

# Hydrophilic Polysulfone-Hydrogel Membrane Material for Improved Nanofiltration in Wastewater Treatment

By

**Francis Ntumba Muya**



A thesis submitted in fulfilment of the requirements for the degree of

**Magister in Scientiae** to the Department of Chemistry,

University of the Western Cape.

*SUPERVISOR:*

***Prof. Priscilla G.L Baker***

November 2013

## I. KEYWORDS

Hydrogels

Polysulfone (PSF)

Glutaraldehyde (GA)

Polyvinyl alcohol (PVA)

Cyclic voltammetry (CV)

Atomic force microscopy (AFM)

Square wave voltammetry (SWV)

Fourier transformer infrared (FTIR)

Scanning electron microscopy (SEM)

Electrochemical impedance spectroscopy (EIS)



## II. Abstract

Over the last decade polysulfone membranes have been demonstrated to be one of the best membrane types in wastewater treatment, especially in ultrafiltration, owing to its mechanical robustness, structural and chemical stability. Regrettably these membranes are mostly hydrophobic by nature and therefore highly vulnerable to fouling due to chemisorptive mechanisms. Fouling may be caused by cake formation on the surface of the membrane or by surface assimilation of the foulants. Many studies have been directed at improving hydrophilic properties of polysulfone membranes by introducing different types of nanoparticle composite such as TiO<sub>2</sub>, ZnO<sub>2</sub>, Au and Ag nanoparticles to the polymer matrix, in order to reduce fouling potential and increase membrane performance. In the present investigation a hydrogel material was developed by crosslinking polyvinyl alcohol (PVA) with polysulfone (PSF), using glutaraldehyde as crosslinker. PVA has excellent film formation, emulsifying and adhesive properties, it is highly flexible and has high tensile strength. Introducing PVA into the PSF polymer matrix was expected to impart its advantageous properties onto the resulting membrane and enhance hydrophilic characteristics of the membrane. The cross linking of PVA and PSF was controlled at three different ratios to evaluate the effect of the PSF contribution i.e. 25:75, 50:50 and 75:25. The crosslinked polymer composites produced three unique hydrogel materials, which were evaluated for the separation of selected small organic molecules, under hydrodynamic conditions, using rotating disk electrochemistry. The hydrogel thin film behaved as a chemical sensor for the oxidation of tannic acid in aqueous solution, with negligible shift in peak potential as a function of concentration. The nanomaterials prepared were characterised using spectroscopic, morphological and electrochemical techniques. Hydrogel

performance in the presence of analyte molecule was evaluated by hydrodynamic voltammetry and electrochemical impedance spectroscopy.

From calibration curves based on cyclic voltammetry, hydrodynamic, macroscopic and spectroscopic techniques, the 75% polysulfone and 25 % polyvinyl alcohol hydrogel (75:25 PSF-PVA) presented the best performance for quantitative detection and best sensitivity toward alginic acid and tannic acid than the corresponding composites (50:50 and 25:75 PSF-PVA). Optical results (contact angle) show an agreement with spectroscopic (EC) and microscopic (AFM) result. A decrease in contact angle gives an increase in roughness and diffusion coefficient. High surface roughness was linked to improved hydrophilicity of the polysulfone.



## II. Declaration of Own Work

I hereby, **Francis N Muya**, understand the University's policy on plagiarism and I certify that this is my own original work, except where indicated by referencing, and that I have followed the good academic practices, declare that all sources have been accurately reported and acknowledged, and that this document has not been previously in its entirety or in part submitted at any higher Education Institution for credit.

**Francis Ntumba Muya**



**November 2013**

Signed.....

A handwritten signature in black ink, appearing to read "Francis Ntumba Muya", written over a grey rectangular background.

### III. ACKNOWLEDGEMENTS

I would like to take this opportunity to sincerely express my gratitude to the following bodies in absolutely no specific order for a tremendous contribution to my entire academic life. I doubt it would have been possible for me to get to this level without their support, whether financial, just social or spiritual.

- **God** Almighty to Him all the glory, honour and adoration for giving me the strength and wisdom through the Holy Spirit to complete this work.
- To chemistry department for financial support
- To my supervisors Prof. P.G. L. Baker and E.I. Iwuoha, thank you very much for seeing my potential and guiding me all the way.
- To my postdoctoral fellow Dr. Tesfaye T. Waryo, Chinwe, Masikini Milua, Stephen Mailu, Euodia Hess, and Janice. Mokgadi, and thank you very much for putting in time to this work. Your tremendous effort is gracefully appreciated
- To my colleagues in SensorLab, University of the Western Cape, specially Dr Fanelwa Ajayi, Lisebo Phelane, Meryck Ward, Godfrey Fuku, L. Willson, Candice and all
- To All grace a la grace members for your spiritual support and prayer.
- To my uncle David Kabamba and his wife Mitchou Mbuyi and my lovely niece Esther Kabamba thanks for all your support in my life which are uncountable, keep it up and don't stop
- To my friends Djo mbaya, Landry katende, Masande yalo, Emile masima, Christian mabiala, Joe Abedi and CrinCESS kamsau Thanks gents for the fun time together.
- To all SensorLab's research team, you guyz rock! Thank you very much

- Much appreciation to all my family members for their love, support and care during the period of study. I felt highly encouraged and loved. Thank you so much. Lastly, not least to my parents Frederick Nkongolo Kabwe and Noella Nkongolo, this is for you. Thank you very much for your love, care, education and upbringing. You are just the best gift from God



#### IV. DEDICATION

This project is dedicated

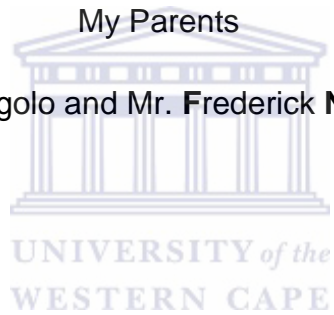
To

**God Almighty**

And

My Parents

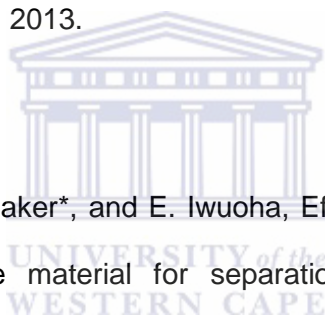
Mrs. **Noella Nkongolo** and Mr. **Frederick Nkongolo Kabwe**





## V. List of publications

1. Lisebo Phelane, **Francis N. Muya**, Heidi L. Richards, Priscilla G.L. Baker\*, Emmanuel Iwuoha, (2013). Polysulfone Nanocomposite Membranes with improved hydrophilicity, *Electrochim. Acta*(2014), <http://dx.doi.org/10.1016/j.electacta.2013.11.156>
2. **Francis N. Muya**, PGL. Baker\*, L. Phelane and E Iwuoha, hydrophilic polysulfone-hydrogel membrane material for improved nanofiltration in wastewater treatment, (in preparation) 2013.
3. **Francis N. Muya**, PGL Baker\*, and E. Iwuoha, Effect of polysulfone contribution into hydrogel membrane material for separation of selected small organic molecules in nanofiltration (in preparation) 2013.



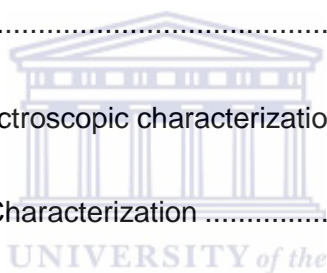
## VI. Table of contents

I.	KEYWORDS .....	i
II.	Abstract.....	ii
II.	Declaration of Own Work.....	iii
III.	ACKNOWLEDGEMENTS .....	iv
V.	List of publications.....	vii
VI.	Table of contents.....	viii
VII.	List of tables .....	xi
VIII.	List of figures.....	xiii
IX.	List of abbreviations .....	xviii
X.	List of units .....	xix
<b>Chapter 1</b>	.....	1
1.	Introduction .....	1
1.1.	Objective of the studies .....	4
1.2.	Motivation.....	5
1.3.	Thesis scope .....	6
<b>Chapter 2</b>	.....	8
	Literature Review .....	8
2.1	Introduction .....	8
2.2.	Classification of Hydrogel .....	10



2.3.	Methods for improving polysulfone hydrophilicity.....	11
2.4.	Applications of hydrogel .....	18
2.5.	Factors affecting hydrogel's characterization and membrane performance .....	18
<b>Chapter 3</b>	.....	21
	Characterisation techniques and methodology .....	21
3.1.	Introduction .....	21
3.2.	Electrochemical characterization .....	21
3.3.	Spectroscopy characterization techniques.....	25
3.4.	Microscopic characterization .....	29
3.6.	Membrane performance .....	36
3.6.1.	Performance under hydrodynamic condition (Rotating disk .. electrode) 36	
3.7.	Methodology and experimental.....	39
3.7.1.	Instrumentation .....	39
3.7.1.1.	Potentiostat Set-up.....	39
3.7.1.2.	Electrode Surface Preparation.....	39
3.7.2.	Materials and reagents.....	40
3.7.3.	Synthesis of Polysulfone –polyvinyl alcohol hydrogel .....	41

<b>Chapter 4</b> .....	45
4.1. Electrochemical characterisation .....	47
4.1.1. Cyclic voltammetry of polyvinyl alcohol on GC electrode .....	48
4.1.2. Cyclic voltammetry of Polysulfone on GC electrode .....	51
4.1.3.1. Cyclic voltammetry of PSF-PVA hydrogels .....	55
4.2. Hydrogel Ageing.....	60
4.3. Spectroscopic characterisation.....	62
4.3.1. Fourier Transform Infrared Spectroscopy (FTIR) Characterisation .....	62
4.3.2. Ultraviolet spectroscopic characterization UV/Vis .....	65
4.4. Macroscopic Characterization .....	68
4.4.1. Scanning Electron Microscopy SEM.....	68
4.4.1.1. Polysulfone film preparation .....	68
4.4.2. ATOMIC FORCE MICROSCOPY (AFM) .....	72
4.5. Optical characterization .....	74
<b>Chapter 5</b> .....	78
5.1. Alginic acid (AA).....	78
5.2. Tannic acid (TA).....	78
5.3. Electrochemical performance in the presence of analyte.....	81



5.4.	Hydrogel performance under Hydrodynamic condition .....	87
	(Rotating disc electrode RDE) .....	87
5.4.1.	Fouling .....	87
5.4.1.1.	Hydrodynamic analyses of hydrogel in the absence of target molecules .....	87
5.4.1.1.1.	Effect of a change in analyte concentration at fixed scan rate and fixed rpm.....	89
5.5.	Electrochemical impedance spectroscopy EIS .....	94
5.5.1.	EIS Hydrogel performance in the presence of analyte .....	94
<b>Chapter 6.</b>	.....	104
6.1.	Conclusion .....	101
6.2.	Recommendations .....	104
	References.....	105



## VII. List of tables

Table 1.	Projected water consumption compared to current sustainable water supply. [3].....	2
Table 2.1:	Application of hydrogel.....	20
Table 3.1:	FTIR stretching vibrations for functional groups present in hydrogels. ....	27

Table 4.1:	The effect of scan rate on anodic and cathodic peak current and peak potentials of PVA in CVs for different scan rates in 2 M HCl Solution.....	50
Table 4.2:	The effect of scan rate on anodic and cathodic peak current and peak potentials for PSF in CVs for different scan rates in 2 M HCl Solution.....	53
Table 4.3:	The effect of scan rate on anodic and cathodic peak current and peak potentials for PSF-PVA hydrogel in CVs for different scan rates in 2 M HCl Solution. ....	57
Table 4.4:	Comparison of PSF, PVA and PSF hydrogels at GC electrode in 2 M HCl.....	58
Table 4.5:	Oxidative and reductive diffusion coefficient of PSF-PVA at GC on different days .....	60
Table 4.6:	Fourier transform Infrared peaks assignment.....	62
Table 4.7:	Hydrogels wavelength and absorbance .....	66
Table 4.8:	Contact angle measurements .....	75
Table 4.9:	Summary of three hydrogels performance .....	76
Table 5.1:	Effect of scan rate on peak current and peak potentials for 50:50 PSF-PVA hydrogel on platinum electrode and glassy carbon electrode in 2 M HCl Solution.....	80
Table 5.3:	Summary of hydrogels performance in alginate acid .....	83
Table 5.4:	Summary of hydrogels performance in tannic acid.....	86
Table 5.5:	Summary of hydrogels performance under RDE in alginate acid..	91
Table 5.6:	Summary of hydrogels performance under RDE in tannic acid ..	93

## ix. List of schemes

Scheme 1 Proposed mechanism of PSF hydrogels formation.....	46
Scheme 2. PVA reaction under acidic condition.....	49

## VIII. List of figures

Figure 1: National noncompliance levels of wastewater treatment plants [2].	2
Figure 2.1: SEM of polysulfone modified with PANI [23].....	14
Figure 3.1: A typical cyclic voltammogram .....	23
Figure 3.2: Schematic drawing of electron and X-ray optics of a combined SEM-EPMA [52].....	29
Figure 3.3: Schematic drawing of Atomic force microscopy [55].....	32
Figure 3.4: Reflux reaction set up.....	41
Figure 3.5: Three electrode electrochemical cell .....	43
Figure 4.1: Cyclic voltammetry of PVA in 1M HCl at different scan rates.....	48
Figure 4.2: Graph of anodic and cathodic peak current ( $I_p$ ) vs. square root of scan rate ( $v^{1/2}$ ) for polyvinyl alcohol film in 2 M HCl solution at different scan rates for peak a and a' .....	51
Figure 4.3: Cyclic voltammetry of PSF in 1M HCl at different scan rates ....	52
Figure 4.4: Graph of anodic and cathodic peak current ( $I_p$ ) vs. square root of scan rate ( $v^{1/2}$ ) for polysulfone film in 2 M HCl solution at different scan rates.....	54
Figure 4.5.(a): Cyclic voltammetry of PSF-PVA (50:50) in 2 M HCl at different scan rates .....	55

Figure 4.5. (b): Cyclic voltammetry of PSF-PVA (75:25) in 2 M HCl at different scan rates .....	55
Figure 4.5. (c): Cyclic voltammetry of PSF-PVA (25:75) in 2 M HCl at different scan rates .....	56
Figure 4.5 (d): Graph of anodic and cathodic peak current ( $I_p$ ) vs. square root of scan rate ( $v^{1/2}$ ) for PSF-PVA Hydrogel in 1 M HCl solution at different scan rates .....	56
Figure 4.6: Variation of diffusion coefficient of GCE based on different number of day .....	61
Figure 4.7: Spectrum of PVA on its own .....	63
Figure 4.8: Spectrum of PSF on its own .....	63
Figure 4.9: Spectrum of PSF-PVA hydrogel 50:50 .....	64
Figure 4.10: Spectrum of PSF-PVA hydrogel 75:25.....	64
Figure 4.11: Spectrum of PSF-PVA hydrogel 25:75.....	65
Figure 4.12: UV/Vis spectrum of PSF and PSF hydrogels.....	66
Figure 4.13: UV/vis absorbance distribution for hydrogels .....	67
Figure 4.14: SEM image of polysulfone .....	68
Figure 4.15: SEM image of PSF-PVA hydrogel 50:50 .....	69
Figure 4.16: SEM image of PSF-PVA hydrogel 75:25 .....	70
Figure 4.17: SEM image of PSF-PVA hydrogel 25:75 at different magnification .....	71
Figure 4.18: AFM image of PSF on its own .....	72
Figure 4.19: AFM image of PSF-PVA hydrogel 50:50.....	72
Figure 4.20: AFM image of PSF-PVA hydrogel 75:25.....	73



Figure 4.21: Surface roughness of PSF and PSF hydrogels.....	73
Figure 4.22: Contact angle variation ( n= 4).....	74
Figure 4.23: Contact angle distribution for hydrogel materials .....	75
Figure 5.1: Anodic and cathodic peak current ( $I_p$ ) vs. square root of scan rate ( $v^{1/2}$ ) for 50:50 PSF-PVA Hydrogel on Platinum electrode in 2 M HCl solution at different scan rates.....	80
Figure 5.2: calibration curves of PSF-PVA hydrogel (50:50) in .the presence of alginate acid in 2 M HCl .....	81
Figure 5.3: Calibration curves of PSF-PVA Hydrogel (50:50) in the presence of alginate acid .....	82
Figure 5.4: Calibration curves of PSF-PVA Hydrogel (75:25) in the presence of alginate acid .....	82
Figure 5.5: Calibration curves of PSF-PVA Hydrogel (25:75) in the presence of alginate acid .....	83
Figure 5.6: Concentration dependant CVs of PSF-PVA hydrogel (50:50) in the presence of tannic acid in 2 M HCl .....	84
Figure 5.7: Calibration curves of PSF-PVA Hydrogel (50:50) in the presence of tannic acid .....	85
Figure 5.8: Calibration curves of PSF-PVA Hydrogel (75:25) in the presence of tannic acid .....	85
Figure 5.9: Calibration curves of PSF-PVA Hydrogel (25:75) in the presence of tannic acid .....	86
Figure 5.10: RDE Voltammogram of Hydrogel at fixed scan rate and change rpm.....	87

Figure 5.11: Plot of rotation speed Vs. peak current response of hydrogel 50:50 at fixed concentration of alginic and tannic acid analyte..	88
Figure 5.12: RDE Voltammogram of Hydrogel 50:50 under hydrodynamic motion at fixed scan rate with an change in alginic acid concentration.....	89
Figure 5.13: RDE Voltammogram of Hydrogel 50:50 under hydrodynamic motion at fixed scan rate with a change in alginic acid concentration.....	90
Figure 5.14: RDE Linear plot of Hydrogel (75:25) current peak response vs an increase in tannic and alginic acid concentration and constant rpm.....	90
Figure 5.15: RDE Voltammogram of Hydrogel 25:75 under hydrodynamic motion at fixed scan rate with a change in alginic acid concentration.....	91
Figure 5.16: RDE Voltammogram of Hydrogel 50:50 under hydrodynamic motion at fixed scan rate with an change in tannic acid concentration.....	92
Figure 5.17: RDE Linear plot of Hydrogel (50:50) current peak response vs an increase in tannic acid concentration and constant rpm....	92
Figure 5.18: RDE Linear plot of Hydrogel (25:75) current peak response vs an increase in tannic acid concentration and constant rpm....	93
Figure 5.19: Equivalent circuit diagram for the PSF hydrogels in the presence of tannic acid.....	95

Figure 5.20: Electrochemical impedance spectra (Nyquist plot) of PSF Hydrogels materials deposited on a platinum working electrode in the presence of tannic acid.....	96
Figure 5.21: Electrochemical impedance spectra (bode plot) of PSF Hydrogels materials deposited on a platinum working electrode in the presence of tannic acid.....	97
Figure 5.22: Electrochemical impedance spectra (bode plot) of PSF Hydrogels materials deposited on a platinum working electrode in the presence of tannic acid.....	97
Figure 5.23: Electrochemical impedance PSF hydrogels plot of Rct vs tannic acid concentration .....	98
Figure 5.24: Electrochemical impedance PSF hydrogels plot of capacitance vs tannic acid concentration.....	99
Figure 5.25: Electrochemical impedance PSF hydrogels plot of Rct vs alginic acid concentration .....	99
Figure 5.26: Electrochemical impedance PSF hydrogels plot of capacitance vs alginic acid concentration .....	100

## IX. List of abbreviations

PSF	:	Polysulfone
GA	:	Glutaraldehyde
PVA	:	Polyvinyl alcohol
TA	:	Tannic acid
AA	:	Alginic acid
DMAc	:	N,N dimethyl acetamide
HCl	:	Hydrochloric acid
KBr	:	Potassium bromide
CV	:	Cyclic voltammetry
SWV	:	Square wave voltammetry
EIS	:	Electrochemical impedance spectroscopy
SPCE	:	Screen printed carbon electrode
Pt	:	Platinum electrode
AFM	:	Atomic force microscopy
UV	:	Ultra violet visible
FTIR	:	Fourier transformer infrared
SEM	:	Scanning electron microscopy
EDX	:	Electron dispersive spectroscopy

MBR	:	membrane bioreactor
Sa	:	Surface roughness
Ra	:	Area roughness
De	:	diffusion coefficient
$\lambda$	:	wavelength
E°	:	formal potential
rpm	:	revolution per minute

## X. List of units



Mw	:	Molecular weight
M	:	Molarity
$\mu$ M	:	Micro-molar
mL	:	Mili-litter
$\mu$ L	:	Micro litter
A	:	Ampere
mA	:	Mili-Ampere
nm	:	nano meter
Cm <sup>2</sup> /s	:	centimetre square per second

# Chapter 1

## 1. Introduction

This thesis describes the development of hydrophilic polysulfone-hydrogel membrane material, for removal of organic material within nanofiltration processes in waste water treatment. There is a large demand for water worldwide owing to an increase in population density. Water is life! 70% of the earth's entire surface is covered by water and 57% of a person's body weight is water. South Africa and Dubai recently announced the deficiency of potable or pure water projected for these countries for the decade to come [1]. The first edition of the National Water Resource Strategy (NWRS) describes how the water resources of South Africa will be protected, used, developed, conserved, managed and controlled in accordance with the requirements of the policy and law. As a result, South Africa's water resources are, in global terms, scarce and extremely limited [1-2]. Mckinsey 2009 forecast that the global water demand would increase from 4500 to 6900 billion m<sup>3</sup> by 2030 [3]. The report further identified India, China, Brazil and South Africa as countries that will account for 40% of the world's population, 30% of the world gross domestic profit, and 42% of the global water demand by 2013 (Table 1) [2 - 3].

**Table 1. Projected water consumption compared to current sustainable water supply. [3]**

Country	Current supply billion m <sup>3</sup>	Demand by 2030 billion m <sup>3</sup>	Demand gap %
<b>China</b>	618	818	32
<b>Brazil</b>	18.7	20.2	8
<b>India</b>	740	1500	102
<b>South Africa</b>	15	17.7	18

South Africa would have to balance water usage between agriculture, industrial activities, and increasing urbanisation. In addition, water resources challenges have been projected based on the water resources available and demand of historical climate conditions. In a recent survey of 14 countries including Canada, USA, Australia, UK and 9 other EU members, South Africa rated 13<sup>th</sup> in terms of the water cost per kilolitre. However, from 2003 to 2008 South Africa rated 3<sup>rd</sup> in terms of the rate at which water costs were increasing [2 - 6]. According to National green drop only 32 of South Africa's approximately 970 waste water treatment plants comply with requirements for safe discharge (Figure 1) [2].

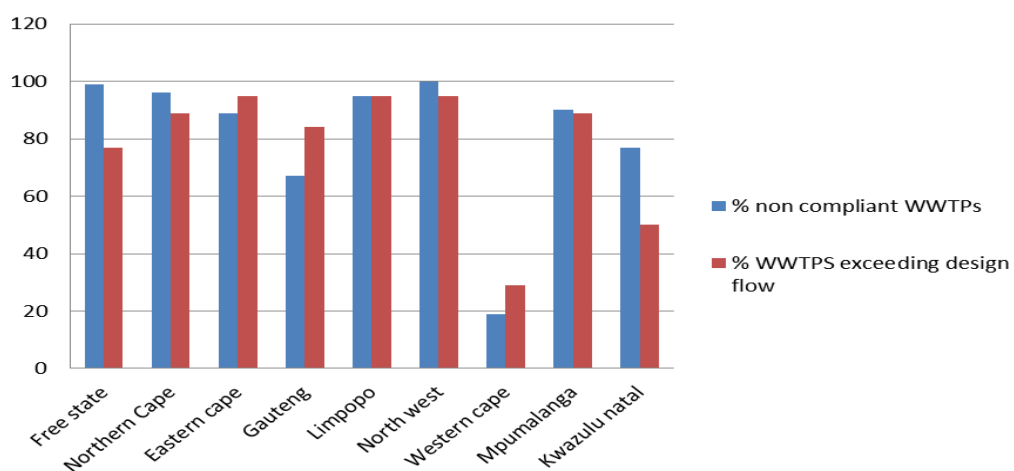


**Figure 1: National noncompliance levels of wastewater treatment plants [2]**

Therefore due to the exponential growth in population and industrialization which is directly proportional to water demand, there is a clear and pressing need for the development of better water treatment processes.

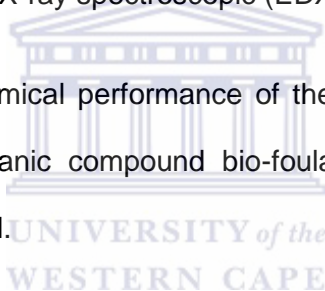
The use of treated wastewater effluent has become a reality and many industries are using this water in their daily production and recycling processes. Membrane technology is still the leading option for water treatment [7]. Membrane bioreactor technology (MBR) is a process for water purification using ultrafiltration or nanofiltration membrane systems. However this technology suffers from major disadvantages such as membrane fouling, irreversibility of the membrane performance and subsequent plant down time. Without improving anti-fouling of membranes this highly efficient technology will remain handicapped. Polysulfone is useful as a main component in membrane technology and ultrafiltration due to its excellent properties such as high tensile strength, durability under heat, pressure resistance, mechanical robustness and structural and chemical stability [7 - 8].

However, the main disadvantage of polysulfone is its hydrophobic nature, which makes its surface prone to fouling by adsorptive mechanisms. These lead to cake formation or adsorption of the foulants on the surface of the membrane and on membranes pores. Cake fouling can occur when foulants are larger than the membrane pores such as sludge flocks and colloids and that form a cake layer on top of the membrane surface which are irreversible by backwashing or water flushing [9].



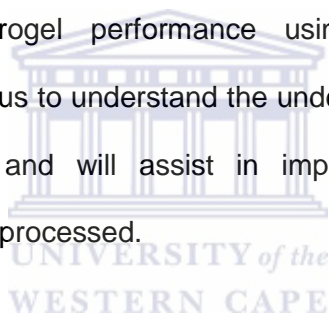
## 1.1. Objective of the studies

1. Preparation of hydrogel material through chemical crosslinking to produce stable hydrogel materials
2. Characterization of hydrogels by :
  - Cyclic voltammetry, rotating disk electrochemistry (RDE), electrochemical Impedance spectroscopic (EIS) and spectroscopy.
  - Morphological and topography evaluation using scanning electron microscopic (SEM), Atomic force microscopic (AFM), Electron dispersive X-ray spectroscopic (EDX or EDS).
  - Electrochemical performance of the hydrogels in the presence of model organic compound bio-foulants such as tannic acid and alginic acid.
3. Evaluation of redox behaviour of tannic acid and alginic acid before the onset of biofouling.
4. Quantifying interfacial electrodynamics morphological and structure in relation to hydrophobicity of prepared PSF materials.



## 1.2. Motivation

South Africa endorses the important international goal of environmental supporter in peaceful manner and safe future for our children and generations to come by providing clean and pure water [1 - 2]. Our contribution in this work will focus on the study of polysulfone hydrogel materials and understanding the physical and chemical properties of polysulfone membranes in the development of hydrophilic nanofiltration membrane materials based on cross-linked PSF-PVA hydrogel. Hydrophilicity of polysulfone has been reported in literature but very few publications refer to the chemically cross-linked polysulfone hydrogel membranes developed in this work. In support of spectroscopic and morphological data, we will also evaluate the hydrogel performance using electrochemical methods. Electrochemistry enables us to understand the underlying mechanisms associated with membrane fouling and will assist in improving the general problems experienced with filtration processed.



### 1.3. Thesis scope

The aims and objectives of the research may be divided into the following chapter which provides pertinent details of synthesis, characterisation and application of the novel hydrogel materials synthesised.

- **Chapter 1:**

This chapter provides a general introduction to polysulfone membrane systems and problems associated with ultrafiltration, reverse osmosis and fouling.

- **Chapter 2:**

In this chapter a critical literature review on the polysulfone membranes systems, the potential of metal nanoparticle incorporation and other methods used to improve hydrophilic nature of the membrane materials.

- **Chapter 3:**

This chapter addresses the preparation and synthesis of PSF-PVA hydrogels and the principles of various analytical techniques and instrument used in these studies.

- **Chapter 4:**

The results obtained from characterizations techniques such as macroscopic, spectroscopic and electrochemical are presented and an evaluation of fouling behaviour as studied using the model organic acids at thin films of hydrogel materials, based on electrochemical impedance spectroscopy interrogation.

- **Chapter 5:**

This chapter provides details of the electrochemistry of hydrogels as sensing material for selected model compound

- **Chapter 6:**

This chapter provides general conclusion and recommendations in terms of improved performance of the membrane after modification as evaluated in standard laboratory experiments



# Chapter 2

## Literature Review

### 2. Introduction

Over the last decade, membrane technology has emerged as the leader in membrane separation techniques, due to its simplicity and environmentally friendly operation [7]. High performance membranes may be produced with good physical and chemical properties as well as high porosity [8]. Hydrogels are networks of polymer chains that are hydrophilic, extremely water swellable and capable of absorbing a large amount of water, whilst not being dissolved themselves [8 - 9]. They are capable of changing chemical energy into mechanical energy and mechanical energy into chemical energy [8]. Physical and chemical properties of hydrogels depend on the types of polymers partaking in hydrogel formation such as polysulfone, polyvinyl alcohol, polyethylene glycol and polyaniline. Consequently, over the last decade, hydrogels made from these polymers have gained widespread recognition as valuable materials for sensors, appropriate membranes for waste water treatment, drug delivery carrier materials, in environmental chemistry and in nosology [10 - 11].

This thesis describes and promotes the application of polysulfone-hydrogels as membranes for nanofiltration in waste water treatment. The improvement of nanofiltration, in membrane bioreactor (MBR) and diffusion reverse osmosis (OR) systems using polysulfone as significant component of the membranes, suffers from many disadvantages associated with the hydrophobic nature of polysulfone [12], which makes its surface vulnerable to fouling. Fouling may be caused by cake formation on the surface of the membrane or by surface assimilation of the

foulants [9]. Polysulfone materials are principally used due to their mechanical, thermal, chemical stability and wide pH range of application [9 - 13]. However its hydrophobic nature results in blocked membrane pore and diminished flux, which shortens the life time of polysulfone membrane [8]. Hydrophobic nature of polysulfone have been improved by using different approaches such as introducing nanoparticles into the polysulfone matrix, [9 - 14] or by crosslinking hydrophilic polymers such as polyaniline, poly(vinyl alcohol), poly(vinyl ester, poly(ethylene glycol) which can network differently based on the position of the functional group [14 - 15].

## 2.1. Mechanism of network formation

Hydrogel formation may refer to the crosslinking of polymer chains that initially leads to the formation of the large branched polymers. However mixing of these branched polymers lead to what is called sol further crosslinking result in **gel** formation [8]. The synthesis approach of polysulfone hydrogel could incorporate chemical modification of a monomeric unit like meth-acrylates and meth-acrylamides mostly known hydrogel [8 & 9], a polymer of (2-hydroxyethyl) methacrylate (HEMA) and ethylene glycol bismethacrylate (EGDMA). These hydrogels could be applied in the assembly of soft contact lenses and as a reservoir for drug delivery [11]. Other hydrogels may be synthesised from chemical modification of prepolymer, such as hydrophilic polymer and some synthesised by cross linking a lower molecular mass hydrophilic polymer e.g. (Hydroxyl poly-ethylene glycol with diisocyanate within the presence of a crosslinker [16]. Chemical modification of polysulfone with polyvinyl alcohol with glutaraldehyde as cross-linker could improve polysulfone hydrophilicity in the absence of additional nanocomposites [14].

## 2.2. Classification of Hydrogel

Hydrogels are classified into categories depending on the types of cross-linking involved [16]. Cross-linking different polymers lead to the formation of hydrogel within the presence or the absence of a cross-linker of alternative. The cross-linked polymers could be classified into different classes [8] some hydrogels are called permanent or chemical when they are covalently bonded. This means involving a cross-linker in which there is bond breaking and new bond formation. Some hydrogels are called reversible or physical when the polymer involved produce a network by molecular entanglement, ionic bonding and hydrogen bonding or even hydrophobic interaction [8].

### 2.2.1. Physical or reversible hydrogel

There has been a lot of interest in physical or reversible hydrogel formation due to the fact that they are relatively easy to produce and the major advantage of reversible hydrogel is that there is no use of cross-linking agents which is significant in terms of reducing cost of preparation. Cross-linking agents affect the integrity of the substances to be entrapped as well as the need for their removal before application. Careful selection of hydrocolloid type, concentration and pH can lead to the formation of broad range of gel textures and is currently an area receiving considerable attention, particularly in the food industry [8]. Various methods that have been reported in literatures for physical cross-linked hydrogels, including:

- Heating and cooling a polymer solution
- Ionic interaction
- Hydrogen bonding
- Maturation (heat induced aggregation) and

- Freeze- thawing (according to Syed K. H and Glyn O Phillips) [8]

### **2.2.2. Chemical or permanent hydrogel**

Chemical cross-linking involves grafting of monomer on the backbone of the chemical compound or the utilization of cross-linking agents to link two polymer chains [8]. The cross-linking of natural and artificial polymers is achieved through the reaction of their functional group like (OH, COOH and NH<sub>2</sub>) with cross-linkers like aldehyde (e.g. glutaraldehyde, adipic acid and dihydrazide) [8 &18]. There are a variety of strategies reported within the literature to produce chemically cross-linked permanent hydrogel [18]. The major chemical strategies include:

- Chemical cross-linkers ( Using Glutaraldehyde)
- Grafting(Activated by gamma rays, electron beam exposure & plasma)
  - Chemical grafting (activated by chemical reagent)
  - Radiation grafting (activated by high energy radiation)
- Radiation cross-linking (gamma rays, X-rays & electron beam)
  - Aqueous state radiation
  - Radiation in paste
  - Solid state radiation
  - Cross-linking in solid state.

### **2.3. Methods for improving polysulfone hydrophilicity**

Hydrogels are hydrophilic polymer chain networks, capable of absorbing water up to 99.9 % owing to its high absorbent nature. They conjointly possess a degree of flexibility, owing to their vital water content. They may also be describes as three-dimensional network structures obtained from a category of artificial or natural



polymer that retain a vital quantity of water [8]. They are present as considerably dilute cross-linked systems that are classified as weak or strong depending on their flow behaviour under steady state conditions. However, traditional hydrogels exhibit very little flow under steady state conditions and has the form of a solid jelly like material with properties similar to the starting material; ranging from soft and weak to mechanically stable and rough [8]. Introducing a crosslinking agent into the polymer network improves the flow behaviour and contributes to the stickiness of hydrogels. Several investigators have developed polysulfone membranes, targeted on improving polysulfone's hydrophobic nature using different approaches and for different applications [19]. Hydrophilic polysulfone membranes are appropriate for use in applications requiring low macromolecule binding and high separation efficiency. The hydrophilic polysulfone membranes are beneficial for a large variety of filtration applications. [20]

Hydrophilic polysulfone may be achieved by incorporating a hydrophilic polymer into the polysulfone network such as polyvinyl alcohol. The hydrophilic functional groups like radical (OH) or carboxyl (COOH) and their characteristic chains are responsible for water storage and water absorption [18]. Hydrogels find application in different areas of separation chemistry such as metallurgy, petrochemical, food industries, medicine (drug delivery and blood purification), electronics (electrical devices) and environmental remediation (water treatment) [8 & 20].

### **2.3.1. Polysulfone modified with polyaniline nanocomposite**

Conducting polymers are a new class of polymers with unique chemical and electrochemical properties. Introducing a conducting polymer such as polyaniline into the polysulfone membrane will enhance the permeability and reduce the fouling of the membrane [21]. The performance of PSF/PANI cobalt nanocomposite membrane was evaluated in terms of pure water permeation flux [21 - 22] as;

$$J = \frac{Q}{\Delta t \times A} \quad (1)$$

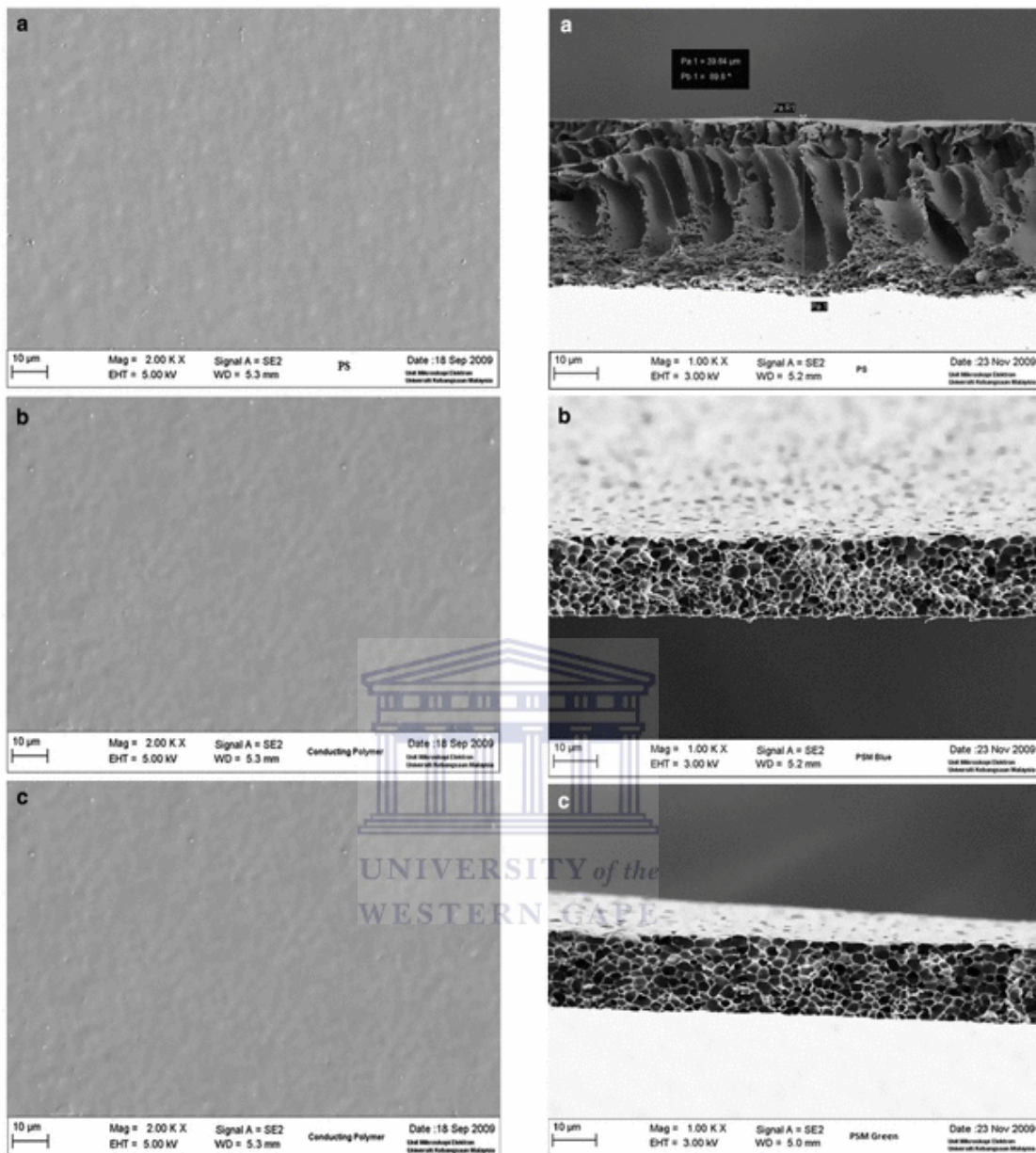
Where by: J (L/m<sup>2</sup>h) is flux permeability membrane for pure water

Q (L) is the volume of permeate solution

Δt is the permeation time (h)

A is membrane area in cm<sup>2</sup>

The authors concluded that pure water flux of the PSF/PANI cobalt nanocomposite membrane was 2.8 times higher compared to that of PSF/PANI membrane. Its salt rejection was 93.4% of sodium chloride for PSF membrane and 97.3% sodium chloride for PSF/PANI cobalt nanocomposite respectively. The contact angle decreased with an increase in polyaniline and cobalt nanocomposite [22]. So Alam and Dass 2012 stated that the deliquescent modification of polysulfone membranes provides all the necessary enhancements required for improved membrane technology [23]. Polyaniline nanoparticles inclusion within the polysulfone membrane improved water flux and salt rejection and not only increased the separation characteristics, but also altered the membrane morphology and surface roughness (Figure 2.1).



*SEM outer surface morphology of a polysulfone, b undoped PSu/PANI, c doped PSu/PANI nanocomposite membrane*

**Figure 2.1:** SEM of polysulfone modified with PANI [23]

### **2.3.2. PSF- Citric acid and sodium bisulfite**

Citric acid and sodium bisulfite are two antioxidants that are widely used in membrane feed water pre-treatment and cleaning. Wei and al 2012 confirmed that adsorption of citric acid and sodium bisulfite into the polysulfone membrane improved the antifouling properties and the membrane salt rejection as well as preventing polysulfone membrane degradation [24]. Pre-adsorption of citric acid and sodium bisulfite were developed as easy ways for polysulfone ultrafiltration membrane modification. It was found that chemical bonding and Van Der Waals attraction could be accountable for the adsorptions of citric acid and sodium bisulfite onto polysulfone membranes. After modification, the surfaces of membranes became hydrophilic, porousness improved and better chlorine tolerance was measured [24].

They confirmed the hydrophilicity of the membrane using contact angle measurement, flux and chlorine tolerance and salt rejection. After pre-adsorption of the antioxidant (citric acid and sodium bisulfite) into the polysulfone membrane and in each case the membrane showed better response for pure water flux of 260.8 L/m<sup>2</sup>h for the modified and 2018 L/m<sup>2</sup>h for the unmodified, salt rejection increased from 98 to 99% and contact angle for the modified membranes was measured as 59.7°.

### **2.3.3. PSF-Nano crystalline cellulose (NCC)**

Huang and Yang 2006 showed that water flux and clearance efficiency of proteins can be adjusted by controlling the pore size of the membrane [25]. Cellulose is renewable natural compound that maintains its characteristic together with hydrophilicity, high strength and tensile modules, biodegradability and renewability [26]. Nano-crystalline cellulose is a very small macromolecular substance with a

large surface areas and surface energy. By introducing nano-crystalline cellulose into polysulfone membrane, the porosity of the membrane appeared to be more controlled and enhanced. High dialysis membranes typically have large pore sizes and high porosity for qualitative analysis which enhance the capability of passing substances of intermediate molecular mass. Incorporating nano-crystalline cellulose into polysulfone membrane was observed to regulate the water flux, salt rejection, contact angle, and purity of water. The interfacial bonding strength was enhanced and the mechanical properties of the membrane were improved and the NCC membrane has proven particularly useful in blood purification studies [26]. Shuai Li, and al confirmed that, introducing nano-crystalline cellulose into polysulfone membrane resulted in an improvement in water flux to 48.4 L/m<sup>2</sup>h mmHg, clearance of lysozyme and urea reached 73.3% to 90.4% and retention ratio of bovine serum albumin (BSA) remained over 96%

1. *Retention ratio and clearance*

Retention ratio of dialysis membrane, reflecting the retention capacity of the composite membrane for a given solute in solution, means that the amount of specific solute retained with the dialysis membrane as percentage of total amount in the solution, may be expressed as:

$$R = 1 - \frac{A_f}{A_i} \times 100\% \quad (2)$$

Where R is the retention ratio (%) and  $A_i$  and  $A_f$  are the absorbencies of initial and filtered sample at 280nm among ultra-violet visible

2. *The clearance may be calculated by*

$$C = \frac{A_o - A_t}{A_o} \times 100\% \quad (3)$$

Where C is clearance and  $A_o$  and  $A_t$  are the absorbencies of the initial sample and sample at time t.

#### 2.3.4. Polysulfone modified with polyvinyl alcohol

Polyvinyl alcohol (PVA) is a colourless and soluble polymer used as main component in manufacturing of textiles, paper and in preparation of hydrophilic membrane [28]. PVA is exclusive among electrochemical polymers owing to its availability of current flow. It can be synthesis from chemical reactions using single-unit of monomers [15]. However, chemical compound such as vinyl resin, polyvinyl resin are formed by dissolving another polymer, vinyl polymer (PVAc), in presence of an alcohol like methanol and an alkaline catalyst like caustic soda. Acetate functional group will be removed by alcoholysis reaction from the PVAc molecules while not disrupting their long-chain structure [28]. The products are very soluble in water and insoluble in most of organic solvents. Incomplete alcoholysis yielded polymer less soluble in water and soluble in certain organic liquids [15].

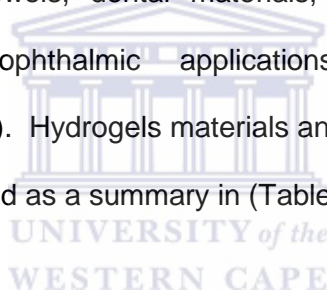
Polyvinyl alcohol (PVA) was characterised as a soluble polymer with extremely hydrophilic properties, physical and chemical stability, PVA is an excellent membrane material for preparation of a hydrophilic membrane [8]. Specifically, PVA-polyvinyl acetate, PVA-vinyl compound, PVA-vinyl resin, these polymer are more desirable for the preparation of hydrophilic membranes due to its low cost, business convenience, high water porosity and smart film-forming properties.

PVA's properties are affected by grease, hydrocarbons, and animal or vegetable oils [15]. To create stable PVA films or films with a desired salt property, PVA can be cross-linked through a range of ways [15], there are many past studies on PVA membranes developed for reverse osmosis and most of those membranes provide comparatively low flux and low salt rejection. Abdel-hameed and El-Aassar 2012 [15] confirmed that membrane preparation of polysulfone modified with PVA and  $\text{TiO}_2$  at  $75^\circ\text{C}$  for a time frame of 60 minutes gave an optimum reverse osmosis

membrane performance for neat PSF/PVA/TiO<sub>2</sub> with permeate flux starting from 9.32 L/m<sup>2</sup>h to 11.56 L/m<sup>2</sup>h with a slight increase in salt rejection from 76.79 to 78% therefore they reported salt rejection improved as a function of crosslinker concentration.

## **2.4. Applications of hydrogel**

Polysulfone hydrogels has been demonstrated to be useful in pharmaceutical and biomedical fields, because of their high water absorption capability and biocompatibility. They have been used in wound dressing [31], drug delivery [11], agriculture, sanitation towels, dental materials, implants, injectable chemical compound systems, ophthalmic applications and hybrid-type organs (encapsulated living cells). Hydrogels materials and their projected corresponding applications is represented as a summary in (Table 2.1)



## **2.5. Factors affecting hydrogel's characterization and membrane performance**

There are many factors contributing to fouling such surface properties, hydrodynamic conditions, ionic strength and solute concentration. However the extent of adsorption depends on the types of solute macromolecule-membrane interactions, such as hydrogen bonding, dipole interaction, van der Waals forces and electrostatic effect. [27, 34 - 35] However an alternative issue affecting the adsorption of the macromolecule into the membrane surface is the charge interaction between the surface of molecules and the macromolecule. Another factor contributing to the membrane aging is an extended exposure to hydrogen

ion concentration (pH) 8 and 10 that produces chain breaking within the radical group of molecules [36]. This results in membrane texture change at microscopic scale, which was closely associated with changes in mechanical properties of the membrane [36-39]. Few chain scissions had a high impact on elongation and tensile strength at break purpose of the membrane material. Membrane permeability appeared to be less sensitive to such changes due to the fact that the permeability depends on skin properties primarily [42]. However, the method of chain breakage was shown to be temperature activated, below 25°C, whilst operation at higher temperatures was to be avoided [36]. These stimuli-sensitive hydrogels can display changes in their swelling behaviour of the network structure according to external environment. They may exhibit positive thermo-sensitivity of swelling, in which polymers with upper critical solution temperature (UCST) will be favoured at this temperature, were the mixture of two liquids immiscible at room temperature, ceases to separate into two phases and shrinking by cooling below the UCST [37].

In this research project we will show that chemical crosslinking produces a stable hydrogel material. The hydrophilicity of the hydrogel materials is expected to reduce substantially. The hydrogel materials will be evaluated by spectroscopy, morphology and electrochemistry to demonstrate the improved physical and chemical properties.



**Table 2.1: Application of hydrogel**

Hydrogel Application	Hydrogel composite (polymer)	References N°
Water treatment	<ul style="list-style-type: none"> <li>• PSF- metal nanoparticle</li> <li>• PSF-PVA- nanocomposite</li> <li>• PSF-PANI nanocomposite</li> <li>• PSF-Citric acid/PSF-Sodium bisulfite</li> <li>• PSF-Oxygen plasma</li> <li>• PSF-Silver nanocomposite</li> <li>• PSF-Isocyanate treated grapheme oxide</li> </ul>	<p>[9 &amp;13]</p> <p>[14,15 &amp; 28]</p> <p>[21 &amp; 22]</p> <p>[24]</p> <p>[53]</p> <p>[62]</p> <p>[27]</p>
Proton exchange	<ul style="list-style-type: none"> <li>• PSF-sulfonate</li> </ul>	[71]
Wound care	<ul style="list-style-type: none"> <li>• PEG, poly(propylene glycol</li> <li>• Poly(vinylpyrrolidone) PEG-Agar</li> <li>• Methyl cellulose</li> </ul>	[8]
Drug delivery	<ul style="list-style-type: none"> <li>• Poly(vinylpyrrolidone)</li> <li>• Poly(acrylic acid, Carboxymethyl cellulose</li> <li>• PVA, acrylic acid, methacrylic acid</li> </ul>	[8 & 11]
Medicinal Blood purification	<ul style="list-style-type: none"> <li>• PSF-Nano crystalline cellulose (NCC)</li> <li>• PSF-Vitamin E</li> </ul>	<p>[25 &amp; 26]</p> <p>[28]</p>
Pharmaceutical and agriculture waste treatment , separation	<ul style="list-style-type: none"> <li>• Starch, PVA</li> </ul>	[17]
Membrane aging	<ul style="list-style-type: none"> <li>• PSF-Hypochlorite</li> </ul>	[30]
Capacitance	<ul style="list-style-type: none"> <li>• PSF-nanocomposite</li> </ul>	[32 & 82]
Gas separation	<ul style="list-style-type: none"> <li>• PSF-modify with additive solvent</li> <li>• PSF-Zeolite</li> <li>• PSF-Silica</li> </ul>	<p>[38, 40]</p> <p>[31]</p> <p>[51]</p>

# Chapter 3

## Characterisation techniques and methodology

### 3.1. Introduction

This chapter presents the preparation procedures for hydrogel synthesis, solvent preparation and instrumental characterization techniques used to study the hydrogels. Different characterization techniques have been used to investigate the properties of polysulfone hydrogels as thin film membranes, prepared onto a conductive electrode surface. These include:

- Electrochemical techniques such as cyclic voltammetry, square waves and Electrochemical Impedance Spectroscopic.
- Spectroscopic techniques used for membrane structure understanding at its molecular level (Fourier transform infrared spectroscopy (FTIR)).
- Microscopic techniques such as (Scanning electron microscopy (SEM), and Atomic force microscopy (AFM)) to evaluate the morphological and topography features;
- Drop shape analysis for the evaluation of contact angle with pure water.

### 3.2. Electrochemical characterization

Electrochemical characterization deals with the connection between electrical and chemical phenomena, also the laws that govern the interaction of these phenomena [44]. Electrochemical studies provide information of the material being analysed from the current response and peak potential response. The signal produced will

enable the calculation of a diffusion constant which may be related to the rate at which electrons move to and into the interfacial region of the transducer [44-45].

Cyclic voltammetry is a widely used electroanalytical technique for the evaluation of redox properties of conductive and semi-conductive materials [45]. The materials under investigation are usually immobilised at a transducer surface, which may be macro-electrodes, predominantly micro-electrodes and even screen printed or interdigitated electrodes [44]. For application in a small electrochemical cells a working, counter and reference electrodes are required. A potentiostat is used to produce the input signal and the resultant output of current against potential is presented as a voltammogram [46]. Throughout the cyclic voltammetry experiment, the potential is ramped from an initial potential,  $E_i$  to an additional negative or positive potential. However, at the tip of the linear sweep, the direction of the potential scan is reversed, sometimes stopping at the initial potential,  $E_i$  [44 & 47].

Current is measured between the working electrode and the counter electrode (auxiliary electrode). The output data are plotted as a voltammogram (Figure 3.1). The forward scan produces a current peak for any analyte that can be reduced or oxidized depending on the initial scan direction over the range of potential scanned. The current increases as it reaches the reduction potential of the analyte, but then decreases as the concentration of the analyte is depleted close to the electrode surface [47]. If the redox couple is reversible, then reversing the applied potential makes it reach a potential that re-oxidizes the product formed in the first reduction reaction, thus producing a current of reverse polarity from the forward scan [47]. The oxidation peak usually has the same shape as that of the reduction peak. As a result, the information about the redox potential and the electrochemical reaction rates of compounds can be obtained. For instance, if the electron transfer is fast at the electrode surface and the current is limited by the diffusion of species to the

electrode surface, then the peak current is proportional to the square root of the scan rate ( $v^{1/2}$ ) [46 & 47].

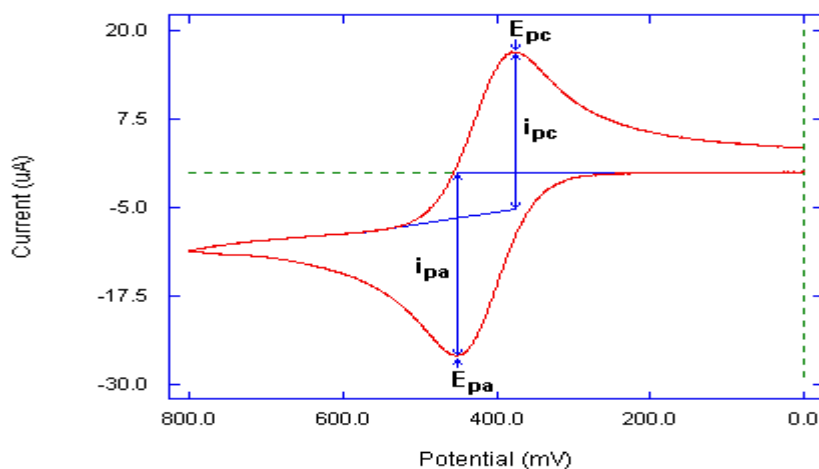


**Figure 3.1: A typical cyclic voltammogram [107].**

Important parameters could be obtained from the cyclic voltammograms analysis of redox properties of conductive or semi-conductive samples. These parameters including peak potential ( $E_{pc}$ ,  $E_{pa}$ ), and peak current ( $I_{pc}$ ,  $I_{pa}$ ) of the cathodic and anodic peaks. The cathodic and anodic peak (peak potential or peak current) provide important information about the sample under investigation [48]. Information about the electrochemical process in terms of reversibility, irreversibility or quasi-reversibility of the sample under investigation and electron movement, mass transfer and diffusion coefficient, may be obtained [49].

### Criteria for reversible system

- $I_{pc} = I_{pa}$  or  $I_{pa} \div I_{pc} = 1$
- The peak potentials ( $E_{p,a}$  and  $E_{p,c}$ ) are independent of the scan rate,  $v$
- The formal potential is positioned midway between  $E_{p,a}$  and  $E_{p,c}$ , so that  

$$(E^{\circ} = (E_{p,a} + E_{p,c})/2)$$

- $I_p$  is proportional to  $v^{1/2}$
- The separation between the peak potentials  $E_{p,a}$  and  $E_{p,c}$  is 59 mV/ $n$  for an  $n$  electron couple at 25 °C [30]. The value for the separation peak potential,  $\Delta E_p$ , arises from the following

$$I_p = 0.4463 \cdot n \cdot F \cdot A \cdot \left( \frac{nF}{RT} \right)^{1/2} \cdot D^{1/2} \cdot v^{1/2} \cdot C_{\text{analyte}}$$

(4)

At room temperature the above equation becomes

$$I_p = 2.69 \times 10^5 n^{3/2} A D^{1/2} v^{1/2} C_0$$

(5)

#### Criteria for irreversible system

- There is no reverse peak
- The  $I_{pc}$  is proportional to  $v^{1/2}$
- The value of  $E_{p,c}$  shifts  $-30/\alpha \cdot n_\alpha$  for each decade increase in  $v$

$$|E_p - E_{p/2}| = \frac{48}{\alpha \cdot n_\alpha} mV$$

- 
- (6)

The property of the current for an irreversible process can be express by the equation below

$$I_p = 0.227 \cdot n \cdot F \cdot A \cdot C \cdot k^0 \cdot e^{-\frac{\alpha \cdot n_\alpha \cdot F}{RT} (E_p - E^*)}$$

(7)

### Criteria for quasi-reversible system

For a quasi-reversible electrochemical process the shape of the peaks and the peak-to peak separation ( $\Delta E_p$ ) depend, through a complex mathematical function  $\Psi$ , from  $\alpha$ ,

$k^o$  and  $\nu$  as shown in the following equation

$$\Psi = \frac{k^o \cdot \left[ \frac{D_{ox}}{D_{red}} \right]^{\alpha/2}}{\left[ D_{ox} \cdot \pi \cdot \nu \cdot \frac{n \cdot F}{R \cdot T} \right]^{1/2}} \quad (8)$$

### 3.3. Spectroscopic characterization techniques

Spectroscopy is the study of the interaction between matter and radiated energy. Traditionally, spectrographic analysis originated through the study of light distributed consistent with its wavelength. Spectrographic analysis and spectrographic are terms which refer to the measurement of radiation intensity as a function of wavelength, and they are typically used for qualitative and quantitative analysis methods and even quantum physics [50].

Spectrographic analysis is employed in physical and analytical chemistry as a result of atoms and molecules have distinctive spectra, which provide qualitative and quantitative information regarding the vibrations of bonds between atoms and molecules. The central idea in spectrographic analysis may be represented by Gauge Boson theory of Energy, which relates resonance energy and its corresponding resonant frequency:

$$E = h\nu \quad (9)$$

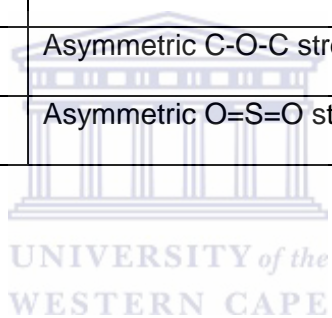
Where E is the energy, h refers to Planck's constant  $6.626 \times 10^{-34}$  J.s and  $\nu$  is the frequency [50]. The equation may be used to calculate bond energy of new bonds formed [50]. In our research we will use FTIR to confirm the formation of the cross linking between starting materials to produce the desired hydrogel products. The FTIR of starting materials and product in the case of PSF hydrogels knowing the starting materials and synthesis product will be compared to obtain information regarding the crosslinking chemistry.

### 3.3.1 Fourier transforms infrared spectroscopic (FTIR)

The term Fourier Transform Infrared Spectroscopic (FTIR) refers to a fairly recent development in the manner in which the data is collected and converted from an interference pattern to a spectrum. The expected functional group stretching vibrations for the starting materials and synthesis product have been identified from literature (Table 3.1)

**Table 3.1:** FTIR stretching vibrations for functional groups present in hydrogels.

Frequency (cm <sup>-1</sup> )	Assignments
3600 & 3200	O-H stretching vibrations
2980 and 2880	Asymmetric and symmetric C-H stretching vibrations involving entire methyl group
1590 & 1485	Aromatic C=C stretching
1412	Asymmetric C-H bending deformation of methyl group
1365	Symmetric C-H bending deformation of methyl group
1325	Double resulting from asymmetric
1298	O=S=O stretching of sulfone group
1244	Asymmetric C-O-C stretching of aryl ether group
1170	Asymmetric O=S=O stretching of sulfonate group





### 3.3.2. Ultra violet (UV/vis) spectroscopic technique

Ultra violet visible (UV/Vis) is a spectroscopic technique that involves the spectroscopy of photons in the UV/visible region. It uses light in the visible and adjacent (ultraviolet (UV) and near infrared (NIR) ranges) [50]. In UV-visible spectroscopy, one can monitor the intensity of colour of a material and the wavelength of absorption, at the same time. The colour monitored is the wavelength at maximum absorption ( $\lambda_{max}$ ), but one compound may have more than one absorption peak associated with energy transitions within the molecule. The optical absorbance, *Abs*, is defined according to the equation:

$$Abs = \log_{10} (T \text{ with no sample}) / (T \text{ with sample}) \quad (10)$$

*T* is the transmittance light through the cell. The absorbance is inversely related to the amount of light transmitted through a cell containing an analyte solution. The absorption spectrum provides information about conjugation within molecules and energy transitions due to excitation by UV light. It is widely used in the quantitative determination of solutions of transition metal ions and highly conjugated compounds. For a material that absorbs UV-visible light, we can monitor its concentration using Beer- Lambert relationship;

$$Abs = \epsilon . C_o l \quad (11)$$

Where the absorbance is determined at fixed wavelength  $\lambda$ ,  $\epsilon$  is the extinction coefficient (cited at the same value of  $\lambda$ ), and *l* is the optical path length. If the magnitude of the extinction coefficient at  $\lambda$  is known, then the amount of analyte (***C<sub>o</sub>***) can be quantified (10). UV-visible spectroscopic is one of the best ways of identifying analyte i.e. qualitative information. This is because each specific analyte absorbs energy in the form of photons at different wavelengths [50].

It is a complementary technique to fluorescence spectroscopy in that it deals with transitions from the ground state to the excited state while fluorescence spectroscopic measures transitions from excited state to the ground state [50].

### 3.4. Microscopic characterization

#### 3.4.1. Scanning electron microscopic

Scanning electron microscopic (SEM) is a microscopic technique used for the study of surface morphological, topography, composition of a material [51- 53]. These studies are performed by scanning the sample to be analysed with a high-energy beam of electron in raster scan pattern. Scanning electron microscopic analysis required a conductive platform for generation of electron that will interact with atom for signal generation, the signal being generate by SEM is based on the collection of back scattered electrons, characteristic of X-rays, light, transmitted electrons or secondary electron.

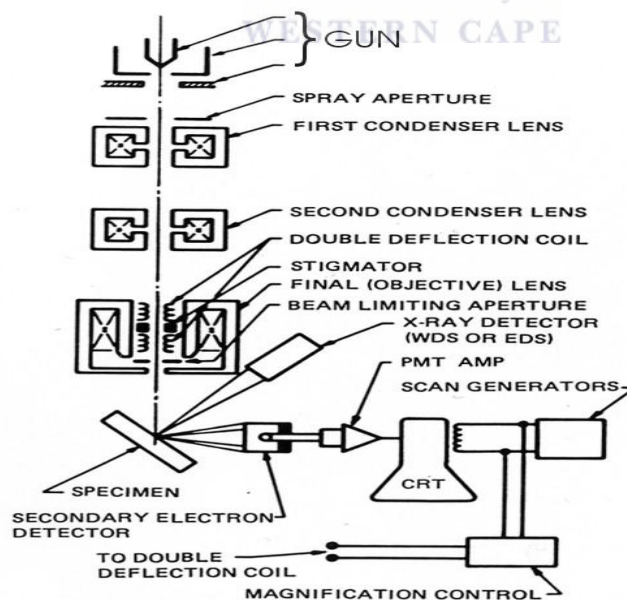
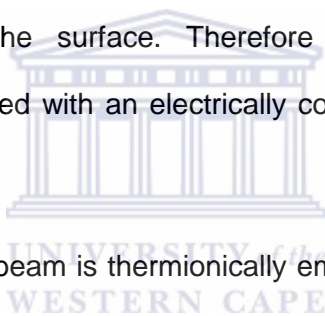


Figure 3.2: Schematic drawing of electron and X-ray optics of a combined SEM-EPMA [52]

The scanning electron microscopic (SEM) is widely use as research technique in membrane technology for identification of surface morphology, porosity and pore sized distribution of a material [51]. A centred beam of high-energy electrons is used to generate secondary electrons that will interact with the surface of solid specimens. The signals derived from electron-sample interactions reveal information regarding the sample morphology, chemical composition, crystalline structure and orientation of materials [52]. Accelerated electrons in SEM carry important amounts of kinetic energy, and this energy is degenerated as a range of signals made by electron-sample interactions once the incident electrons are decelerated within the solid sample and at the surface. For conventional imaging in SEM, electrically conductive and electrically grounded specimens are required to prevent the accumulation of electrostatic charge at the surface. Therefore non-conductive specimens like polymers, need to be coated with an electrically conductive material such as carbon and gold nanoparticle. [53]



In SEM analysis, electron beam is thermionically emitted from electron gun fitted with a metal filament cathode (tungsten). As a result, the electromagnetic wave that has energy from 0.2 keV to 40 keV, is concentrated by 2 condenser lenses of 0.4 nm to 5 nm in diameter. The beam passes through pairs of scanning coils that deflect the beam within the x and y axes so that it scans in a raster pattern over an oblong space of the sample surface. Once the first electromagnetic wave interacts with the sample the electrons lose energy by continual random scattering and absorption among a teardrop-shaped volume of the specimen [53]. The energy exchange between the electromagnetic wave and the sample ends up in the reflection of high-energy electrons by elastic scattering, emission of secondary electrons every of which may be detected by specialised detectors The beam current absorbed by the specimen may be detected and used to produce image. To which an Energy-dispersive x-ray spectroscopy (EDS or EDX) could be associated for elemental analysis or chemical

characterization of the sample. The instrument used for all SEM analysis in this work is the Zeiss Auriga, High resolution (Fegsem) field emission gun.

### **3.4.2. Atomic Force microscopic (AFM)**

The Nanosurf easyScan 2 is an atomic force microscope system that can make nanometer scale resolution measurements of topography and several other properties of a sample. Atomic force microscopy (AFM) or scanning force microscopy (SFM) is one of the first instruments that were developed for image manipulation and nanoscale measurement [54]. It has a very high-resolution scanning probe, with demonstrated resolution on the order of fractions of a nanometer, atomic force microscopy is better than optical diffraction because it can measure at 1000 times higher resolution. [54-55]. The force between a probe and the sample is measured [54]. Hydrogel analysis was done using contact mode cantilever which measured the angle of deflection between the sample and cantilever probe and its feedback to regulate the force on the hydrogel. It does not only measure the force acting on the material but also regulates it, and acquisition of images was done at very low forces. The feedback loop consists of the tube scanner that controls the height of the tip; the cantilever and optical lever, which measures the local height of the sample and a feedback circuit that attempts to keep the cantilever deflection constant by adjusting the voltage applied to the scanner. This instrument is capable of different modes of imaging at nanoscale. It has different component such as piezoelectric scanner which expands and contracts proportionally to an applied voltage, cantilever and tip (contact and non-contact), a laser, photodiode and detector and electronic device for feedback (figure 3.3)

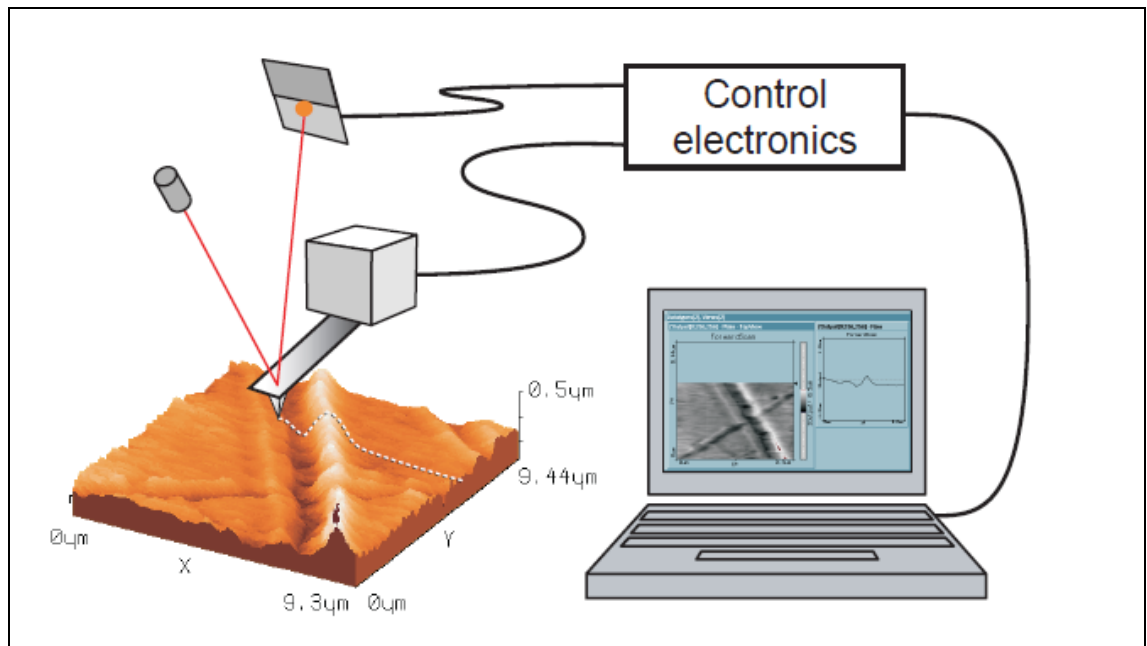


**Figure 3.3:** Schematic drawing of Atomic force microscopic [55]

#### 3.4.2.1. Contact mode

In contact mode the measurement is based on static tip deflection which is used as a feedback signal. The low stiffness cantilevers are used to boost the deflection signal. However, close to the surface of the sample, attractive forces can be quite strong, causing the tip to "snap-in" to the surface. The force between the tip and the surface is kept constant during scanning by maintaining a constant deflection. [55]

#### 3.4.2.2. Non-contact mode

In non-contact mode, the tip of the cantilever doesn't contact the sample surface. The cantilever is instead oscillated at either its resonant frequency (frequency modulation) or simply higher than (amplitude modulation). The amplitude of oscillation is often a few nanometers (10 nm) right down to a few picometers. The decrease in resonant frequency combined with the electrical circuit system maintains a relentless oscillation amplitude or frequency by adjusting the common tip-to-

sample distance. Measuring the tip-to-sample distance at every (x,y) point provides information that permits the scanning software to construct a topographic image of the sample surface [54 & 55].

### 3.4.2.3. Tapping mode

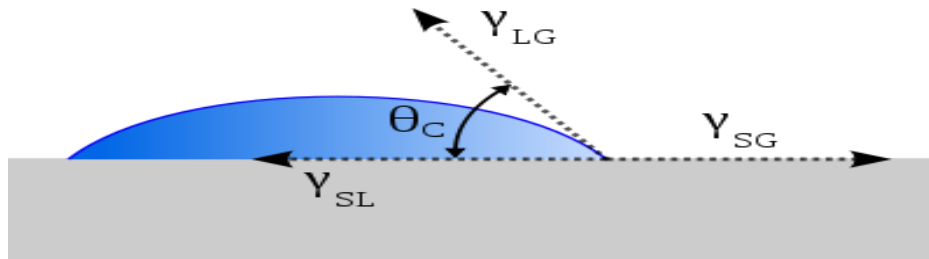
In tapping mode, the cantilever is driven to oscillate up and down at close to its resonance frequency by a little electricity component mounted within the AFM tip holder the same as non-contact mode. However, the amplitude of this oscillation is usually 100 to 200 nm. The interaction of forces exerted on the cantilever once the tip comes near the surface. A tapping AFM image is created by imaging the force of the intermittent contacts of the tip with the sample surface [55].

## 3.5. Contact angle measurement

Drop shape analyser (DSA25, Kruss) was used to confirm the hydrophobic nature of the membrane by measuring the angle formed between the film of PSF and a drop of water. It was illuminated from one side and a camera at the opposite end of the optical bench recorded an image of the drop. Contact angle is a measure of the wettability and is used as a a measurement of hydrophobicity or hydrophilicity of a material. It is also possible to calculate surface free energy of solids and the surface tension of pendant drops. The concept is to measure the angle of a droplet being form on plate solid surface, and the shape of the droplet is determined by the Young's relation [72].

$$0 = \gamma_{SG} - \gamma_{SL} - \gamma_{LG} \cos \theta_C$$

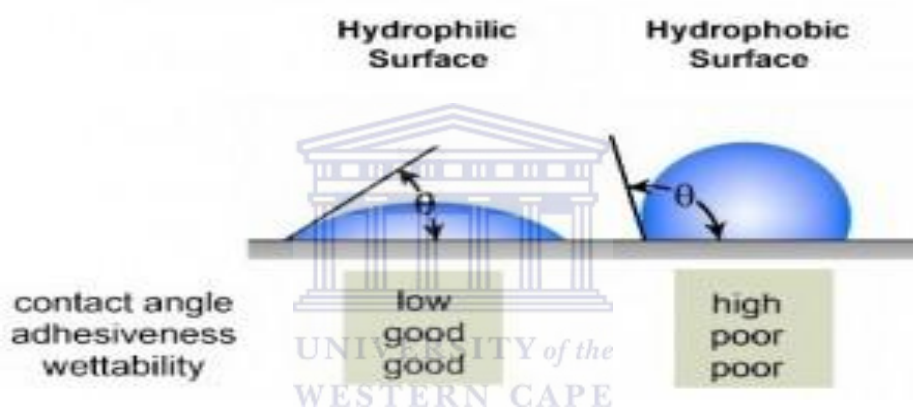
(12)



$\gamma_{SG}$  : interfacial tension between the solid and gas

$\gamma_{SL}$  : Interfacial tension between solid and liquid

$\gamma_{LG}$  : Interfacial tension between liquid and gas



### 3.5.1. Surface tension

Surface tension in a liquid is the forces of attraction between the molecules that make up the liquid or can be thought of force that holds a liquid together [72]. In the absence of other forces, the molecules attraction caused the liquid to coalesce to form spherical droplets. For example a raindrop falls on a freshly waxed body of a car. Surface tension is directly proportional to the presence of polar groups present in a molecule such (e.g. O-H group), the lower the surface tension of a liquid coating, the easier it will be to form a satisfactory wet film onto it [72]. The greater the proportion of polar groups (e.g. O-H groups) in a molecule the stronger the attractive forces between them. Strong attractive forces give rise to a high surface

tension and a tendency to form discrete droplets on a surface rather than wet it evenly. The large proportion of O-H groups in water is responsible for its high surface tension as opposed to alcohols, with their smaller proportion of O-H groups. Surface tension can therefore be quantified in terms of the forces acting on a unit length at the liquid-air interface. The units are dynes per centimetre (dyn/cm) or Newton per metre (Nm<sup>-1</sup>). 1 dyn/cm is equal to 0.001 Nm<sup>-1</sup> or 1 mNm<sup>-1</sup> [72 - 73].

### **3.5.2. Surface energy**

Energy may be defined as the capacity to do work and if we take the example of the average wooden desk top it is difficult to find evidence that it is engaged in any form of work that results in displacement, but it does have inherent potential energy [73]. In other words the surface tension forces that hold the water droplets together have been overcome. It takes energy to overcome the surface tension forces and this energy has to come from somewhere [73]. In fact it comes from the surface of the sample holder and more specifically from the forces that hold the molecules of the desktop material together. Surface energy is quantified in terms of the forces acting on a unit length at the solid-air or the solid-liquid interface. The units of measurement are exactly the same as for surface tension.

### **3.5.3 Contact angle**

Contact angle is a quantitative measure of the wettability of a solid by a liquid. The deliquescent and hydrophobic properties is predicted by the contact angle being measured. If the water contact angle is smaller than 90° it is indication of hydrophilic and if its water contact angle is larger than 90° it is indication of hydrophobic nature of the material. Contact angle was used as the physical method for quantifying the improved hydrophilic nature of hydrogels synthesised.



## 3.6. Membrane performance

### 3.6.1. Performance under hydrodynamic condition (Rotating disk electrode)

Rotating disk electrode (RDE) and cyclic voltammetry (CV) both operate using a three electrode system. The working electrode in (RDE) consistently rotates throughout experiments causing a flux of analyte to the electrode. The disk's rotation is sometimes delineating in terms of angular speed, because the fluid mechanics physical phenomenon is dragged by the spinning disk [84]. The speed of the solution flow will be controlled by the electrode's angular speed. The steady-state current is controlled by mass transport instead of diffusion. This is often the distinction between quiet and agitated experiments like cyclic voltammetry where the steady-state current is restricted by the diffusion of substrate [84].

This can be understood by returning to the concept of the diffusion layer thickness generated due to flux of material to the electrode surface. The rotation speed increases the space that material will diffuse from the surface before being removed by convection [84]. The mass transport restricted current arises from the fact that the system reaches a steady state once the product concentration reaches equilibrium at the surface [85]. We can analyse the variation of the mass transport restricted current as a function of the rotation speed. This was first resolved mathematically by Levich who established the relationship between current and rotation speed for a reversible electron transfer reaction (equation 13). Therefore by plotting Current vs the root of the rotation speed ( $\omega$ ) over a range of scan rates, a straight line may be obtained.

These types of plots will be used to evaluate the reaction kinetics of the reactions where the mass transport of selected model compounds will be investigated.

Rotating disk electrochemistry also allows the investigation of diffusional or flux phenomena under hydrodynamic conditions. It is possible to calculate diffusion coefficients from rotating disk electrochemistry data. Therefore the hydrogel diffusion coefficients may also be evaluated and used as a quantitative measure to assess flux of ions and electrons to the hydrogel interface..

$$i = (0.620) nFAD^{2/3} \omega^{1/2} \nu^{-1/6} C_{\text{analyte}} \quad (13)$$

### 3.6.2. Electrochemical impedance spectroscopic (EIS)

In cyclic voltammetry and other dynamic electro analysis, an applied potential is either constant (potentiostat) or changing (potentiodynamic) when ramped at a constant rate of  $v = dE/dt$  [87]. However, in impedance, a small perturbing potential is applied to the perturbing signal which results in a sinusoidal output signal that is a representative of the magnitude of the impedance of the electrochemical cell and the time lag or lead imposed on the sinusoidal output signal [88-105]. The induced current alternates because the voltage changes in a cyclic manner, and hence the term alternating current (AC).

The term impedance is therefore a measure of the ability of a circuit to resist the flow of an alternating current (AC) [105]. It is synonymous to resistance ( $R$ ) used in direct current (DC), which is defined by Ohm's law as the ratio between voltage ( $E$ ) and current ( $I$ ). Electrochemical impedance spectroscopic is an excellent, non-destructive, accurate and rapid in situ technique for examining processes occurring at the electrode surface. During a controlled-potential EIS experiment, the electrochemical cell is held at equilibrium at a fixed DC

potential, and a small amplitude AC wave form is superimposed on the DC potential to generate a response from the equilibrium position [106].

The response to the applied perturbation, which is generally sinusoidal, can differ in phase and amplitude from the applied signal. This response is measured in terms of the AC impedance or the complex impedance,  $Z^*$  (overall or complete impedance), of the system, which permits analysis of electrode process in relation to diffusion, kinetics, double layer, coupled homogeneous reactions, etc. The complex impedance ( $Z^*$ ) is made up of a resistive or real part  $Z'$ , attributable to resistors (in phase with the applied voltage), and a reactive or imaginary part  $Z''$ , attributable to the contributions of capacitors. This is related to the resistance ( $R$ ), reactance ( $X$ ) and capacitance. The experimental data collected from an impedance experiment is often presented as Nyquist plot of real versus imaginary impedance [106].

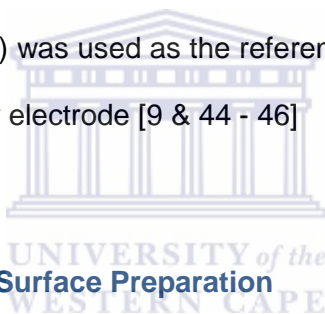
The Nyquist plot of impedance spectra includes a semicircle portion and a linear portion, with the former at higher frequencies corresponding to the electron transfer process and the latter at lower frequencies corresponding to the diffusion process. The electron transfer resistance ( $R_{ct}$ ) at the electrode surface is equal to the semicircle diameter, which can be used to describe the conductivity of the electrode interface [107].

## 3.7. Methodology and experimental

### 3.7.1. Instrumentation

#### 3.7.1.1. Potentiostat Set-up

All electrochemical experiments were performed and recorded with a computer interfaced to a BAS-100/W electrochemical analyser with BAS-100/W software (Bioanalytical Systems, Lafayette, IN, USA), using either cyclic voltammetry (CV), or Oysteryoung square wave voltammetry (OSWV). A conventional three electrode system was employed. The working electrode was a platinum disc electrode Bioanalytical Systems, Lafayette, IN, USA). Silver/silver chloride (Ag/AgCl – 3 M NaCl type) was used as the reference electrode and a platinum wire was used as auxiliary electrode [9 & 44 - 46]



#### 3.7.1.2. Electrode Surface Preparation

Prior to use, platinum and glassy carbon electrodes were polished using aqueous slurries of 1  $\mu\text{m}$ , 0.3  $\mu\text{m}$  and 0.05  $\mu\text{m}$  alumina powder. After thorough rinsing in deionised water followed by acetone, the electrodes were etched for about 5 minutes in concentrated  $\text{H}_2\text{SO}_4$  and rinsed again with copious amounts of deionised water.

The polished electrodes were then cleaned electrochemically by cycling the potential scan between - 200 and + 1200 mV in 2 M HCl at the scan rate of 100  $\text{mV}\cdot\text{s}^{-1}$  until the CV characteristics for a clean Pt or GC electrodes were obtained. The platinum (Pt) counter electrode was regularly cleaned before and after synthesis and in between synthesis and analysis. This involved flaming

the Pt electrode in a Bunsen burner until it was white hot, followed by rinsing with copious quantities of deionised water [56].

### 3.7.2. Materials and reagents

**Polyvinyl alcohol:** PVA of 89,000-98,000 molecular weights, 99+ % hydrolysed was supplied by sigma Aldrich, South Africa cape town with lot number MKBL028IV, Product code 10001444119 this product was used as received from the supplier without any modification and was stored at room temperature.

**Polysulfone:** Polysulfone (MW = 35.000, 0.2%w/v in CH<sub>3</sub>Cl<sub>3</sub> 25°C) was supplied by sigma Aldrich, South Africa Cape Town (product code 428302-100g). This product was used as received from the supplier without any modification and stored at room temperature.

**Glutaraldehyde:** The cross linker glutaraldehyde (GA) or pentane 1, 5 dial solutions Grade I, 25% in water, total impurities ≤ 0, 05% free of carboxylic acid (product code 1001381318) was supplied by Sigma Aldrich, South Africa Cape Town. GA was stored in the freezer at a temperature of below -25°C

**N,N- dimethylacetamide (DMAc):** DMAc of a molecular formula C<sub>4</sub>H<sub>9</sub>NO, (product code 100990279), purity ≥ 99.5% (G.C) was supplied by Sigma Aldrich South Africa cape town.

**Hydrochloric acid:** 32% HCl product was supplied by Seabreeze suppliers CC, with batch number 508098 in which 2M HCl was prepared out of the 32% by dilution using the following formula.

$$C_1 \times V_1 = C_2 \times V_2 \quad (14)$$

The concentration of the 32% could be calculated from the following

$$C = \frac{\text{Purity} \times \text{density} \times 10}{Mw} \quad (15)$$

### 3.7.3. Synthesis of Polysulfone –polyvinyl alcohol hydrogel

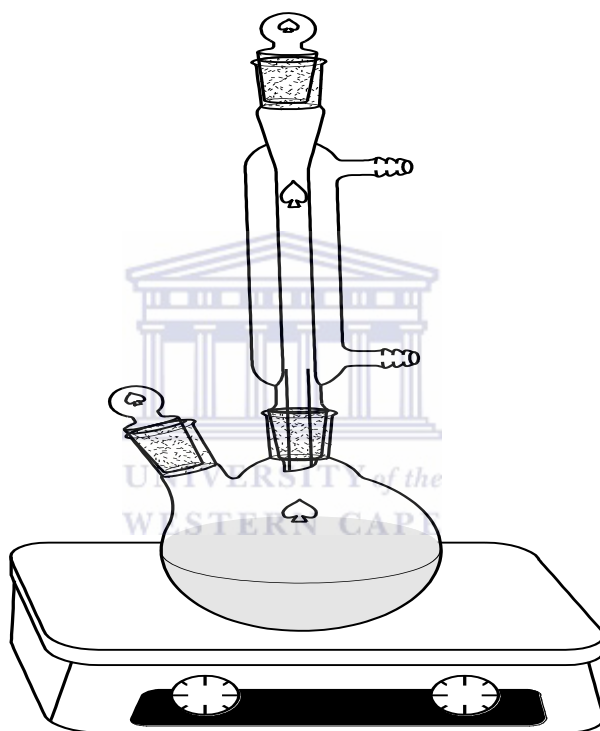


**Figure 3.4:** Reflux reaction set up

To the reflux equipment setup, a temperature control device was attached for temperature moderation. The presence of the controller device was to avoid reaching polyvinyl alcohol boiling point. Polysulfone-PVA hydrogels was synthesised by dissolving 0,4421g of polysulfone crystal into 50 mL of N,N-dimethylacetamide (DMAc) to produce 0.0554 M PSF-solution after 1 hour of sonication. 5 mL of this solution was transferred to a round bottom flask, to

which 2,5895g of PVA was added. To the mixture 1 mL glutaraldehyde cross-linker solution was added followed by the catalyst in order to speed up the reaction during the crosslinking process. An excess of acid was required for protonation and reduction of the aldehyde into alcohol. 1 mL of 2 M HCl catalyst was added the reflux mixture and the mixture was allowed to for 3 hours at 75°C with constant stirring.

After three hours the mixture was stored at a room temperature for 10 days in order to ensure completeness of cross-linking reaction. The cross linking of PVA and PSF was controlled at three different ratios to evaluate the effect of the PSF contribution i.e. 25:75, 50:50 and 75:25. The crosslinked polymer composites produced three unique hydrogel materials, which were evaluated for the separation of selected small organic molecules, under hydrodynamic conditions, using rotating disk electrochemistry.

#### **3.7.3.1. Hydrogel thin films prepared by drop coating method**

Polysulfone – polyvinyl alcohol hydrogels was physical adsorbed onto the platinum electrode (Pt/E) by drop coating 10 µl of the hydrogels onto the Pt/E. For each experiment the same amount of 10 µl of the hydrogels of the same concentration was drop coated and dried at a room temperature for 24 hours to allow the interaction between the hydrogels and the surface of the electrode for a good conductivity.

#### **3.7.3.2. Cyclic voltammetry analysis of hydrogels**

Cyclic voltammetry (CV) was performed at a normal scan rate of 100 mV.s<sup>-1</sup> to study the redox behaviour of hydrogels by applying potential scan between -200 mV and + 1200 mV (vs. Ag/AgCl). Cyclic voltammograms were obtained in the absence and the presence of model organic compounds (tannic acid and alginic acid) respectively.

Sequential 10  $\mu\text{L}$  aliquots of 0.2 M tannic and 0.05 M alginic acid were added to 1 mL of 2 M HCl solution, degassed with argon and a blanket of gas was kept for few seconds. The solution was stirred after each addition of tannic or alginic acid. This was done to ensure homogeneity of the solution before measurements were taken.

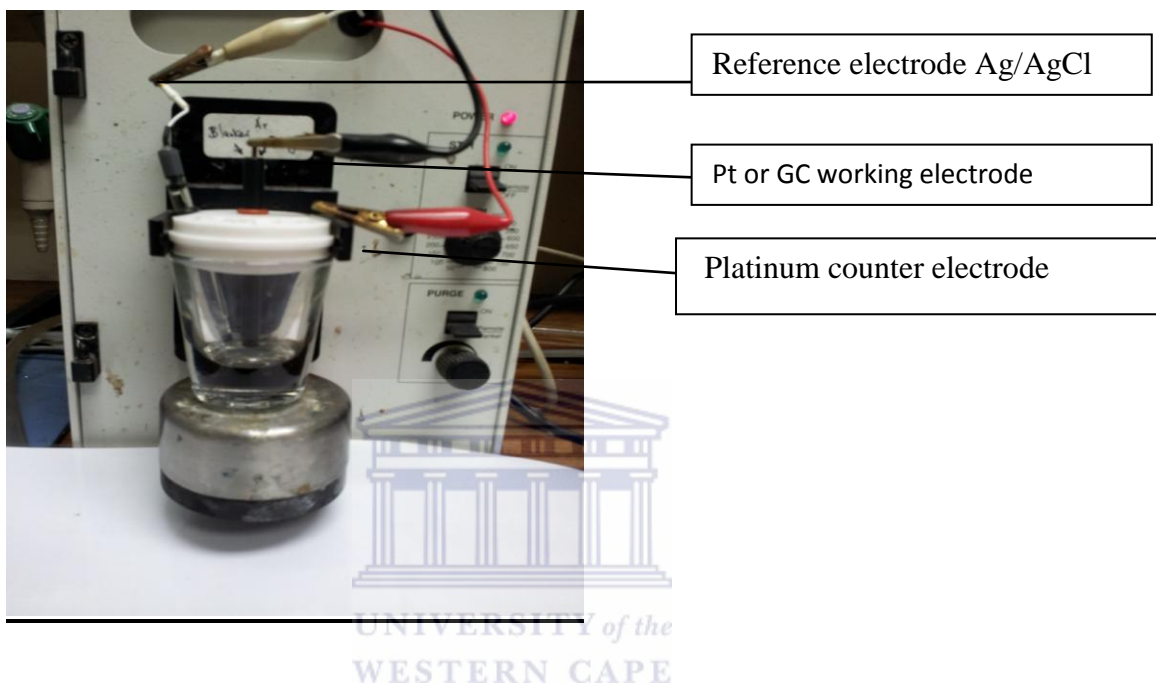


**Figure 3.5:** Three electrode electrochemical cell

### 3.7.3.3. Square Wave Voltammetry Analysis of PSF-PVA hydrogels

Osteryoung square wave voltammetry (OSWV) was performed immediately after cyclic voltammetry analysis in 1 mL of 2 M HCl solution, containing different concentrations of tannic and alginic acid under normal conditions. The anodic difference square wave voltammogram (SWV) was collected in an oxidation direction only by applying a linear potential scan between -200 mV to 1200 mV (vs. Ag/AgCl), at a frequency of 10 Hz, and a square wave amplitude of 10 mV. The SWV was obtained in the absence and the presence of tannic and alginic acid.



The Instrumental method detailed in this chapter was used to gain information about the hydrogel formal potentials and electrochemical mechanistic details. Tannic acid was selected to represent polyphenol and alginic acid was selected to represent polysaccharides. These are two main categories of compounds responsible for biofouling in nanofiltration.



# Chapter 4

## Result and Discussions

This section of the work provides evidence of the proposed polysulfone-hydrogels mechanisms. The proposed mechanism involve three steps, firstly protonation of alcoholic oxygen, secondly reduction of aldehyde into primary alcohol followed by crosslinking through the oxygen functionality.

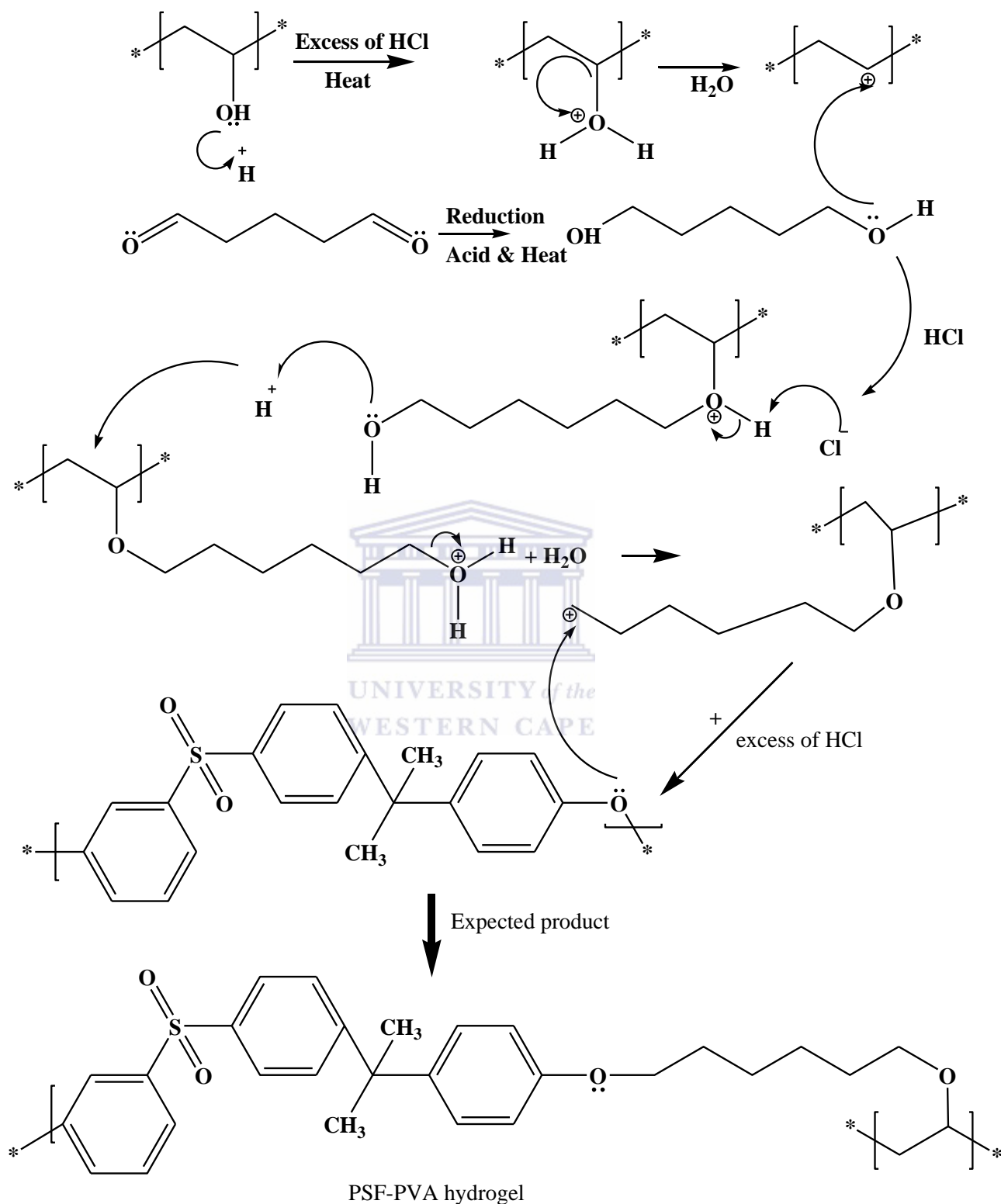
The detailed steps of the proposed mechanism may be summarised as follows:

Steps 1: Protonation of the alcoholic oxygen in PVA makes it a better leaving group. This step is very fast and reversible [60]. The lone pairs of electron on the oxygen make it a Lewis base. Cleavage of the C-O bond allows for the loss of the good leaving group as a neutral water molecule, leaving behind a primary carbonation intermediate which is very reactive. This step is the rate determining step (bond breaking endothermic).

Steps 2: In general reduction of an aldehyde leads to a primary alcohol. [60] Reduction of glutaraldehyde essentially involves the addition of a hydrogen atom to each end of the carbon-oxygen double bond to form an alcohol (1, 5 pentanol). This will further undergo protonation of alcoholic oxygen to form a primary carbocation.

Steps 3: Attack of the primary carbocation to an available oxygen site (ester or sulphone oxygen) to produce polysulfone /PVA hydrogels. (Scheme 1)

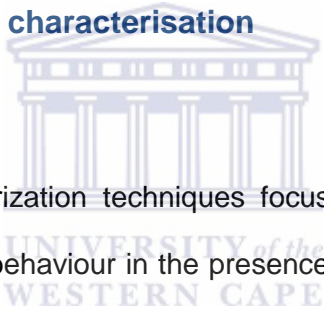
## PSF-PVA Hydrogel composite Mechanism of formation



Scheme 1 Proposed mechanism of PSF hydrogels formation

From the proposed mechanism some questions may arise i.e.: why ether oxygen is more favoured than sulphur oxygen. We know from literature that the intermediate primary carbocation is more reactive than secondary and tertiary carbocation. We also know that sulphur is more electron negative compare to carbon and will pull electrons toward it. However both oxygen in ether and sulphone are in a dipole moment. Attachment of carbocation to sulphur oxygen will result in instability of the structure, and cleavage of the ionic benzene ring is not favoured in these conditions. Therefore it is more likely that the carbocation would attack the ether oxygen, hence we propose that ether oxygen should be the more favoured position for linkage.

#### 4.1. Electrochemical characterisation



Electrochemical characterization techniques focused on understanding PVA, PSF and PSF hydrogel redox behaviour in the presence and absence of target molecules before it fouls the membrane. Polyvinyl alcohol membrane film was prepared by dissolving 2.59 g of PVA in 50 mL of deionised water, and the reaction mixture was sonicated in a water bath until a clear homogenous solution were obtained. For a thin film, 10  $\mu\text{L}$  aliquot of the solution was drop coated onto a glassy carbon electrode (GCE) with a micropipette and left to dry overnight before analysis. Electrochemical characterization was performed by cycling the potential scan between - 200 and + 1200 mV in 2 mL of 2 M HCl, at the scan rate range from 10 to 300  $\text{mV}\cdot\text{s}^{-1}$ . The platinum (Pt) counter electrode was regularly cleaned before and after synthesis and in between synthesis and analysis.

#### 4.1.1. Cyclic voltammetry of polyvinyl alcohol on GC electrode

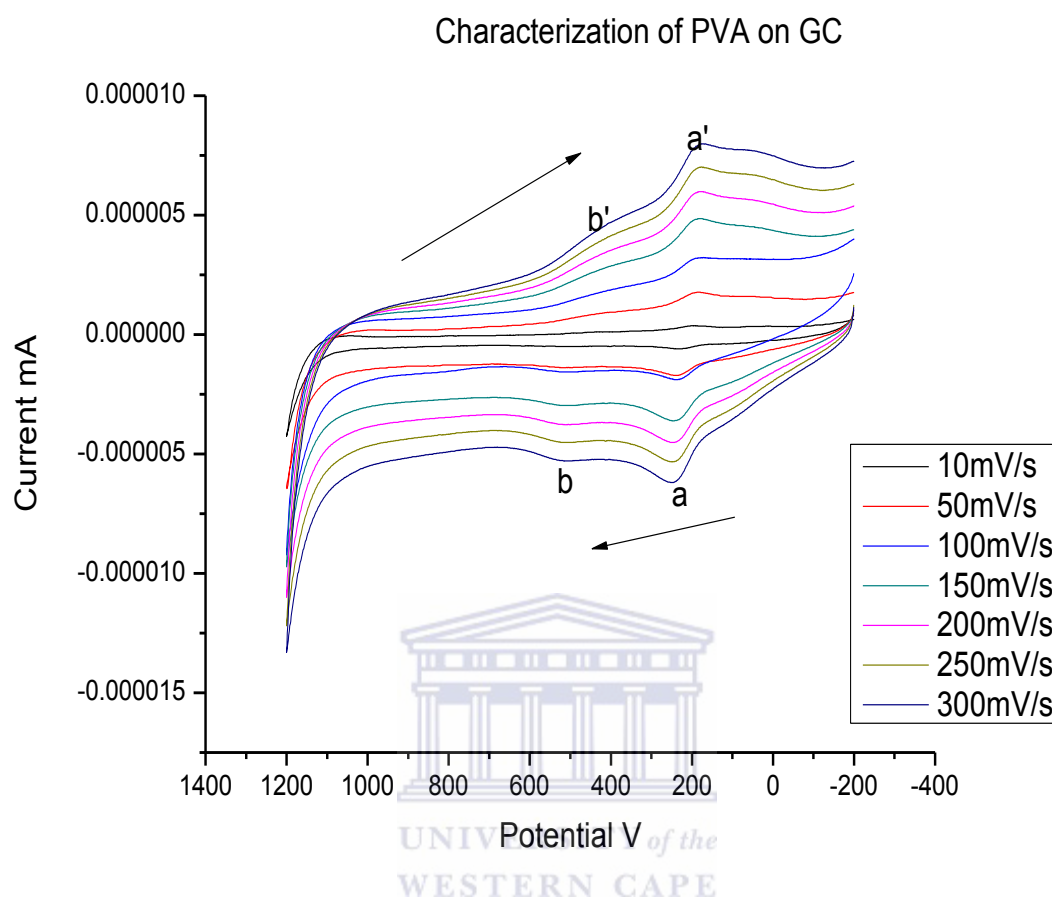
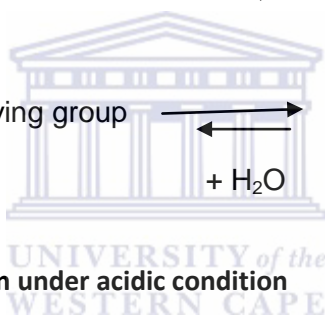
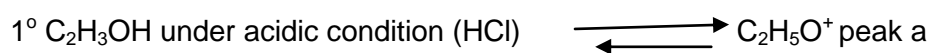


**Figure 4.1:** Cyclic voltammetry of PVA in 1M HCl at different scan rates

The starting material PVA and PSF as individual polymers was characterised electrochemically and the influence of scan rate on peak current and peak potential was evaluated (Figure 4.1) for PVA. Cyclic voltammogram showed an increase in the cathodic and anodic peak currents as a function of increase scan rate, in a near linear relationship. According to equation (5) the number of electrons transferred was calculated to be 1, for a surface confined electrochemical process [64].

The redox peaks **a** and **b** in Figure 4.1 result from the protonation of the alcoholic oxygen in PVA. This step is very fast and reversible [92]. In the presence of catalyst and under applied potential PVA becomes protonated to generate a water molecule. As a leaving group, it will have its own electrochemistry, and produces peak **a**. Once the H<sub>2</sub>O molecule is lost, a carbocation is formed with its own unique electrochemistry producing peak **b**. Peak **b** is smaller than **a** due to the fact that carbocation is short lived unstable species which will undergoes stabilisation and return to the starting material. Therefore the redox peak **a**, **a'** and **b**, **b'** are due to electrochemical protonation of PVA and carbocation formation (scheme 2).



**Scheme 2. PVA reaction under acidic condition**

The choice of peak **a** is based on the proposed mechanism, where electron protonation of alcoholic oxygen is the rate determining step. Therefore all results reported in this work are based on the rate determining step peak **a** and **a'**

The Table 4.1 provide the electrochemical parameters calculated from scan rate dependent CV data. Peaks **a** and **b** are anodic, while peaks **a'** and **b'** are for the cathodic processes. The Randles Sevcik equation (5) was used to determine the rate of electron transport (*De*) within the polymer layer. The electron transport diffusion coefficient, *De*, was found to be slightly smaller for oxidation ( $1.45002 \times 10^{-9} \text{ Cm}^2/\text{s}$ ) compared to reduction ( $3.2654 \times 10^{-9} \text{ Cm}^2/\text{s}$ ) with the formal potential for the redox couple **a/ a'** determined as 211mV (vs Ag/AgCl).

**Table 4.1:** *The effect of scan rate on anodic and cathodic peak current and peak potentials of PVA in CVs for different scan rates in 2 M HCl Solution.*

Scan rate $\nu$ mV/s	Square root of scan rate $\nu^{1/2}$ mV/s $^{1/2}$	Anodic peak current $I_{pa}$ mA (peak a)	Cathodic peak current $I_{pc}$ mA (peak a')	Anodic peak potential $E_{pa}$ mV (peak a)	Cathodic peak potential $E_{pc}$ mV (peak a')	Peak potential separation potential $\Delta E^{\circ}$	$I_{pc}/I_{pa}$ (peak a/a')
10	3.16	5.98e-7	3.58e-7	205.9	226.50	20.60	0.61
50	7.07	1.72e-6	1.77e-6	197.0	230.70	33.70	1.03
100	10.00	1.85e-6	3.10e-6	190.0	232.10	42.10	1.68
150	12.25	3.63e-6	4.88e-6	184.4	244.70	60.30	1.35
200	14.14	4.60e-6	5.96e-6	187.2	247.50	60.30	1.29
250	15.81	5.31e-6	6.94e-6	184.47	251.70	67.00	1.31
300	17.81	6.26e-6	7.96e-6	183.0	250.30	67.30	1.27

These results in Table 4.1 were used to plot a graph of change in current vs. root of scan rate ( $\nu$ ) as shown in Figure 4.2. A straight line was obtained, with high correlation coefficient which confirmed diffusion controlled behaviour at the interface according to the Randles-Sevcik equation.

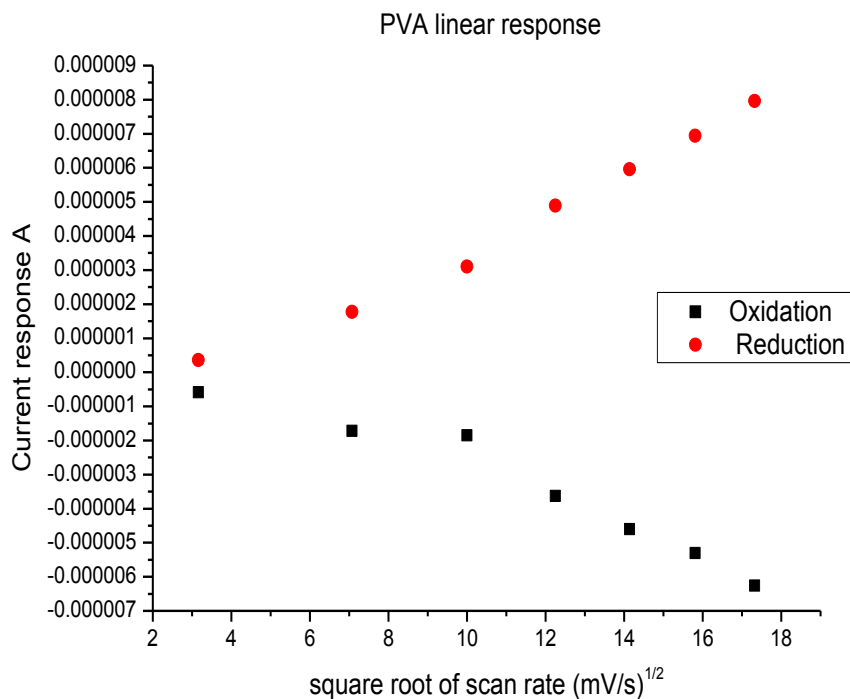


**Figure 4.2:** Graph of anodic and cathodic peak current ( $I_p$ ) vs. square root of scan rate ( $v^{1/2}$ ) for polyvinyl alcohol film in 2 M HCl solution at different scan rates for peak a and a'

The results in Table 4.1 further indicate that the peak potential separation, anodic and cathodic peak current and anodic and cathodic peak ratio increased relatively with the scan rate. The trends observed in this table are indicative of a reversible system [44].

#### 4.1.2. Cyclic voltammetry of Polysulfone on GC electrode

Polysulfone membrane film was prepared by dissolving 0.44 g of polysulfone in 50 mL N, N-dimethyl acetamide and the action mixture was sonicated in a water bath until a clear homogenous casting suspension was obtained. For a thin film, 10  $\mu$ L aliquot of the solution was drop coated onto a glassy carbon electrode (GCE) with a micropipette and left to dry overnight before analysis.



Electrochemical characterization was performed by cycling the potential between -200 and +1200 mV in 2 mL of 2 M HCl, at the scan rate range from 10 to 300 mV.s<sup>-1</sup> (figure 4.3). The platinum (Pt) counter electrode was regularly cleaned before and after synthesis.

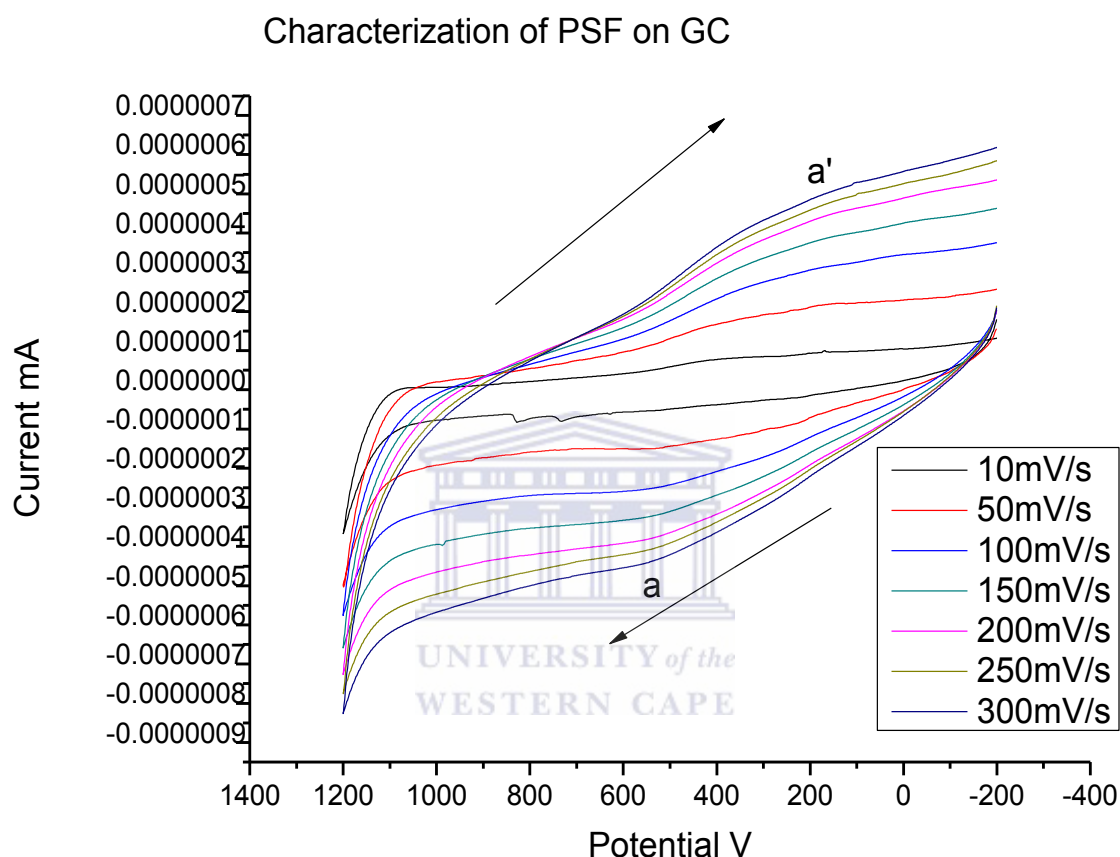


**Figure 4.3:** Cyclic voltammetry of PSF in 1M HCl at different scan rates

Cyclic voltammogram showed a redox peak resulting from electron delocalization and the growth of a semi conducting polysulfone film on the electrode as the scan rates increased. The separation of oxidation and reduction current showed a near square shaped voltammogram indicative of the capacitive nature of polysulfone. To date, not much has been reported on polysulfone electrochemistry. However from organic chemistry considerations, the redox peaks observed (Figure 4.3) were ascribed to the delocalisation of the double bonds. Strong resonance delocalization of the lone pairs

of electrons on ester oxygen throughout the structure occurs, which resulted in the redox peak observed as we increased the scan rate [60].

**Table 4.2:** *The effect of scan rate on anodic and cathodic peak current and peak potentials for PSF in CVs for different scan rates in 2 M HCl Solution.*

Scan rate, mV/s	Square root of scan rate, mV/s <sup>1/2</sup>	Anodic peak current I <sub>pa</sub> , mA (peak a)	Cathodic peak current I <sub>pc</sub> , mA (peak a')	Anodic peak potential E <sub>pa</sub> , mV (peak a)	Cathodic peak potential E <sub>pc</sub> , mV (peak a')	Peak potential separation potential, ΔE°	I <sub>pc</sub> /I <sub>pa</sub>
10	3.16	-2.29e-8	9.96e-8	413.00	495.80	82.80	0.23
50	7.07	-8.72e-8	2.29e-7	392.20	511.20	119.00	0.38
100	10.00	-1.41e-7	3.16e-7	351.00	528.10	177.10	0.46
150	12.25	-1.76e-7	3.94e-7	316.20	543.50	227.30	0.47
200	14.14	-1.99e-7	4.55e-7	288.20	550.50	262.30	0.47
250	15.81	-2.25e-7	5.15e-7	236.30	557.50	321.20	0.46
300	17.81	-2.40e-7	5.36e-7	222.20	561.70	339.50	0.48

For the peak potential separation ( $\Delta E_p$ ) reported in Table 4.2, different values were obtained as a function of scan rate. At faster scan rate  $\Delta E_p$  was found to be 339.5 mV whereas at slower scan rates it was 82.8 mV. The I<sub>pa</sub>/I<sub>pc</sub> ratio centred around 0.4 which was indicative of quasi reversible electrochemistry. Formal potential was calculated to be 439.6 mV (vs Ag/AgCl, which is twice that of polyvinyl alcohol and within the theoretical range reported in literature [60].

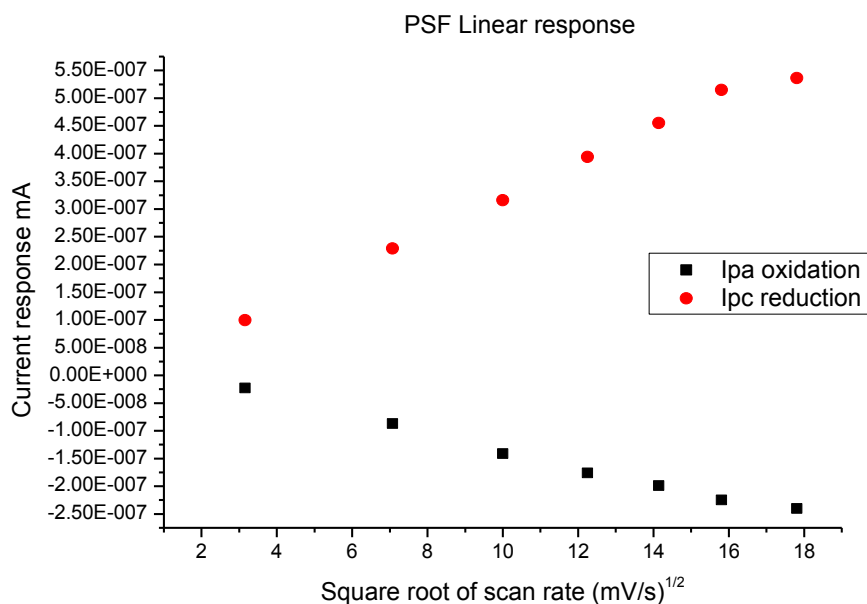


**Figure 4.4:** Graph of anodic and cathodic peak current ( $I_p$ ) vs. square root of scan rate ( $v^{1/2}$ ) for polysulfone film in 2 M HCl solution at different scan rates.

The calculation of diffusion coefficient from oxidation current ( $3.625 \times 10^{-12} \text{ Cm}^2/\text{s}$ ) was observed to be lower than diffusion coefficient from reduction current ( $8.15635 \times 10^{-12} \text{ Cm}^2/\text{s}$ ), indicating that the kinetics of the system favour the reduced state.

#### 4.1.3. Cyclic voltammetry of Polysulfone-polyvinyl alcohol (PSF-PVA) Hydrogel on GC electrode

Polysulfone-polyvinyl alcohol hydrogels was synthesised as detailed previously and prepared as thin films by drop coating 10  $\mu\text{L}$  aliquot of the hydrogel solution onto a glassy carbon electrode (GCE) with a micropipette and leaving to dry overnight before analysis. Cyclic voltammetry was performed by cycling the potential range between - 200 and + 1200 mV in 2 mL of 2 M HCl, at scan rates from 10 to 300  $\text{mVs}^{-1}$ . The cyclic voltammetry and the square Wave voltammetry were evaluated for the effect of PSF contribution (i.e. 25:75, 50:50 and 75:25) to the overall hydrogel performance. Diffusion coefficient and the formal potential were calculated as before.

### 4.1.3.1. Cyclic voltammetry of PSF-PVA hydrogels

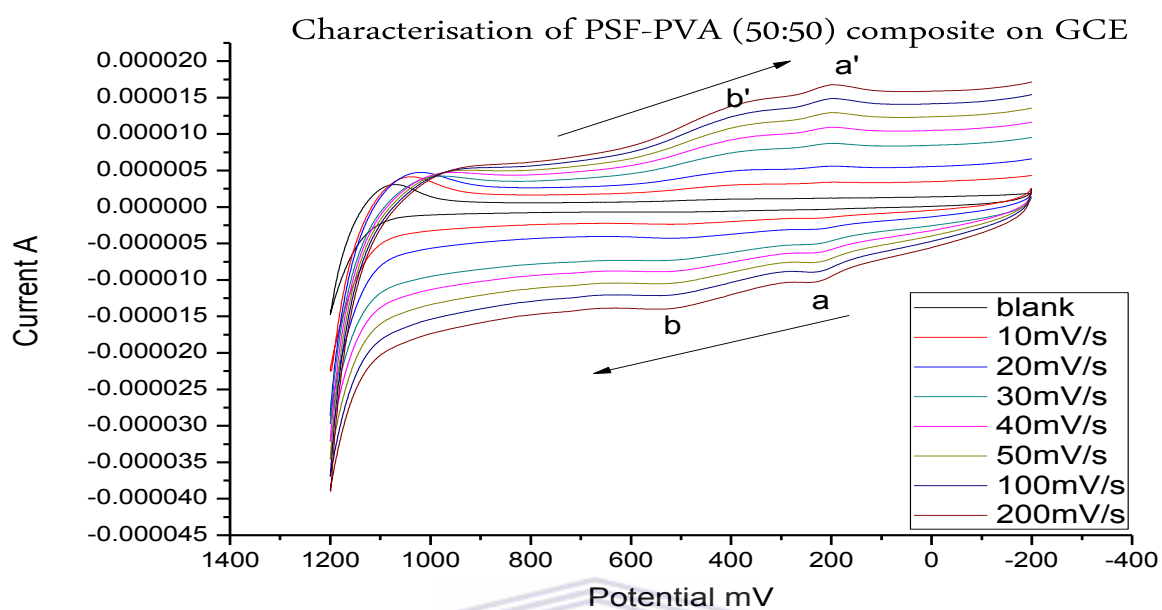


Figure 4.5.(a): Cyclic voltammetry of PSF-PVA (50:50) in 2 M HCl at different scan rates

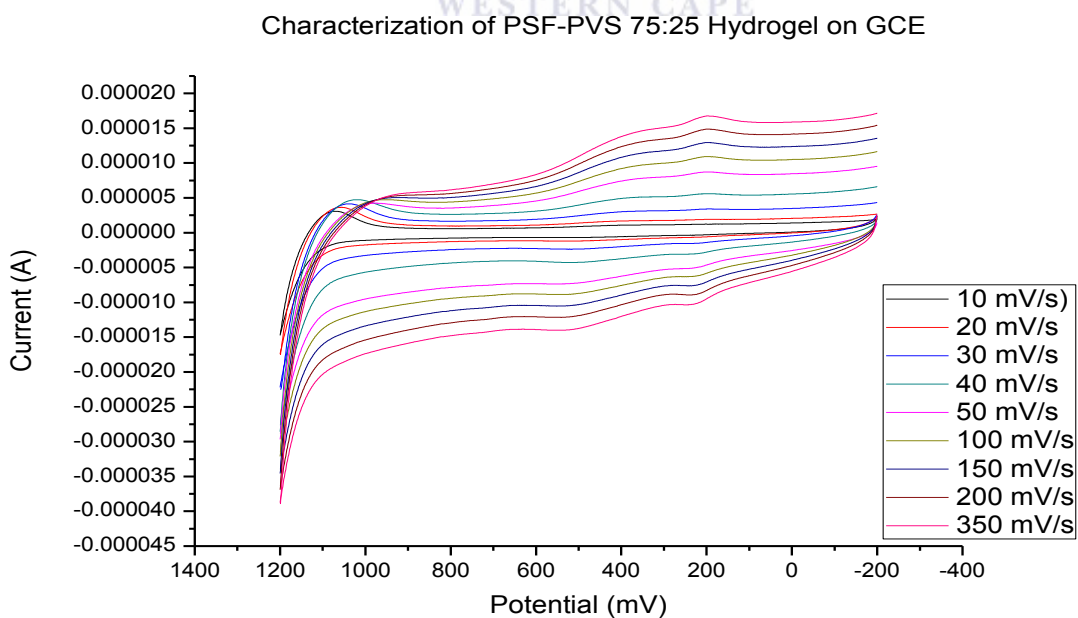
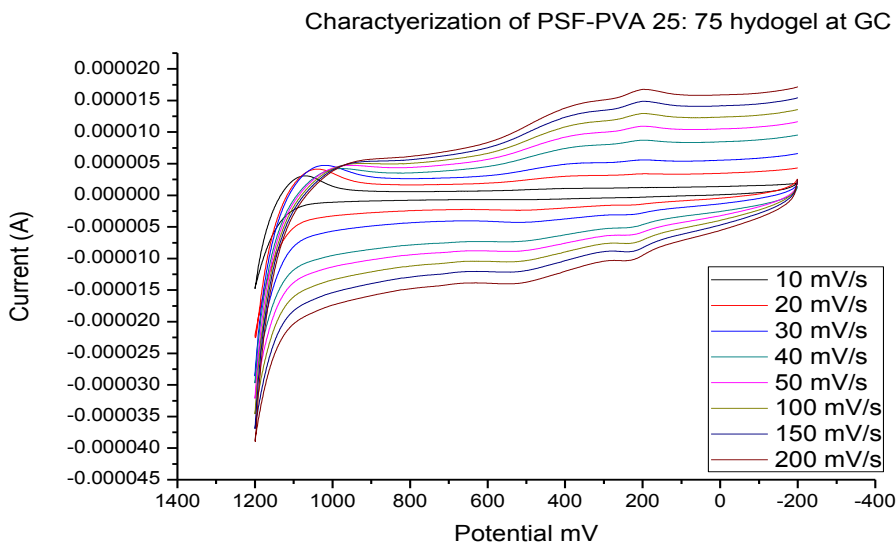
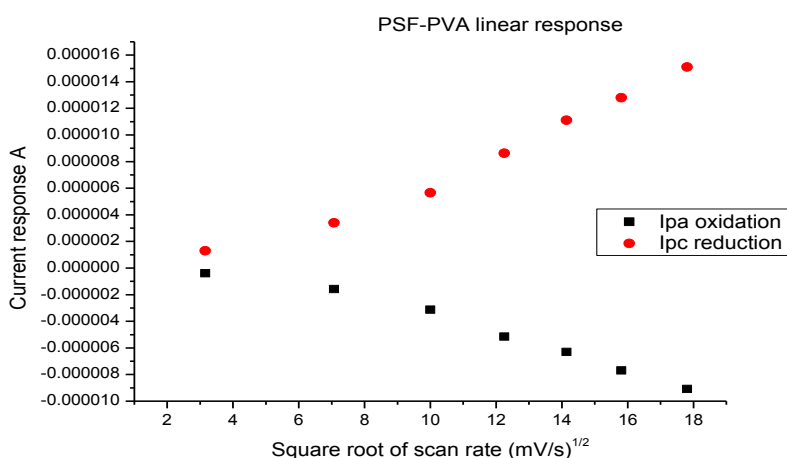


Figure 4.5. (b): Cyclic voltammetry of PSF-PVA (75:25) in 2 M HCl at different scan rates



**Figure 4.5. (c): Cyclic voltammetry of PSF-PVA (25:75) in 2 M HCl at different scan rates**

The redox peaks **a**, **a'** and **b**, **b'** observed were similar to the electrochemical performance observed in PVA. No additional peaks were observed due to the presence of polysulfone, but the increased peak separation was ascribed to the presence of polysulfone. All results reported for the hydrogel systems were based on the performance of the redox couple **a/a'** which was identified as the rate determining step (Figure 4.5 a, b, c).



**Figure 4.5 (d): Graph of anodic and cathodic peak current ( $I_p$ ) vs. square root of scan rate ( $v^{1/2}$ ) for PSF-PVA Hydrogel in 1 M HCl solution at different scan rates**

**Table 4.3:** *The effect of scan rate on anodic and cathodic peak current and peak potentials for PSF-PVA hydrogel in CVs for different scan rates in 2 M HCl Solution.*

Scan rate $v$ mV/s	Square root of scan rate $v^{1/2}$ mV/s <sup>1/2</sup>	Anodic peak current $I_{pa}$ A (peak a)	Cathodic peak current $I_{pc}$ A (peak a')	Anodic peak potential $E_{pa}$ mV (peak a)	Cathodic peak potential $E_{pc}$ mV (peak a')	Formal potential $\Delta E^\circ$	$I_{pc}/I_{pa}$
10	3.16	-3.88e-7	1.30e-6	453.70	413.00	-40.70	3.34
50	7.07	-1.58e-6	3.40e-6	436.90	431.30	-5.60	2.15
100	10.00	-3.12e-6	5.65e-6	407.40	455.10	47.70	1.81
150	12.25	-5.15e-6	8.62e-6	382.20	476.20	94.00	1.67
200	14.14	-6.30e-6	1.11e-5	369.50	486.00	116.50	1.75
250	15.81	-7.70e-6	1.28e-5	349.90	500.00	150.10	1.67
300	17.81	-9.09e-6	1.51e-5	340.10	515.40	175.30	1.66

Scan rate dependent cyclic voltammetry or current behaviours in cyclic voltammetry was used to predict the capacitance nature of the starting material, and of the proposed structure PSF-PVA hydrogels. According to the block shape curves and peaks separation observed between the three cyclic voltammograms (Figure 4.1, 4.3 and 4.5.). So there is a change in current which indicate the formation of a new material.

**Table 4.4:** Comparison of PSF, PVA and PSF hydrogels at GC electrode in 2 M HCl

Membrane	Diffusion coefficient (Cm <sup>2</sup> /s)		Formal potential (mV) ΔE°	I <sub>pc</sub> /I <sub>pa</sub>
	Oxidation	Reduction		
PSF	3.63e <sup>-12</sup>	8.16e <sup>-12</sup>	439.60	0.46
PVA	1.45e <sup>-9</sup>	3.26e <sup>-9</sup>	211.00	1.68
PSF/PVA 50:50	3.26e <sup>-11</sup>	9.06e <sup>-9</sup>	431.25	1.81
PSF/PVA 75:25	6.35e <sup>-10</sup>	9.85e <sup>-8</sup>	575.85	1.52
PSF/PVA 25:75	8.54e <sup>-10</sup>	9.46e <sup>-8</sup>	410.50	1.84

It is evident from the diffusion coefficient calculations that the PVA strongly improves the electron transport efficiency in all the cross linked hydrogel systems. The diffusion coefficient based on the reduction current was improved from 10<sup>-12</sup> to 10<sup>-8</sup> Cm<sup>2</sup>.s<sup>-1</sup> which is largely due to the influence of PVA electron mobility characteristics. The formal potential for the a/a' redox couple in all three hydrogels (~470 mV vs Ag/AgCl) on the other hand, showed the characteristic behaviour of the PSF electrochemical observed.

The electrodynamic parameters therefore serve to confirm the incorporation of PVA and PSF into the new hydrogel materials. The ratio control of starting polymers had a significant effect on the formal potential of the resultant hydrogel (standard deviation STD = 73.5%, n=3) but the diffusion coefficients of the three hydrogels were not significantly different (STD = 16.5 %, n=3). A higher degree of PSF in the starting ratio resulted in a hydrogel with formal potential at least 100 mV more positive, than any other hydrogel or the respective starting materials. Energy efficient catalytic systems usually benefit from lower formal potentials.

Polysulfone, polyvinyl alcohol and PSF hydrogels in 2 M HCl showed linear response with an increase in current as scan rates increase, clearly confirmed the diffusional transport of the analyte to the film surface. The linear response was used to calculate the diffusion coefficient from the Randles- Sevcik equation (16).

$$i_p = 2.69 \times 10^5 n^{3/2} A D^{1/2} C v^{1/2} \quad (16)$$

$$\text{Slope} = (2.69 \times 10^5) \times n^{3/2} \times A \times C \times D^{1/2} \quad (17)$$

Diffusion coefficient could then clearly be interpreted as measurement of ions and electrons across a concentration gradient in solution. From diffusion coefficients obtained for the three hydrogels it was evident ionic mobility was not impaired by the introduction of hydrophobic PSF, but that the cross linking chemistry and PVA electronics enhanced the electron mobility and ion diffusion in the hydrogel materials. Crosslinked PSF with conductive polymer such as PVA shows an improved in polysulfone conductivity.



## 4.2. Hydrogel Ageing

Hydrogel Ageing could be defined as the accumulation of changes in the performance of hydrogels over time. Therefore its stability over time was, assessed using, diffusion coefficients as the indicating parameter. Thin films of the hydrogels were prepared as before from aliquots of synthesised hydrogel which was left to age in the absence of stirring or heating. Diffusion coefficients were calculated from the slope of Randles-Sevcik plots, for hydrogel thin films prepared every day, over a period of 10 days (Table 4.5)

**Table 4.5:** *Oxidative and reductive diffusion coefficient of PSF-PVA at GC on different days*

<b>Number of Hours</b>	<b>Oxidative diffusion coefficient Cm<sup>2</sup>/s</b>	<b>Reductive diffusion coefficient Cm<sup>2</sup>/s</b>
<b>24</b>	3.26 e-11	9.06 e-11
<b>48</b>	3.63 e-12	3.63 e-12
<b>72</b>	2.27 e-11	5.85 e-11
<b>96</b>	8.16 e-12	1.45 e-11
<b>120</b>	8.16 e-12	1.45 e-11
<b>144</b>	3.63 e-12	1.45 e-11
<b>168</b>	8.16 e-12	1.80 e-11
<b>192</b>	3.63 e-12	1.45 e-11

## Hydrogel stability

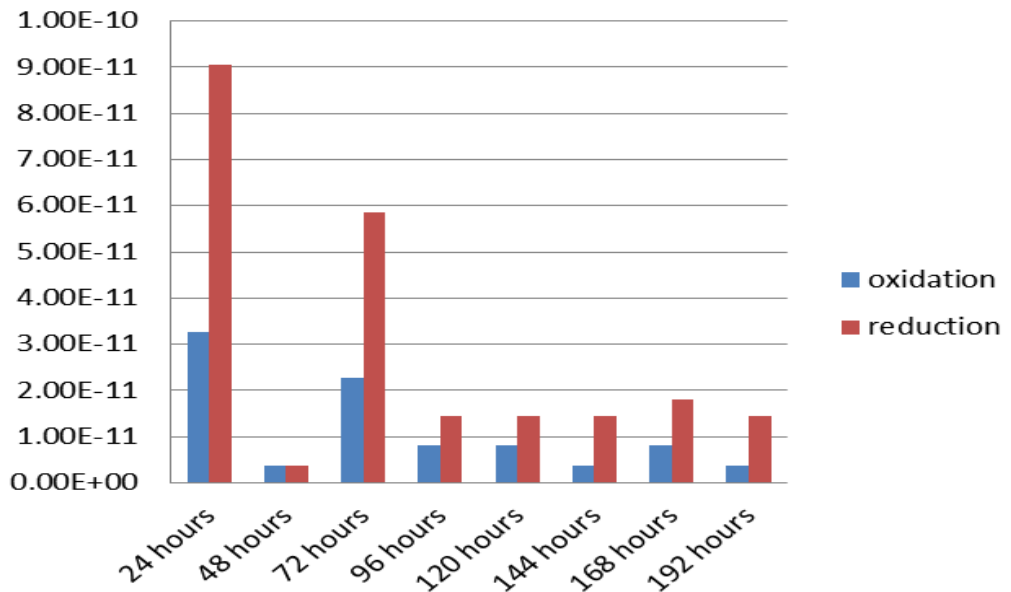


Figure 4.6: Variation of diffusion coefficient of GCE based on different number of day

This process was performed for a period of 10 days until a stable diffusion coefficient was observed (Figure 4.6). It was concluded that the complete cross-linking between the polymers occurs after 10 days meaning that after synthesis the hydrogel should be allowed to stabilise under normal condition of temperature and pressure for ten days.

### 4.3. Spectroscopic characterisation

#### 4.3.1. Fourier Transform Infrared Spectroscopic (FTIR) Characterisation

For FTIR analysis, a small portion of the hydrogel was placed between two filter papers and a physical force was applied to it for dryness. The hydrogel was then dried at room temperature for 24 hours and then compressed as a KBr disk, prepared by grinding approximately 1% mixture of a solid sample in KBr using a hydraulic press. PVA and PSF were also analysed separately (Figure 4.7 and 4.8). All the characteristic functional groups were present in both PSF and PVA spectra. The spectrum of the PSF-PVA hydrogels confirmed the cross-linking of the two polymers by the presence of both functional groups found in PSF and PVA with a band C-H at  $3125\text{ Cm}^{-1}$ , C=C at  $1800\text{ Cm}^{-1}$ , SO<sub>2</sub> at  $1300\text{Cm}^{-1}$  and C-C at  $1100\text{ Cm}^{-1}$ . The absence of OH groups from PVA was interpreted as evidence of its involvement in crosslinking (Figure 4.10,11 & 12) [62, 69 - 71].

**Table 4.6:** *Fourier transform Infrared peaks assignment*

Functional groups	Wavenumbers $\text{Cm}^{-1}$	Bond types
C=C	1600- 1500	In aromatic ring
C-C	1200-1600	
C-H	3000-2800	Stretch
C-H	1500-1400	Bend
OH	3600-2400	
SO <sub>2</sub>	1150-1300	

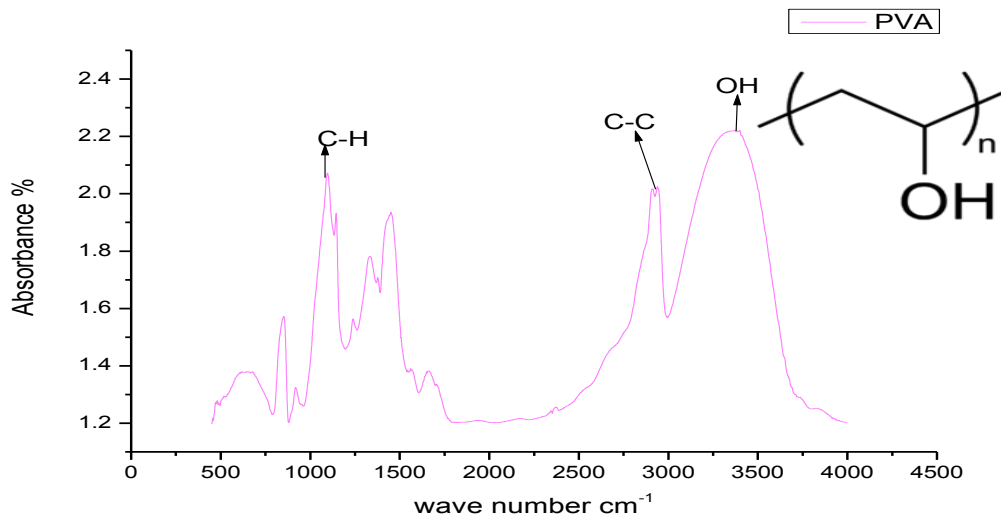


Figure 4.7: Spectrum of PVA on its own

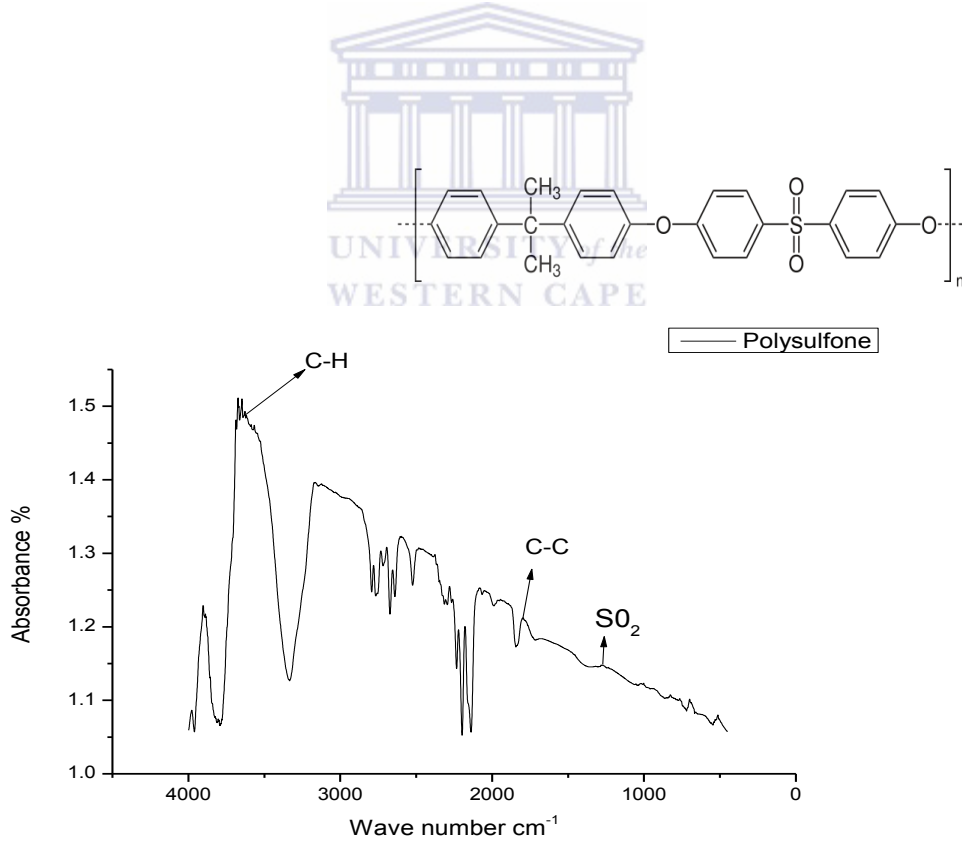
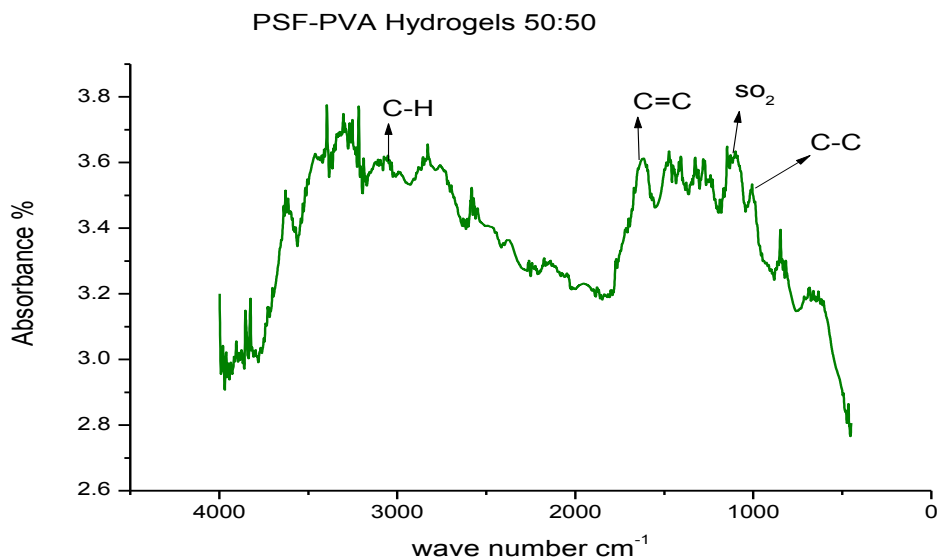
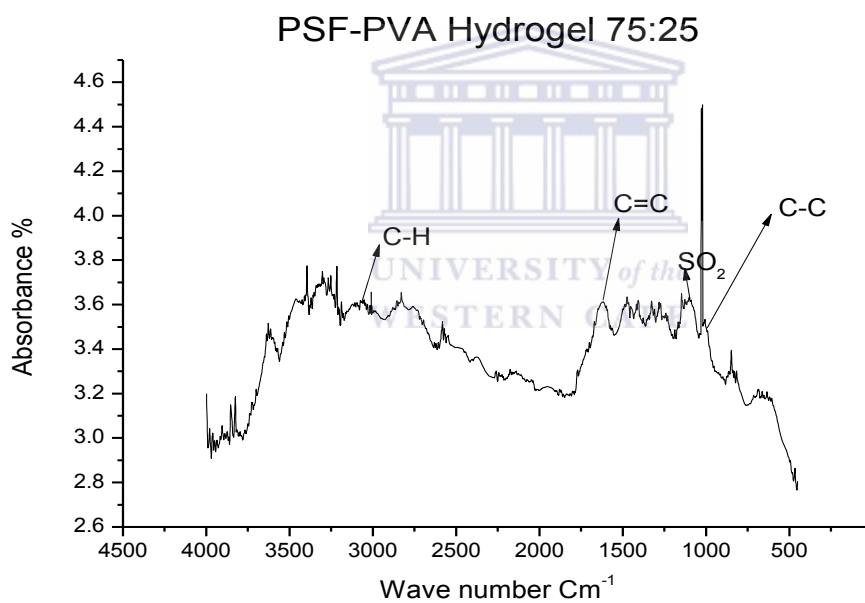


Figure 4.8: Spectrum of PSF on its own



**Figure 4.9:** Spectrum of PSF-PVA hydrogel 50:50



**Figure 4.10:** Spectrum of PSF-PVA hydrogel 75:25

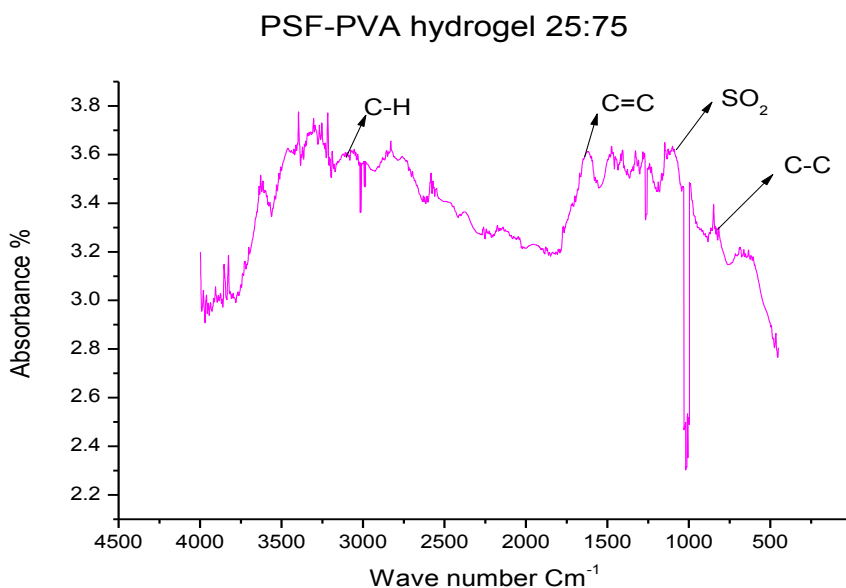


**Figure 4.11: Spectrum of PSF-PVA hydrogel 25:75**

From the proposed mechanism the two possibilities were identified for the position at which carbocation attachment could occur either at the ester oxygen, or sulphur oxygen. Fourier transform infrared analysis provides some evidence of point of linkage. The spectra of the PSF-PVA hydrogels confirmed cross-linking of the two polymers by the absence C-O-C which is involved in cross linking (Figure 4.9,10 & 11) [71]. This indicates that the ester oxygen was the site for cross linking to form the hydrogel. The sulphone oxygen vibrations were still visible in the spectrum of the hydrogel products.

#### 4.3.2. Ultraviolet spectroscopic characterization UV/Vis

Ultraviolet visible UV/vis analysis was done by adding 10  $\mu\text{L}$  of the PSF, PVA and PSF/PVA hydrogels to solvent DMAc in 1 mL cuvette respectively and recording the absorbance spectra between 100 and 700 nm. The spectrum on (Figure 4.12) showed PSF with the highest wavelength (285 nm) and absorbance (2.8) follow by the hydrogels (Table 4.7).

The ultraviolet visible UV/vis analysis was carried out to investigate the extent of crosslinking in the hydrogels based on polysulfone absorbance parameters i.e. whether the ratio control introduced any contribution to the degree of crosslinking in hydrogels.

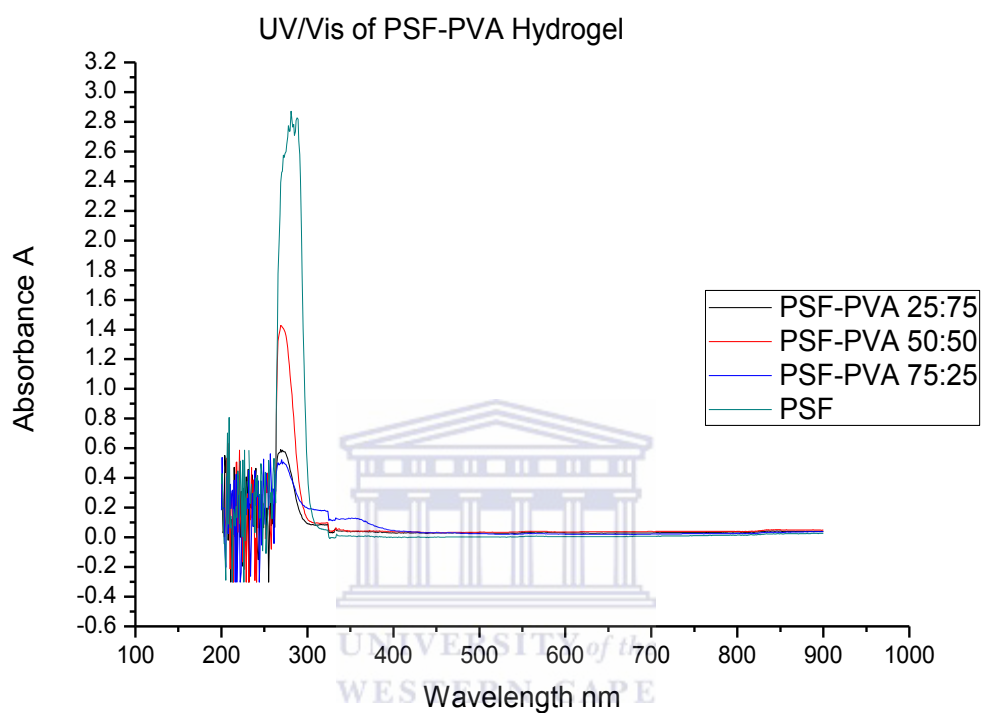


**Figure 4.12:** UV/Vis spectrum of PSF and PSF hydrogels

**Table 4.7. Hydrogels wavelength and absorbance**

Membrane	Absorbance (A)	Wavelength
PVA	0.1	285 nm
PSF	2.8	285 nm
PSF hydrogel 50:50	1.42	275 nm
PSF hydrogel 75:25	0.53	273 nm
PSF hydrogel 25:75	0.6	273 nm

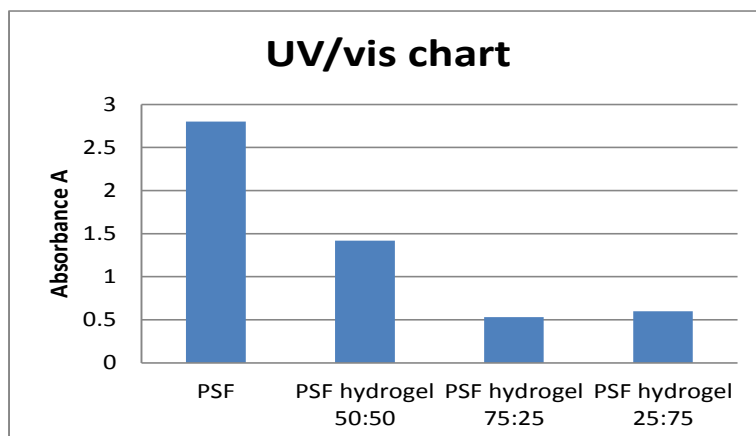


**Figure 4.13: UV/vis absorbance distribution for hydrogels**

Absorbance and wavelength distribution of PSF hydrogels, gives a standard deviation (STD) of 0.4% (n=3) for absorbance and 1% for wavelength. Therefore no significant differences in hydrogel wavelength of the three hydrogels prepared (Figure 4.13). The ratio control has no direct effect on the hydrogel UV/vis absorbance except that at 50:50 ratio a concomitant 50% absorbance reduction was observed compare to PSF on its own.

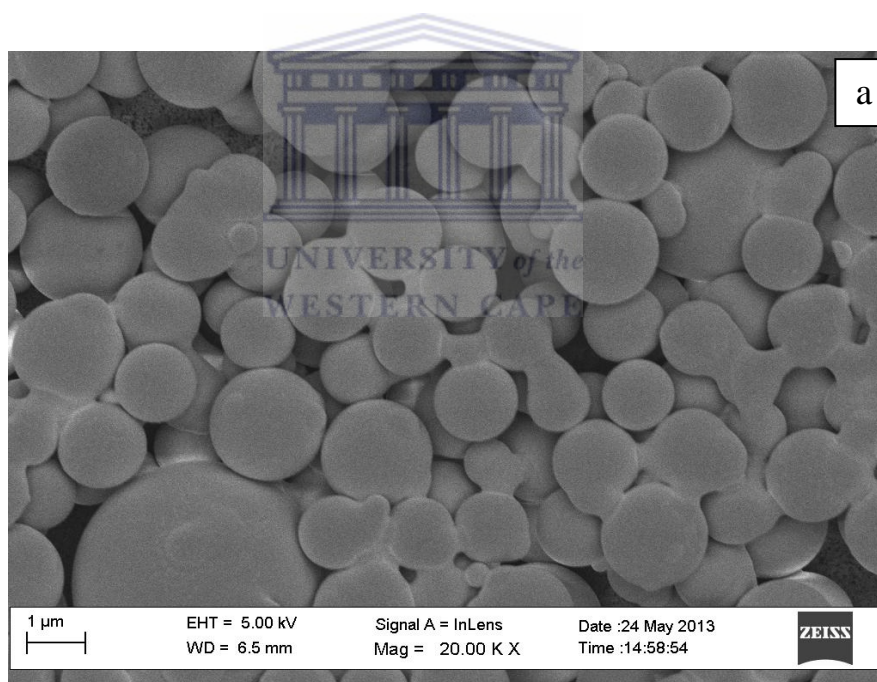


## 4.4. Macroscopic Characterization

### 4.4.1. Scanning Electron Microscopy SEM

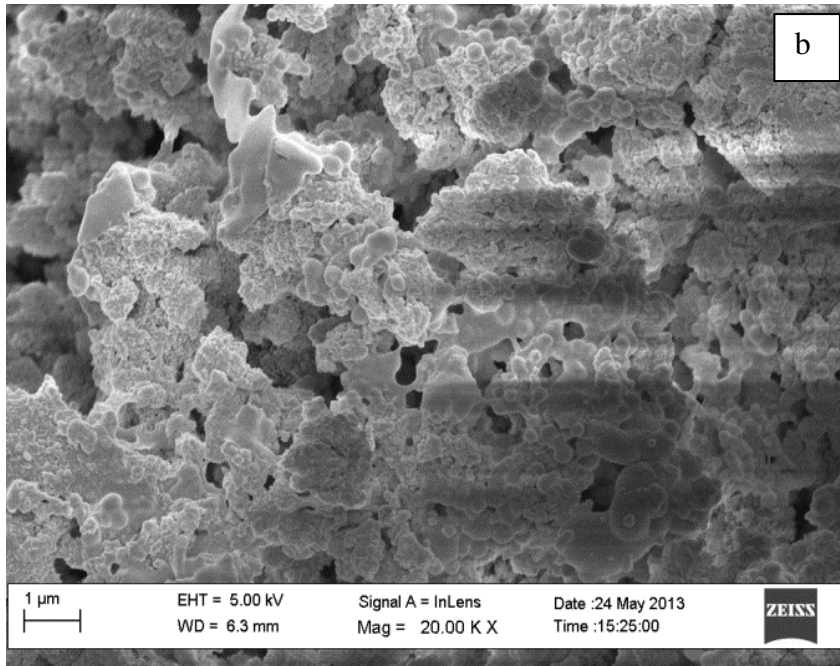
#### 4.4.1.1. Polysulfone film preparation

Thin films were prepared by drop coating 10  $\mu\text{L}$  aliquot of PSF solution and PSF hydrogels onto screen printed carbon electrode (SPCE) with a micropipette and left to dry overnight before imaging. Each sample was coated for viewing with gold dust to enhance the conductivity of the thin film.



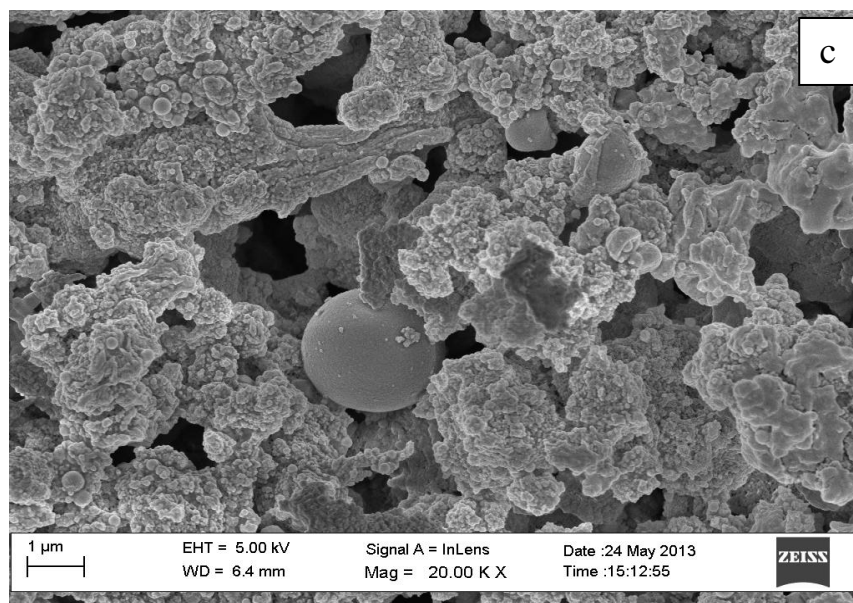
**Figure 4.14:** SEM image of polysulfone

Scanning electron microscopic image on (Figure 4.14) shows that polysulfone has a spherical shape with fairly uniform size distribution of spheres in the order of 1  $\mu\text{m}$ . The uniformity in colour of the image indicated the absence of charging due to interaction with the incident electron beam.



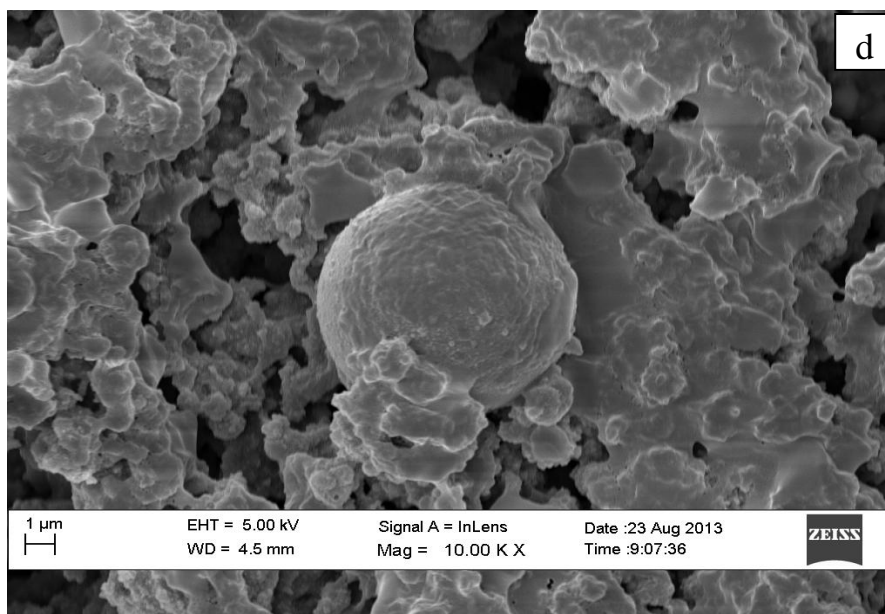
**Figure 4.15: SEM image of PSF-PVA hydrogel 50:50**

Figure 4.15, shows PSF-PVA hydrogel 50:50 contribution, which when compared to polysulfone on its own, confirmed a change in morphology due to the integration of both PVA and PSF. Polyvinyl alcohol introduction resulted in a decrease in size of the surface morphology features. Very little PSF spheres were visible, but it was evident that PSF spheres directed the growth of PVA polymer, which is consistent with expectation for efficient crosslinking.



**Figure 4.16: SEM image of PSF-PVA hydrogel 75:25**

Scanning electron microscopic images for PSF-PVA hydrogels 75:25 and 25:75 showed that the dominant component also dominates the morphology. When PSF was present as the 73% ratio in synthesis mixture the resultant hydrogel morphology showed evidence of unreacted PSF spheres (Figure 4.16) whereas when PVA was the dominant component its finer textured morphology dominates and no unreacted PSF spheres were observed (Figure 4.17). Evidence of crosslinking was observed at all three ratios. The smaller scale morphology of PVA was visibly filling up the spaces between PSF beads. In Figures 4.16 and 4.17 the template effect of PSF directing the growth of PVA was directly observed.



**Figure 4.17:** SEM image of PSF-PVA hydrogel 25:75 at different magnification

Morphology plays an important role in membrane technology, electrical conductivity and mechanical properties of the materials. Electrical conductivity is related to surface morphology [53]. Bulk polymer tends to aggregate in large particles in the form of large globules. This is probably due to an increased inter-chain interaction compared to its stabilized particles, in which the polymeric surfactant chains act as a limiting factor for such an interaction. However from the colour and size distribution observed in the polymers and composites we can conclude that efficient crosslinking was achieved with evidence of PSF templates directing the crosslinking morphology.

#### 4.4.2. ATOMIC FORCE MICROSCOPY (AFM)

Atomic force microscopy has been used to characterise the surface roughness which has been regarded as one of the most important surface properties. It has a significant role in membrane permeability and fouling behaviour. Surface roughness determined from roughness parameters such as the average roughness ( $R_a$ ) and root mean square roughness ( $R_{rms}$ ), could also be related to hydrophobicity of the thin film [55]. Imaging of prepared thin films samples were obtained using Nanosurf easyScan 2 (Wirsam).

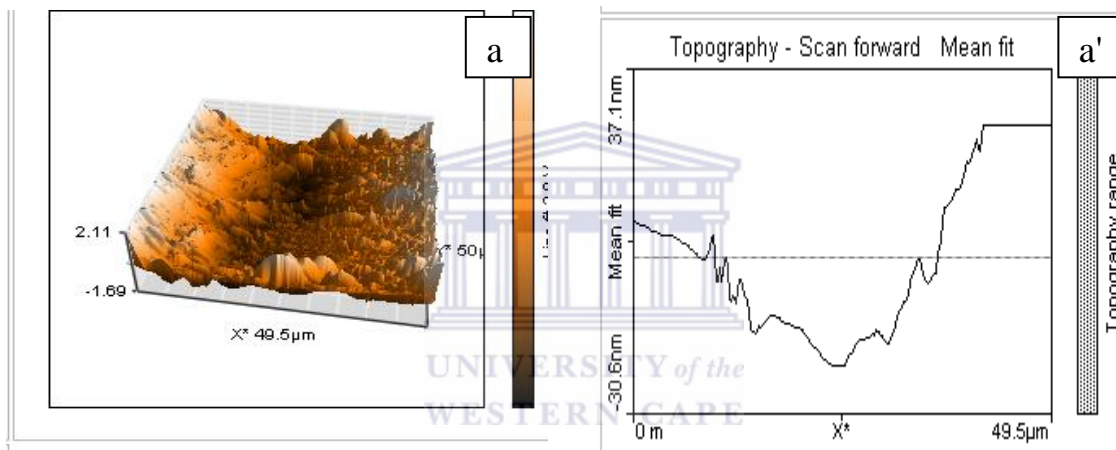


Figure 4.18: AFM image of PSF on its own

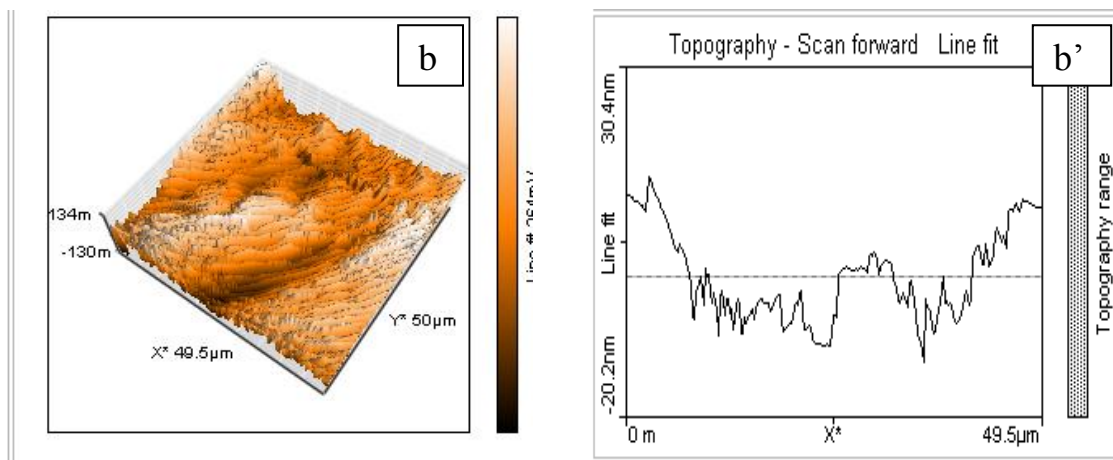
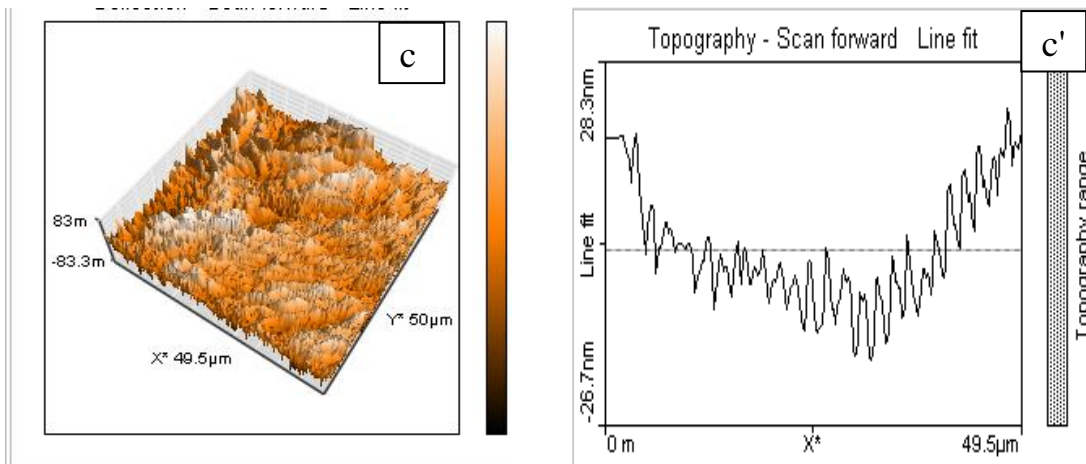
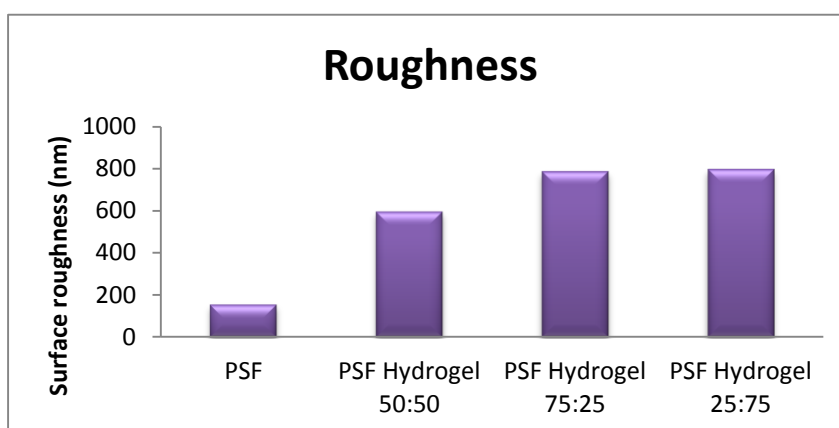


Figure 4.19: AFM image of PSF-PVA hydrogel 50:50



**Figure 4.20: AFM image of PSF-PVA hydrogel 75:25**

Higher surface roughness was measured for polysulfone (Figure 4.18), compared to polysulfone hydrogels (Figure 4.19 and 4.20). This height distribution was in good agreement with the observed surface features of the polymers from SEM, The Sa and Ra values show a clear distribution of roughness associated with PSF contribution respectively. And a clear increase in trend upon modification with PVA was observed. Surface roughness could be associated with hydrophilicity of material. The more rough the surface the more hydrophilic it becomes [55]. This topography trend is in good agreement with contact angle drop shape analysis and SEM images.



**Figure 4.21: Surface roughness of PSF and PSF hydrogels**

Roughness distribution for the three hydrogels showed no significant variations for PSF; PVA ratio (STD= 6.8, n=3)

#### 4.5. Optical characterization

Kruss drop shape analyser (DSA25) was used to measure the contact formed between the film of PSF, and a drop of water. A drop is placed on a sample located on the sample table. It was illuminated from one side while a camera at the opposite end recorded an image of the drop. The image recorded was used for determination of contact angle (Figure 4.22).

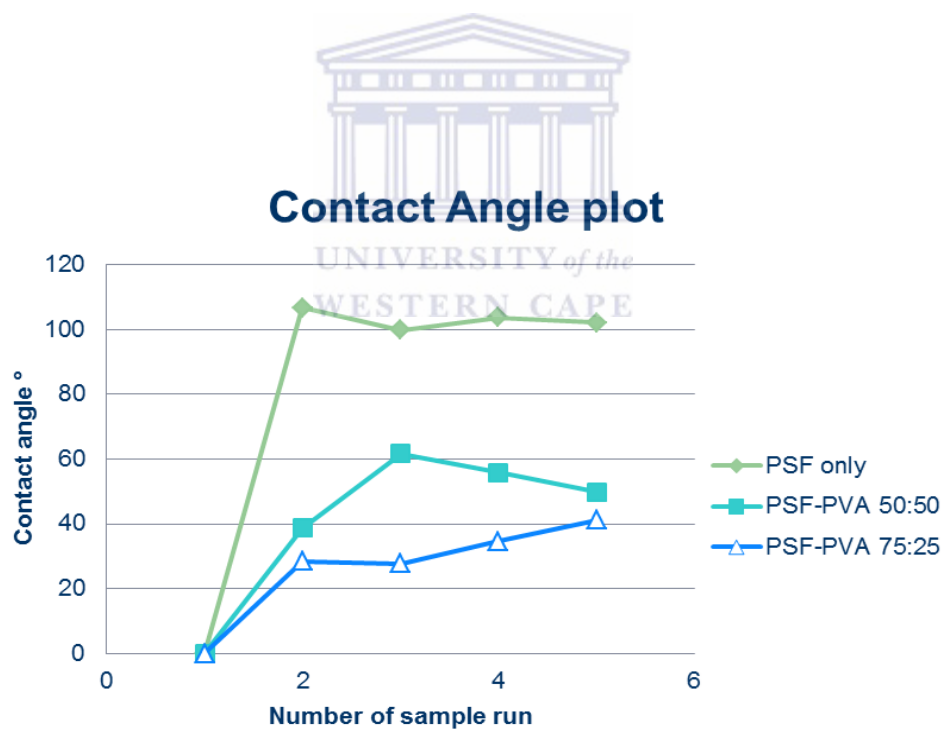
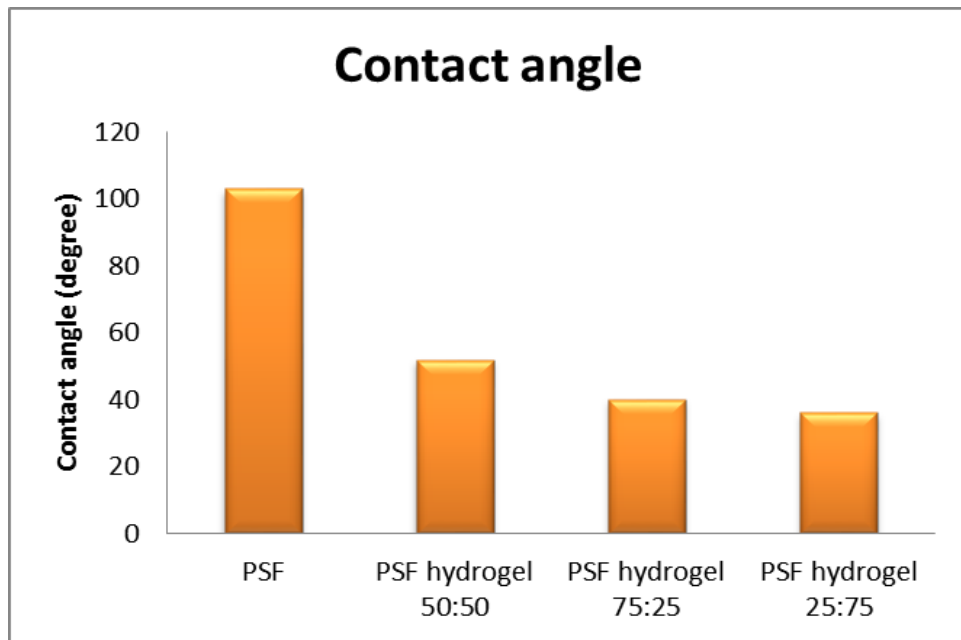


Figure 4.22: Contact angle variation ( n= 4)



**Figure 4.23:** Contact angle distribution for hydrogel materials

**Table 4.8:** Contact angle measurements

Membranes	Contact angle average (°), n = 4	STD n = 4
Polysulfone	103	4.5
Polysulfone- polyvinyl alcohol 50:50	52	8.5
Polysulfone- polyvinyl alcohol 75:25	40	2.9
Polysulfone- polyvinyl alcohol 25:75	36	5.1

Membranes are defined as hydrophobic once its contact angle is greater than 90° and hydrophilic when it's less than 90°. Polysulfone on its own shows a contact angle of greater than 90° which confirm it hydrophobic nature. After incorporation of 50% PVA, it showed a decrease in contact angle by 51% with a contact angle of (52°). This result confirms the improvement of PSF hydrophobicity. Previous research from our group have shown improvement of hydrophilic properties of polysulfone



membranes by introducing different metal nanoparticles such as Co, Ni and Ag to the polymer matrix [9 & 13]. Introducing an electrochemically conductive polymer such as PVA into PSF polymer matrix imparts its advantageous properties onto the resulting membrane and enhances hydrophilic characteristics of the membrane with a contact angle equal or much better than that achieved by modification with nanoparticles [12 - 15 & 62]. Optical results (contact angle) shows an agreement with spectroscopic (EC) and microscopy (AFM) data (Table 4.9)

**Table 4.9: Summary of three hydrogels performance**

Hydrogels	Contact angle	Roughness (nm)	Diffusion coefficient	
			D <sub>o</sub> Cm <sup>2</sup> /s	D <sub>R</sub> Cm <sup>2</sup> /s
PSF:PVA 50:50	52°	595.60	3.21e-11	9.06e-9
PSF:PVA 75:25	40°	786.80	6.32e-10	9.88e-8
PSF:PVA 25:75	36°	789.90	8.54e-10	9.45e-8

A decrease in contact angle gives an increase in roughness and diffusion coefficient. High surface roughness was linked to improved hydrophilicity and was also shown to agree with improved electron mobility within the polymer matrix. Hence a more hydrophilic interface was linked to the improved conductivity for the hydrogels. Crosslinking PSF with PVA reduced the hydrophobic nature of PSF as evidenced by surface features such as shape and size distribution as well as surface roughness. Crosslinking PSF and PVA also improved electron transfer properties.

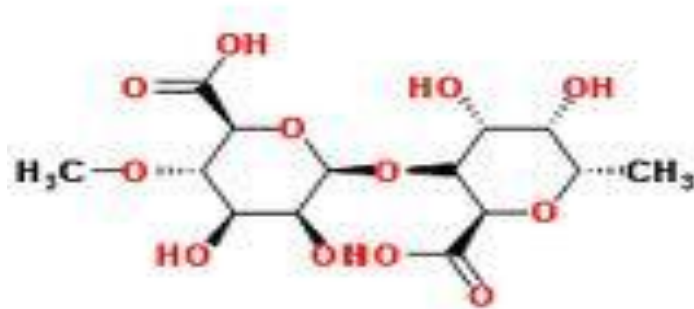
# Chapter 5

## 5. Electrochemistry of hydrogels as sensing material for selected model compound.

At very low levels of concentration tannic acid and alginic acid redox electrochemistry may be evaluated quantitatively, in order to calculate the concentration loading that may result in fouling the hydrogel surface area. Membrane filtration processes are vulnerable to fouling. Natural organic matters are the major fouling agents during the membrane filtration processes. Compounds such as polysaccharides, proteins, humic acid, fulvic acid and organic acids are examples of the organic matter. Polysaccharides are produced during biological waste water treatment and they are part of the soluble microbial products.

Alginic acid is a type of a polysaccharide produced by bacteria and algae. Studies investigating the properties of alginic acid due to the role played by alginic acid bio-flocculation have been reported, however there are no studies that describe the role of alginic acid in the reverse osmosis membrane fouling [75]. Tannic acid (TA) is not a true acid because it does not contain the carboxyl group (COOH) present in all organic acids; instead it is a polyphenol  $(C_5H_5OH)_n$ . As a water soluble polyphenolic compounds, TA has been demonstrated to be toxic to aquatic organism, such as algae, phytoplankton, fish and invertebrates. Moreover, TA will react with chlorine during water treatment and sterilization and produce carcinogenic disinfection by-products (DBPs), which cause cancer and affect the health of human beings very seriously [76].

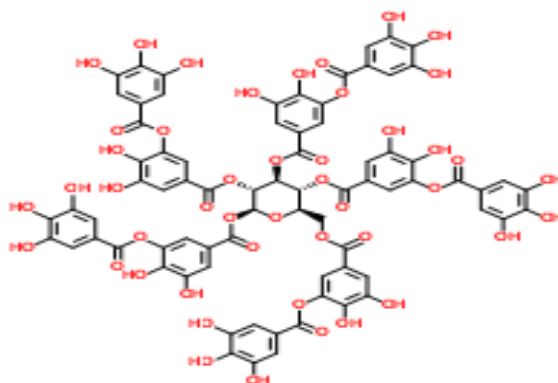
### 5.1. Alginic acid (AA)



Alginic acid

Alginic acid (algin or alginate) is one of the anionic polyose distributed within the cell walls of alga. It forms a viscous gum once in contact with water and absorbs water quickly [74] it's capable of engrossing 200-300 times its own weight in water. It has a colour ranges from white to yellowish-brown. Alginic acid is a linear polymer with homopolymeric blocks of (1-4)-linked  $\beta$ -D-mannuronate (M) and its C-5 epimer  $\alpha$ -L-glucuronate (G) residues, severally, covalently joined along in several sequences or blocks. [74 - 75].

### 5.2. Tannic acid (TA)



Tannic acid

Tannic acid is a specific industrial variety of tannin, a sort of polyphenol. Its weak acidity (pKa around 10) is as a result of the many phenol teams within the structure. The statement for industrial tannin is commonly given as  $C_{76}H_{52}O_{46}$ , that corresponds with decagalloyl aldohexose, however a mixture of polygalloyl glucoses or polygalloyl quinic acid esters with the quantity of galloyl moieties per molecule starting from a pair of up to twelve counting on the plant supply wont to extract the tannin [76].

Electrochemistry of PSF hydrogels in the presence of target molecules, alginate and tannic acid showed measurable redox performance before onset of fouling. Polysulfone hydrogels redox chemistry was evaluated using cyclic voltammetry and square wave voltammetry from which kinetic parameters associated with alginate and tannic acid was determined. Cyclic voltammetry evaluation of PSF hydrogels were done at different concentration of the analyte, to measure the sensitivity of the modified electrode where the oxidation and reduction was taking place and diffusion coefficients were calculated.

Hydrogel thin films were prepared as before at a platinum working electrode and the organic acids were introduced to the analytical solution. Before concentration analysis, the diffusion coefficients of the 50:50 hydrogel was evaluated at the platinum electrode and compared to the values previously determined at the glassy carbon electrode, because the transducer material is known to affect the charge transfer at the interface. The platinum electrode experiments were performed in 2 mL of 2 M HCl as electrolyte solution as before, within the potential window between -200mV to 1200 mV.

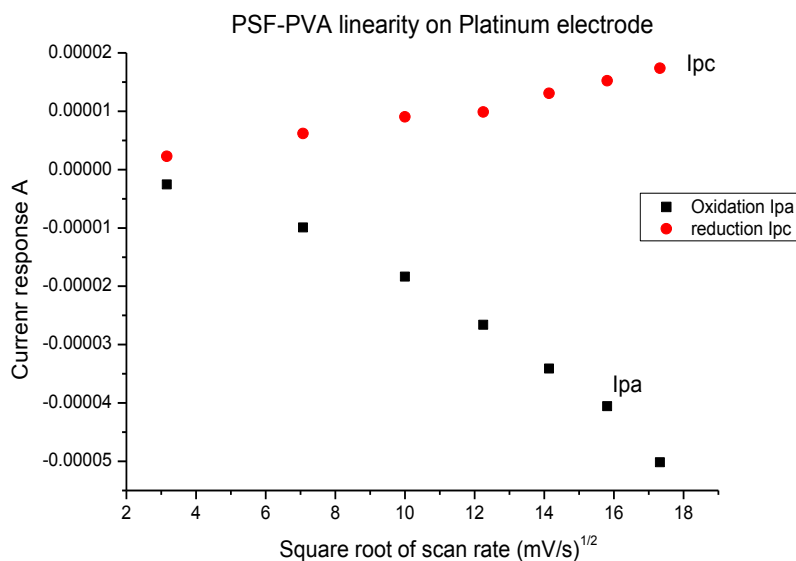


**Figure 5.1:** Anodic and cathodic peak current ( $I_p$ ) vs. square root of scan rate ( $v^{1/2}$ ) for 50:50 PSF-PVA Hydrogel on Platinum electrode in 2 M HCl solution at different scan rates.

**Table 5.1:** Effect of scan rate on peak current and peak potentials for 50:50 PSF-PVA hydrogel on platinum electrode and glassy carbon electrode in 2 M HCl Solution.

	Intercept	Slope	Statistic	Kinetics
	A	A/mVs <sup>-1</sup>	Adjusted R <sup>2</sup>	Diff coeff Cm <sup>2</sup> /s
<b>Oxidation (Pt)</b>	1.18615e-5	-3.327e-6	0.96258	1.264e-14
<b>Reduction (Pt)</b>	-1.38600e-6	1.037e-6	0.97822	1.228e-13
<b>Oxidation (GCE)</b>	2.3318e-6	6.1878e-7	0.9692	3.260e-11
<b>Reduction (GCE)</b>	2.93716e-6	9.7869e-7	0.97085	9.06e-9

The correlation between peak current and scan rate conformed to the expected linear correlation for diffusional control following the Randles Sevcik treatment of data. The diffusion of charged species at the 50:50 hydrogel/Pt interface was found to be slower (1.264e-14 and 1.228e-12 Cm<sup>2</sup> /s respectively for oxidation and reduction)

compared to the diffusion coefficients at GCE/hydrogel interface. However the electron mobility was observed to favour the reduced state as before.

### 5.3. Electrochemical performance in the presence of analyte

#### 5.3.1. Hydrogels performance in alginic acid

The analytical current response to changing alginic acid introduced to 2 M hydrochloric acid solution as aliquots, was evaluated by CV.

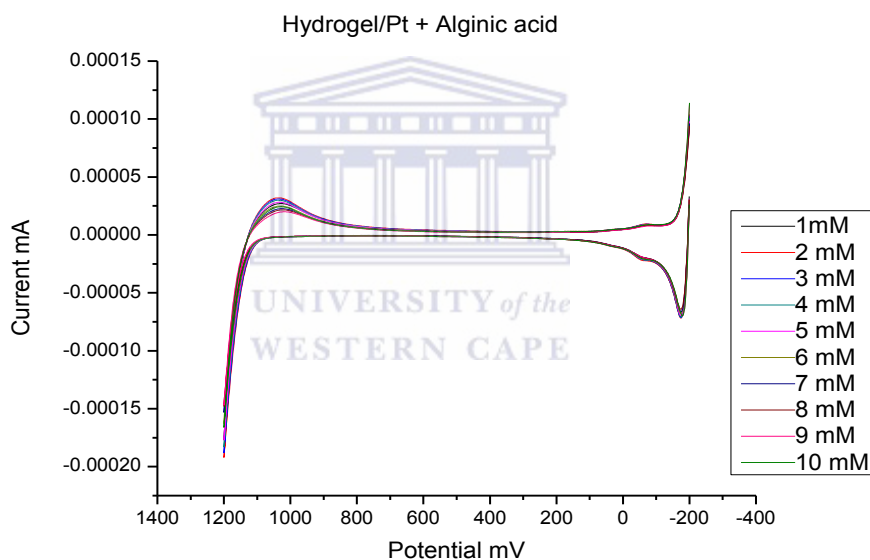


**Figure 5.2:** Concentration dependant CVs of PSF-PVA hydrogel (50:50) in the presence of alginic acid in 2 M HCl

This voltammogram showed a decreasing trend in analytical current with every increase in concentration (Figure 5.2). Alginic acid was observed to be partially soluble in water especially in acidic medium, however the electrochemical characterization was continued in acidic medium, to simulate environmental conditions and a linear concentration response was established.

Secondly, alginic acid did not show any unique electrochemistry of its own and the transducer electrochemistry was used to identify a suitable analytical signal at 110 mV (vs Ag/AgCl) which was used to evaluate its concentration effect at all three hydrogels.

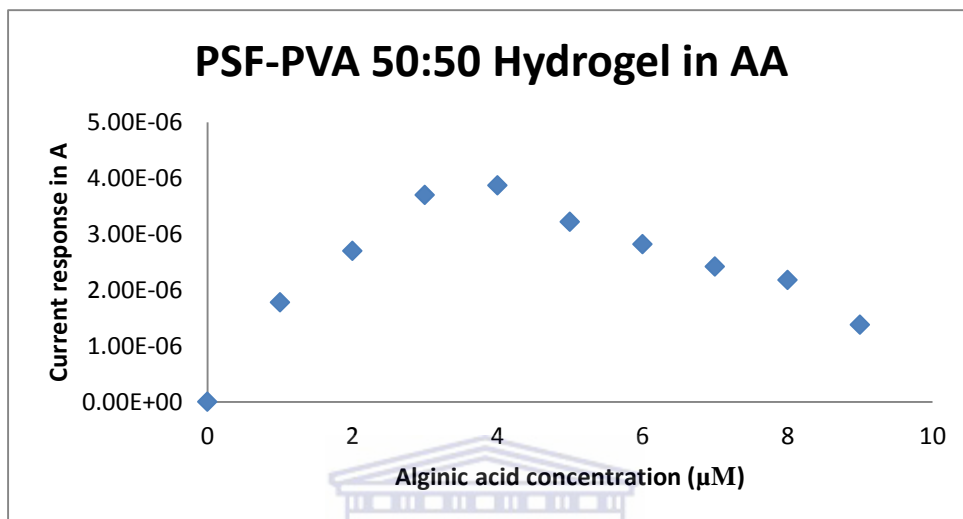


Figure 5.3: Calibration curves of PSF-PVA Hydrogel 50:50 in the presence of alginic acid

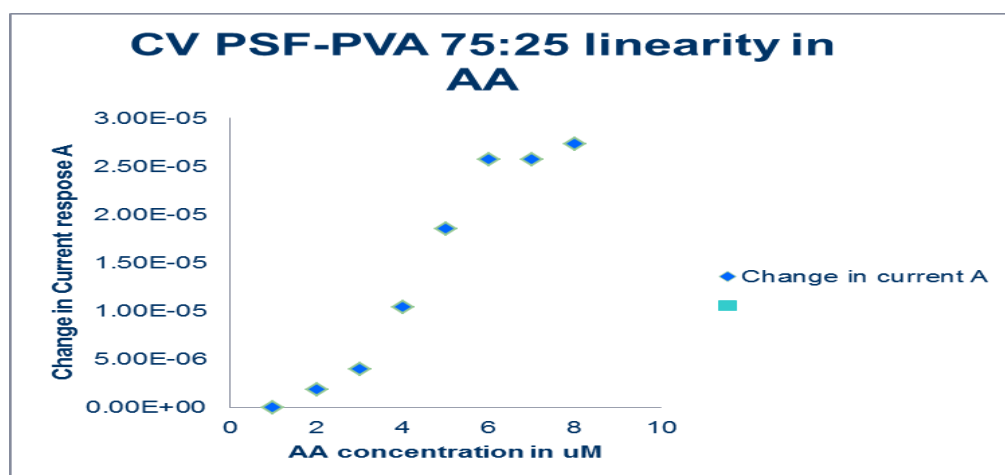


Figure 5.4: Calibration curves of PSF-PVA Hydrogel 75:25 in the presence of alginic acid

### PSF:PVA 25:75 in AA

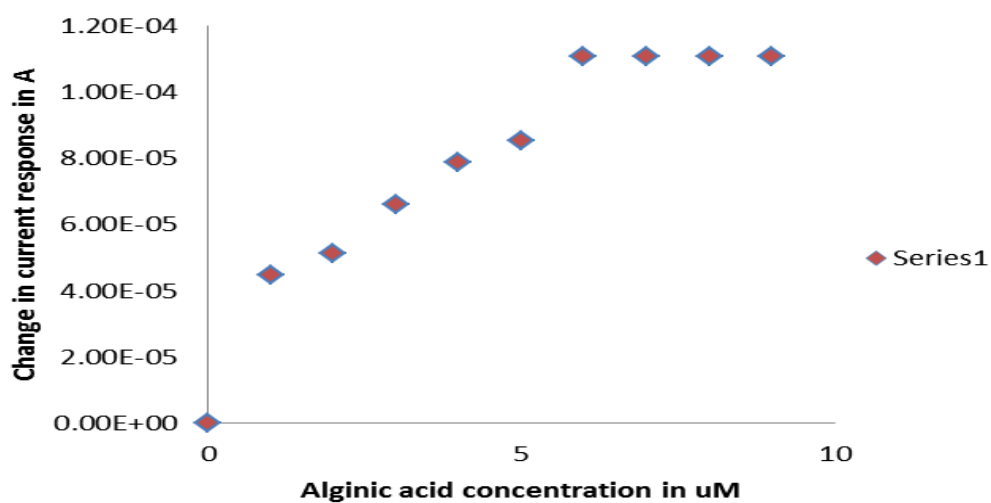


Figure 5.5: Calibration curves of PSF-PVA Hydrogel 25:75 in the presence of alginic acid

Table 5.3: Summary of hydrogels performance in alginic acid

	Hydrogel 50:50	Hydrogel 75:25	Hydrogel 25:75
Analytical peak	110 mV	110 mV	110 mV
Correlation coefficient $R^2$	0.97	0.98	0.99
Sensitivity	2.e-6A/ $\mu\text{M}$	5e-05A/ $\mu\text{M}$	3e-05A/ $\mu\text{M}$
LOD	5 $\mu\text{M}$	6 $\mu\text{M}$	6 $\mu\text{M}$

The 50:50 hydrogel showed the lowest sensitivity towards the presence of alginic acid in the concentration range 1-6  $\mu\text{M}$ . The diffusion coefficient for the analyte towards the 50:50 hydrogel interfaces was also calculated to have the lowest value and this supports the conclusion that the concentration response was diffusion



controlled. The decreasing trend observed for alginic acid was indicative of an adsorption mechanism and hence the LOD was relatively small.

### 5.3.2. Hydrogels performance in tannic acid

Following a similar protocol as for the preceding alginic acid, the analytical current response to changing tannic acid introduced to 2 M hydrochloric acid solution as aliquots, was evaluated by CV.

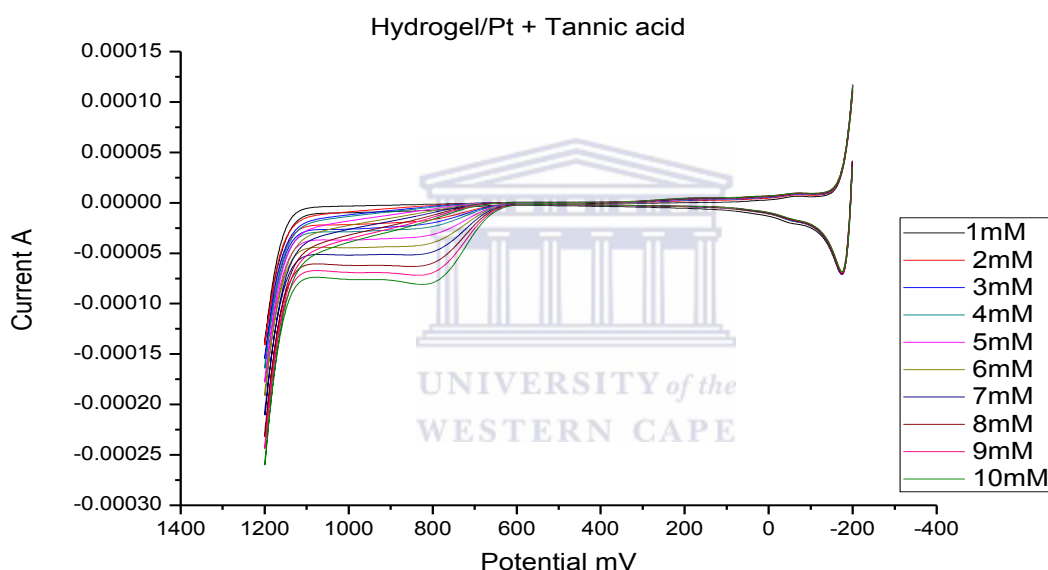


**Figure 5.6:** Concentration dependant CVs of PSF-PVA hydrogel (50:50) in the presence of tannic acid in 2 M HCl

Cyclic voltammetry clearly showed the development of a new oxidative peak at 800 mV (vs Ag/AgCl) due to the increasing tannic acid in solution (Figure 5.6). This peak was used as the analytical signal to evaluate the effect of tannic acid oxidation at the hydrogel interfaces respectively (50:50, 75:25, and 25:75). In this case the hydrogel thin film behaved as a chemical sensor for the oxidation of tannic acid in aqueous solution, with negligible shift in peak potential as a function of concentration.

The increase in the peak current observed at 800 mV was consistent with an electro-catalytic mechanism.

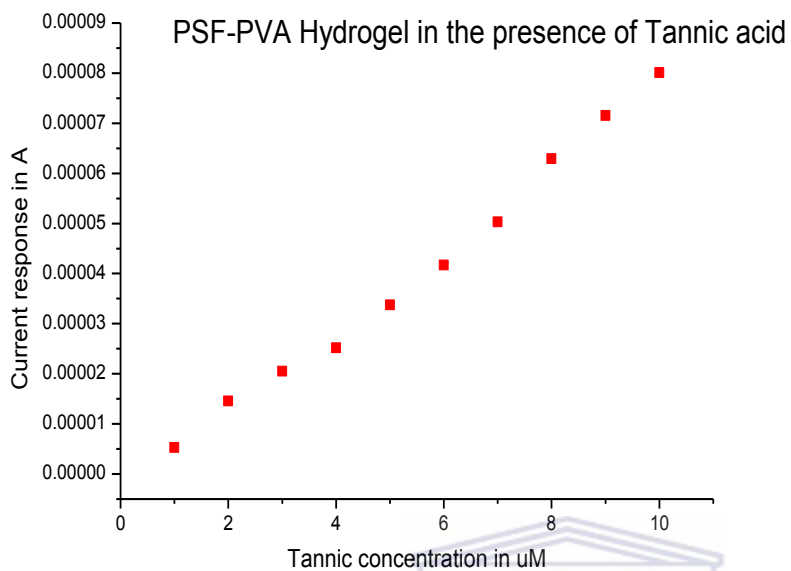
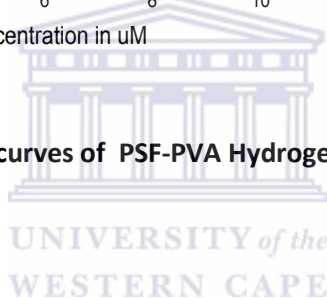


Figure 5.7: Calibration curves of PSF-PVA Hydrogel 50:50 in the presence of tannic acid



### CV PSF-PVA 75:25 linearity in TA

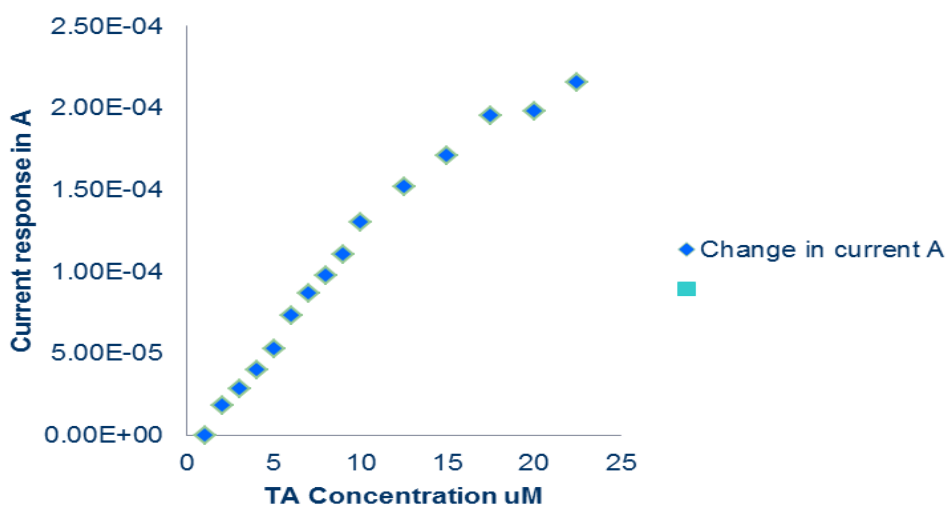
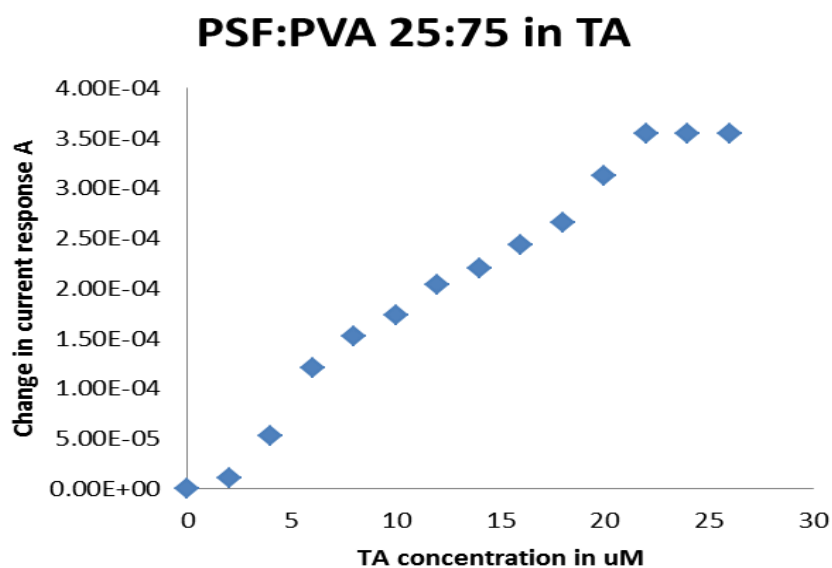


Figure 5.8: Calibration curves of PSF-PVA Hydrogel 75:25 in the presence of tannic acid.



**Figure 5.9:** Calibration curves of PSF-PVA Hydrogel 25:75 in the presence of tannic acid



**Table 5.4:** Summary of hydrogels performance in tannic acid

	<b>Hydrogel 50:50</b>	<b>Hydrogel 75:25</b>	<b>Hydrogel 25:75</b>
Analytical peak	800 mV	800 mV	800 mV
Correlation coefficient R <sup>2</sup>	0.99	0.96	0.97
Sensitivity	8e-5A/ μM	9e-05A/μM	1e-05A/ μM
LOD	20 μM	18 μM	20 μM

An increase in sensitivity of the 75:25, 50:50 and 25: 75 hydrogel current responses towards tannic acid was observed. The 50:50 hydrogel showed the lowest sensitivity towards tannic acid. However due to the different mechanisms of interaction between the alginate (adsorptive) and the tannic acid (electro-catalytic) much higher linear range of concentration analysis was established for tannic acid.

## 5.4. Hydrogel performance under Hydrodynamic condition (Rotating disc electrode RDE)

### 5.4.1. Fouling

#### 5.4.1.1. Hydrodynamic analyses of hydrogel in the absence of target molecules

This experiment was done in order to study effect of hydrodynamic motion on diffusion at the hydrogel interface. The analysis was done over a wide range of rotation speed i.e. 20 – 400 rpm and fixed scan rate of 100 mV/s (Figure 5.10). It was observed that current response increased as rotation speed increases. Platinum /PSF hydrogels upper limit was reached at 150 revolutions per minute (rpm) and a drop in current response was observed at a higher rotation speed. This experiment confirmed that a concentration response for tannic acid and alginic acid could be obtained at slow scan rates i.e. below 150 rpm. However, at fixed scan rate and fixed concentration of tannic acid and alginic acid respectively, showed a decreasing trend up to rotation speed of 350 rpm (Figure 5.11)

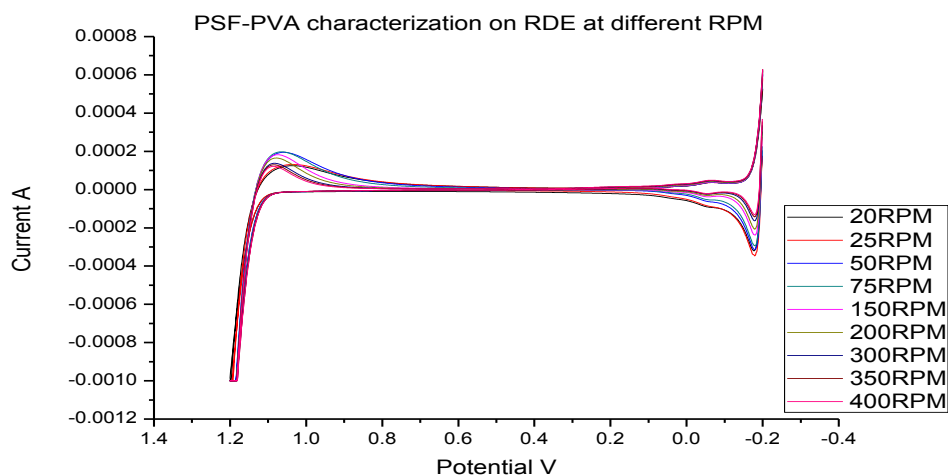
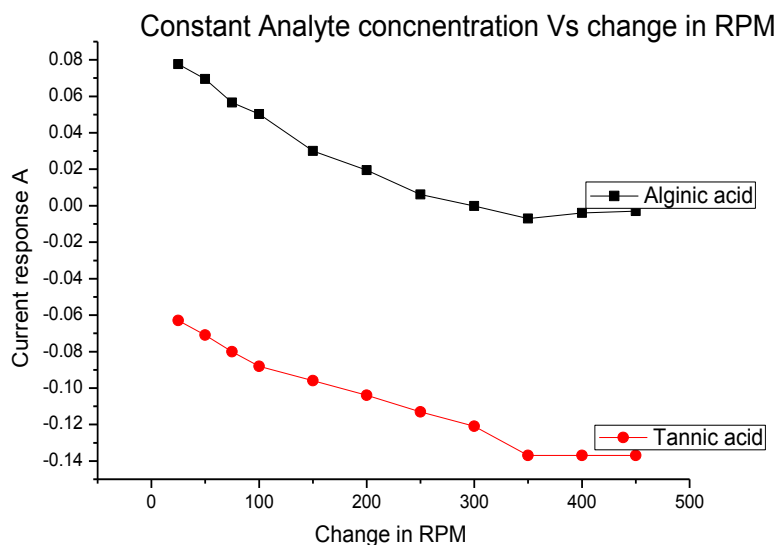


Figure 5.10: RDE Voltammogram of Hydrogel at fixed scan rate and change rpm.



**Figure 5.11:** Plot of rotation speed Vs. peak current response of hydrogel (50:50) at fixed concentration of alginic and tannic acid analyte

The higher rotation speed tolerance observed for the diffusion controlled charge transfer of tannic acid (800 mV) and alginic acid (110 mV) indicated an electro-catalytic effect on the mechanism, of interaction between analyte and 50:50 hydrogel interface. The 75:25 and 25:75 hydrogel diffusion controlled charge transfer behaviour in the presence of alginic acid and tannic acid evaluated in the same way, confirmed a tolerance of rotation speed of the same magnitude i.e. 300 rpm. This confirmed that all the hydrogels would be suitable for flux studies in a membrane through flow cell at low flow rates.

#### 5.4.1.1.1. Effect of a change in analyte concentration at fixed scan rate and fixed rpm

In subsequent experiments the scan rate was fixed at 100 mV/s and the rotation speed was kept constant at 100 rpm. Under these conditions the response of the hydrogel to analyte concentration was evaluated as a concentration effect. The analytical current response at 110 mV as a function of increasing alginic acid concentration was obtained from CV (Figure 5.12). Similarly, the analytical current response at 800 mV as a function of increasing tannic acid concentration was obtained from CV (Figure 5.13).

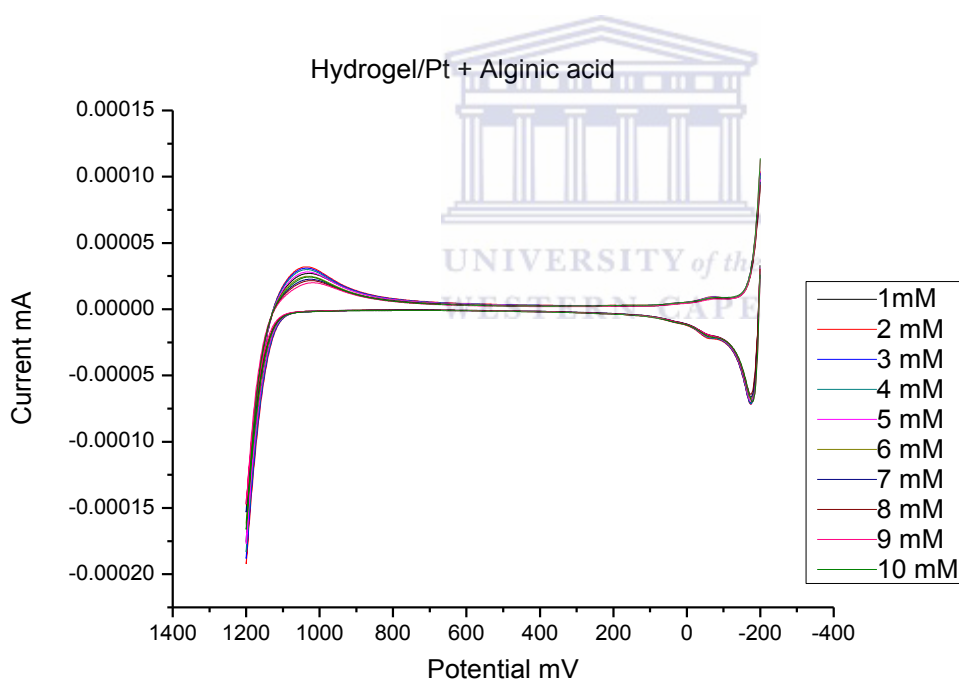


**Figure 5.12:** RDE Voltammogram of Hydrogel (50:50) under hydrodynamic motion at fixed scan rate with an change in alginic acid concentration

Calibration plots were derived from the concentration response of each hydrogel to alginic acid (Figure 5.13,14 and 15) and tannic acid respectively (Figure 5.17, 5.14 and 5.18).

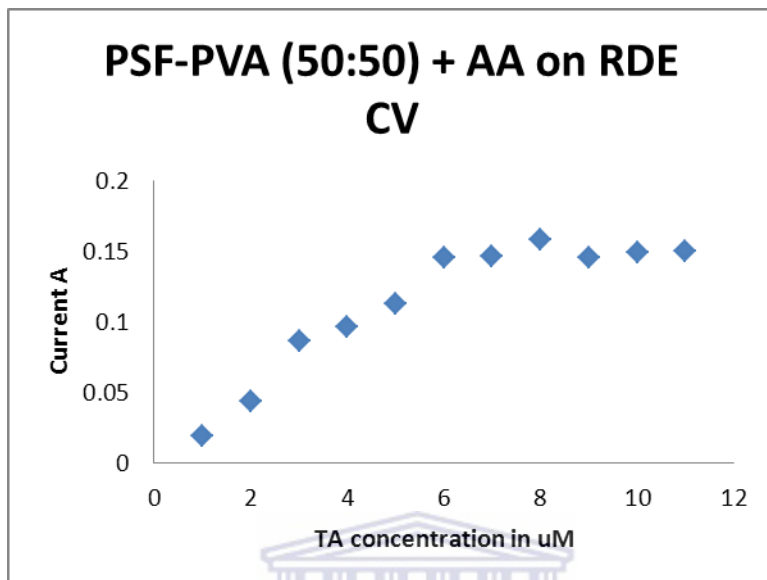


Figure 5.13: RDE Voltammogram of Hydrogel (50:50) under hydrodynamic motion at fixed scan rate with a change in alginic acid concentration

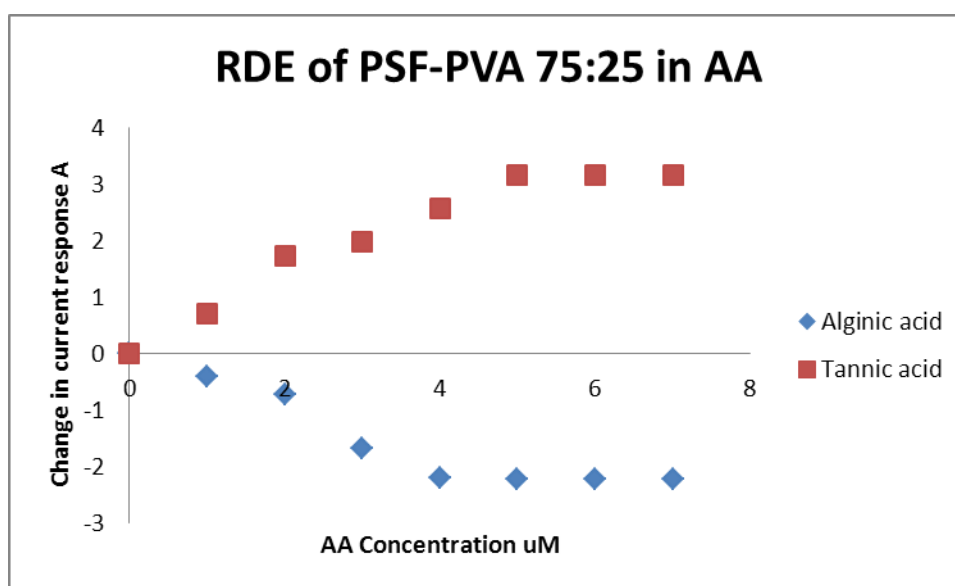
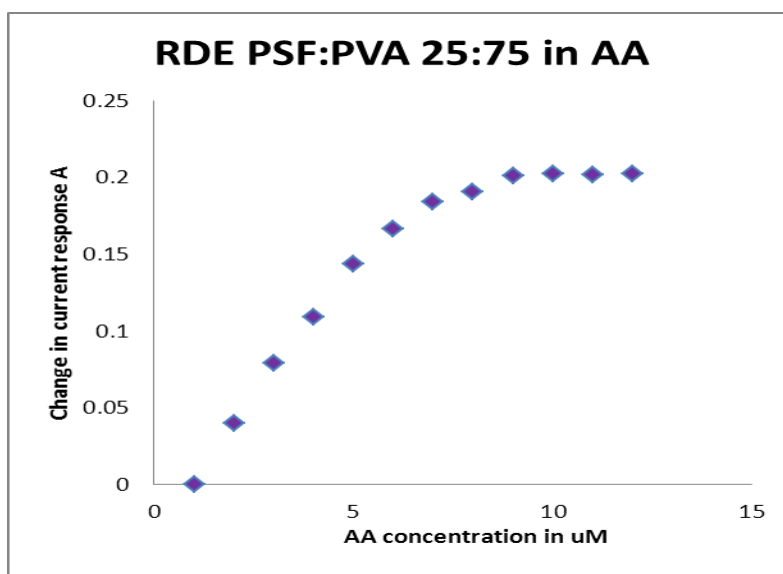


Figure 5.14: RDE Linear plot of Hydrogel (75:25) current peak response vs an increase in tannic and alginic acid concentration and constant rpm.



**Figure 5.15:** RDE Voltammogram of Hydrogel (25:75) under hydrodynamic motion at fixed scan rate with a change in alginic acid concentration

**Table 5.5:** Summary of hydrogels performance under RDE in alginic acid

	Hydrogel 50:50	Hydrogel 75:25	Hydrogel 25:75
Analytical peak	110 mV	110 mV	110 mV
Correlation coefficient R <sup>2</sup>	0.97047	0.9843	0.98807
Sensitivity	0.0128 A/ μM	0.3526 A/ μM	0.0231 A/ μM
LOD	8 μM	6 μM	6 μM



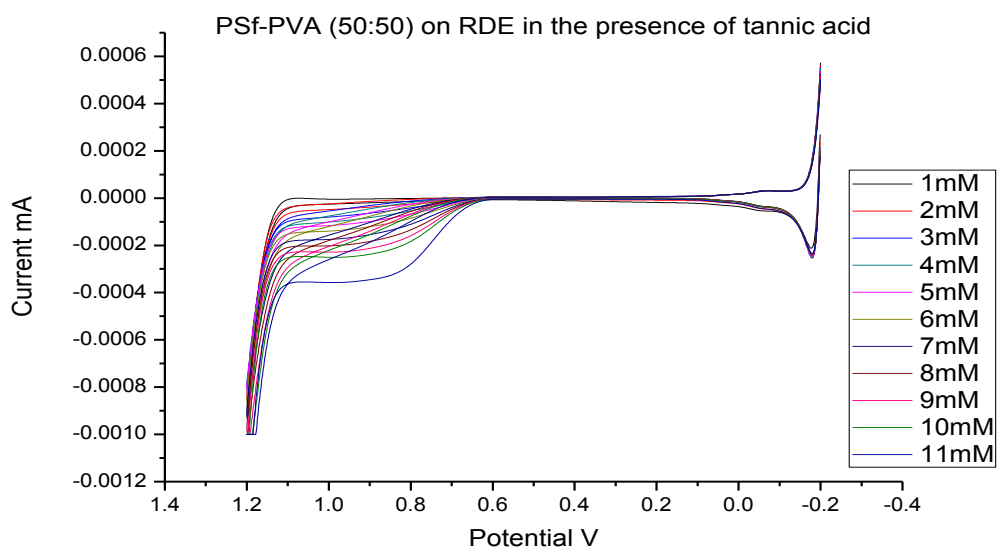


Figure 5.16: RDE Voltammogram of Hydrogel (50:50) under hydrodynamic motion at fixed scan rate with an change in tannic acid concentration

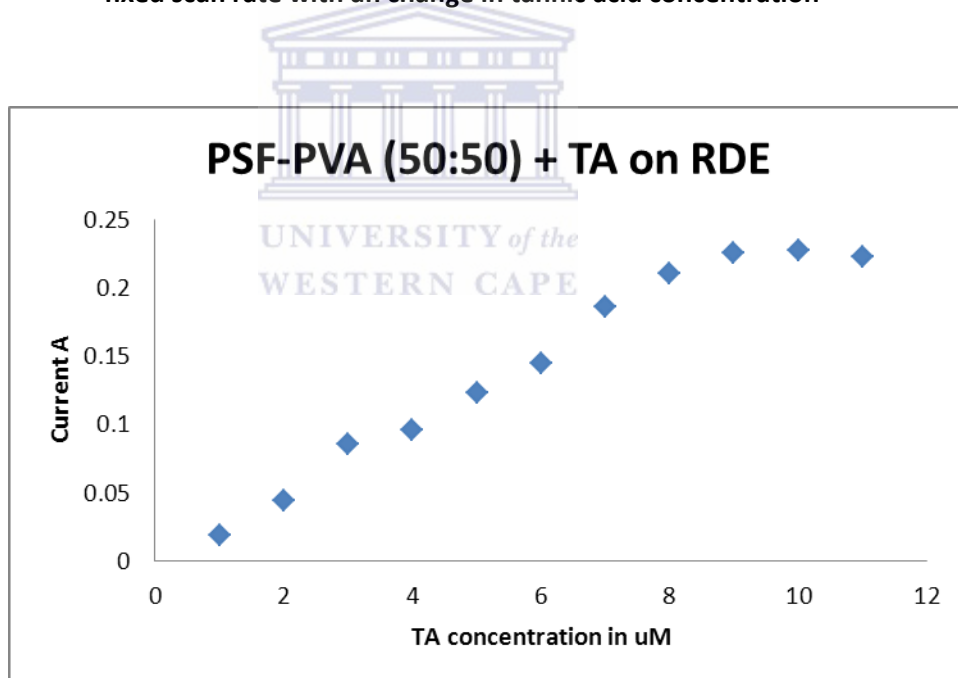


Figure 5.17: RDE Linear plot of Hydrogel (50:50) current peak response vs an increase in tannic acid concentration and constant rpm

### RDE PSF:PVA 25:75 in TA

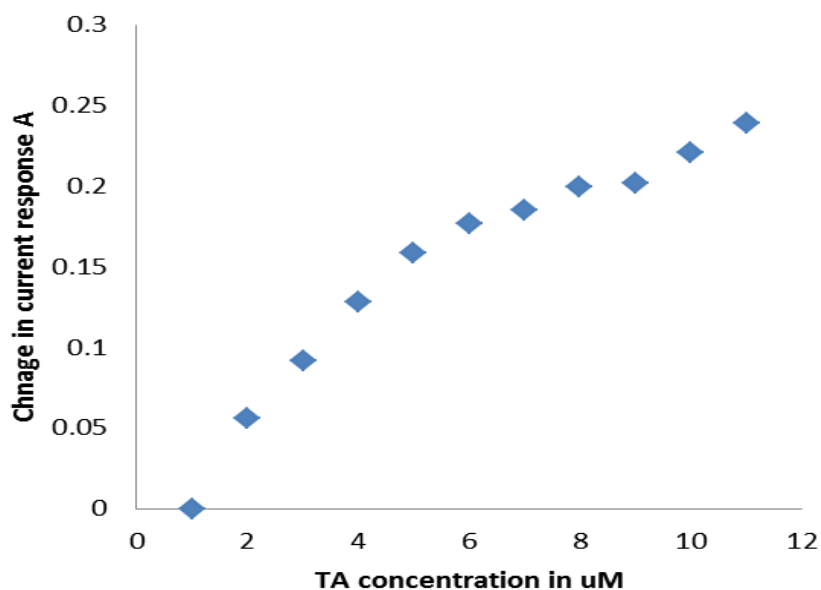


Figure 5.18: RDE Linear plot of Hydrogel (25:75) current peak response vs an increase in tannic acid concentration and constant rpm

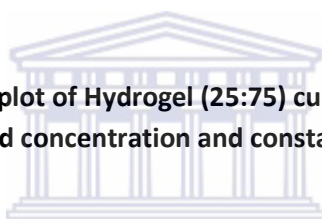


Table 5.6: Summary of hydrogels performance under RDE in tannic acid

WESTERN CAPE

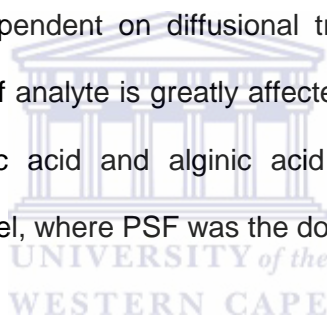
	Hydrogel 50:50	Hydrogel 75:25	Hydrogel 25:75
Analytical peak	110 mV	110 mV	110 mV
Correlation coefficient R <sup>2</sup>	0.98047	0.9873	0.98207
Sensitivity	0.0225 A/ µM	0.5935 A/ µM	0.0214 A/ µM
LOD	9 µM	6 µM	6 µM

Effect of a change in analyte concentration at fixed scan rate and fixed rotation speed, was used as a test for fouling behaviour of PSF hydrogels. Fouling may be defined as the accumulation of unwanted material on solid surfaces to the detriment of function. In this work the saturation point of the hydrogel response to analyte

concentration was interpreted as the onset of fouling, since the hydrogel no longer responded as a catalytic interface.

Convection was seen to speed up the transports of the analyte to the electrode interface, and this was reflected in diffusion coefficient and sensitivity evaluated from Randles Sevcik treatment (Table 5.5 AA and Table 5.6 TA)

We observed that the dynamic linear range for alginic acid was not affected by rotation speed, but that the dynamic linear range for tannic acid was greatly reduced. This may be understood in the light of the different reaction mechanisms that govern the respective analysis. Alginic acid follows an adsorptive mechanism that is not affected by low rotation speed, whereas tannic acid follows an electro-catalytic mechanism, which is dependent on diffusional transport of analyte the detection interface. The diffusion of analyte is greatly affected by rotation speed. The highest sensitivity towards tannic acid and alginic acid concentration respectively, was observed at 75:25 hydrogel, where PSF was the dominant component.



## **5.5. Electrochemical impedance spectroscopy EIS**

### **5.5.1. EIS Hydrogel performance in the presence of analyte**

Electrochemical impedance spectroscopy studies were performed by immobilising 10  $\mu\text{L}$  of PSF hydrogels respectively onto a Pt working electrode, the experiment was performed in three cell system in which silver/silver chloride ( $\text{Ag}/\text{AgCl} - 3 \text{ M NaCl}$ ) as the reference electrode and a platinum wire was used as auxiliary electrode in 2 mL of 2 M HCl as the electrolyte solution at fixed potential 800 mV which represents the formal potential for tannic acid oxidation, and 110 mV for alginic acid. The frequency

range used was from 100 mHz – 1 KHz. The Randles circuit was used to model the data, where  $R_s$  represent the solution resistance,  $R_{ct}$  represent charge transfer resistance. The CPE was used instead of pure capacitor to model the capacitance.

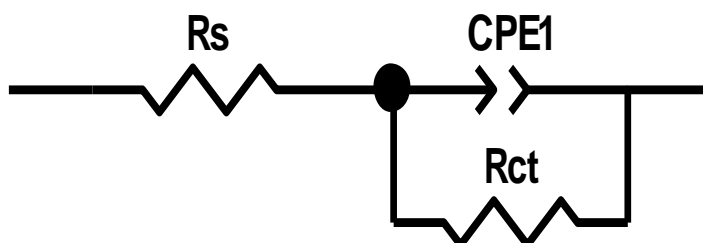


**Figure 5.19:** Equivalent circuit diagram for the PSF hydrogels in the presence of tannic acid

Double-layer capacity and Warburg impedance of the Randles circuit are replaced by the constant-phase elements [89]. In general, the appearance of a CPE may arise from:

- (i) A distribution of the relaxation times as a result of non-homogeneities existing at the electrode-electrolyte interface;
- (ii) Porosity;
- (iii) The nature of the electrode;
- (iv) Dynamic disorder associated with diffusion.

However, for PSF hydrogels in the same electrolyte solution, the equivalent circuit consists of an active electrolyte resistance  $R_s$  in series with the parallel combination of the double-layer capacitance  $C_d$  and an impedance of the Faradic reaction. The impedance of the Faradic reaction consists of an active charge transfer resistance

$R_{ct}$  and a specific electrochemical element of diffusion  $W$ . The results imply that the electrode behaviour follow the Randles equivalent circuit model [109].

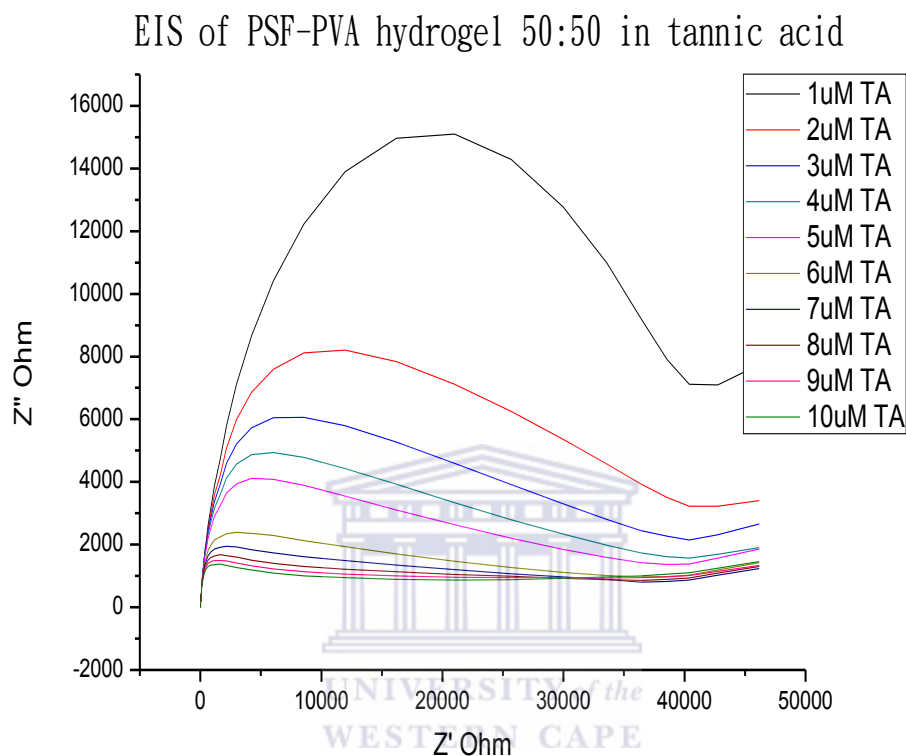


**Figure 5.20: Electrochemical impedance spectra (Nyquist plot) of PSF Hydrogels materials deposited on a platinum working electrode in the presence of tannic acid**

Electrocatalysis of tannic acid followed typical diffusion control kinetics as evidenced by semi-circle in the Nyquist plot at low frequency in the concentration range evaluated and was modelled as Randles circuit using CPE to model non-homogeneity at the interface (Figure 5.20).

In the Bode representation where phase angle and total impedance as a function of frequency, are presented as separate plots, the oxidation of tannic acid was confirmed to follow a one-step catalytic mechanism as evidenced by the single phase

angle maximum (Figure 5.21). The total impedance Bode plot showed a decreasing trend with increasing concentration. (Figure 5.23)

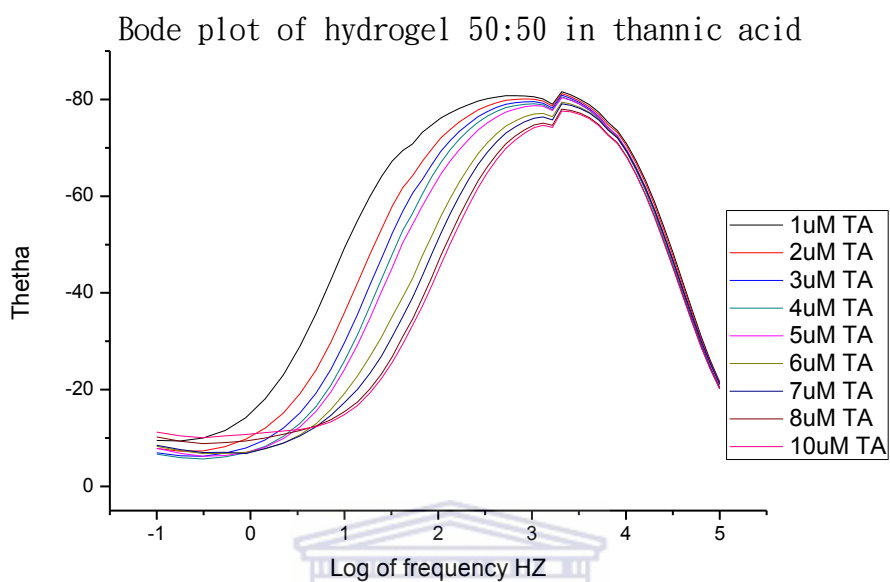


**Figure 5.21:** Electrochemical impedance spectra (bode plot) of PSF Hydrogels materials deposited on a platinum working electrode in the presence of tannic acid

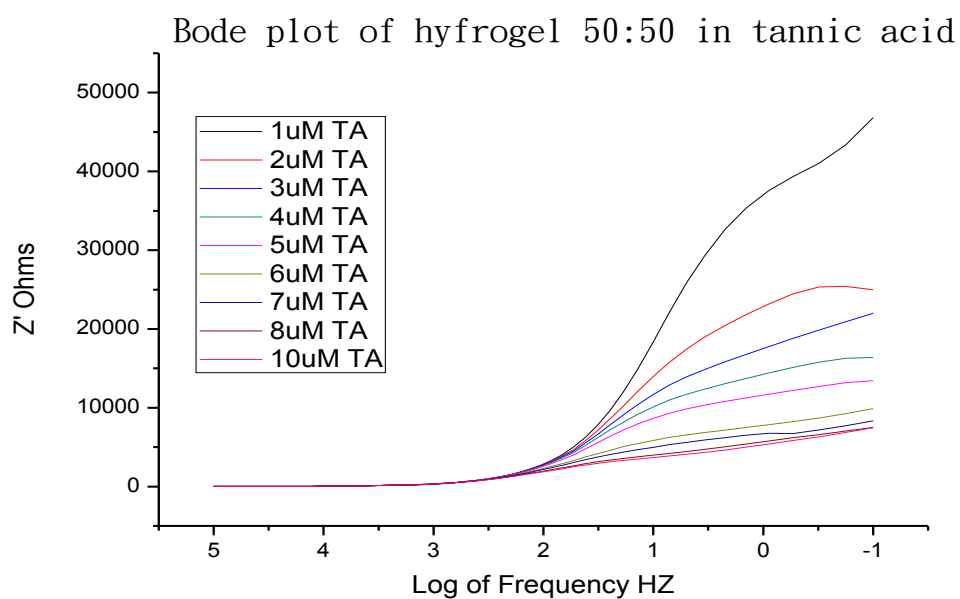


**Figure 5.22:** Electrochemical impedance spectra (bode plot) of PSF Hydrogels materials deposited on a platinum working electrode in the presence of tannic acid

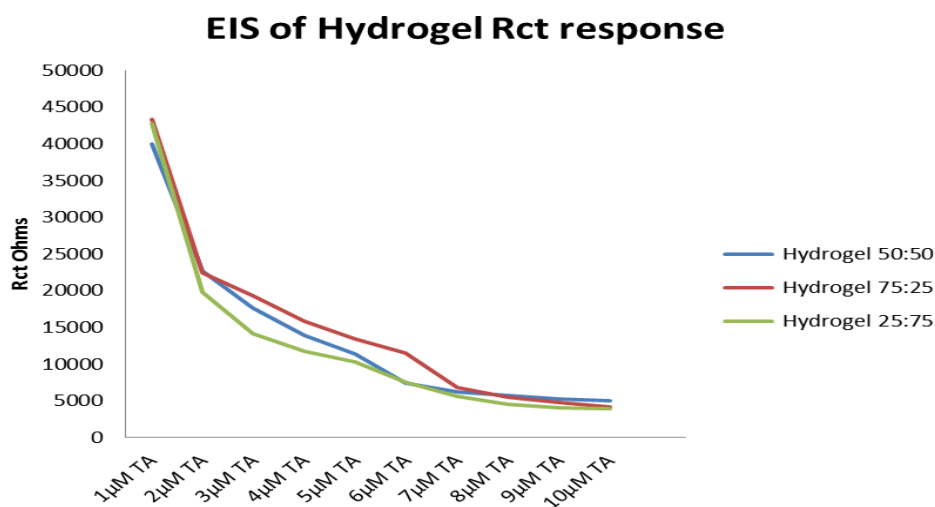


**Figure 5.23:** Electrochemical impedance PSF hydrogels plot of Rct vs tannic acid concentration

The impedance data was modelled as equivalent electrical circuits for the quantitative evaluation of charge transfer and capacitance behaviour. The hydrogel interface was observed to increase in conductivity (decrease in Rct) due to the charging effect of the applied analytical potential, but still facilitated a linear response to tannic acid concentration (Figure 5.23). To major change in the interfacial capacitance was expected, since the tannic acid oxidation was electrocatalytical driven and indeed the change in capacitance remains fairly constant until limit of detection had been reached (Figure 5.24).

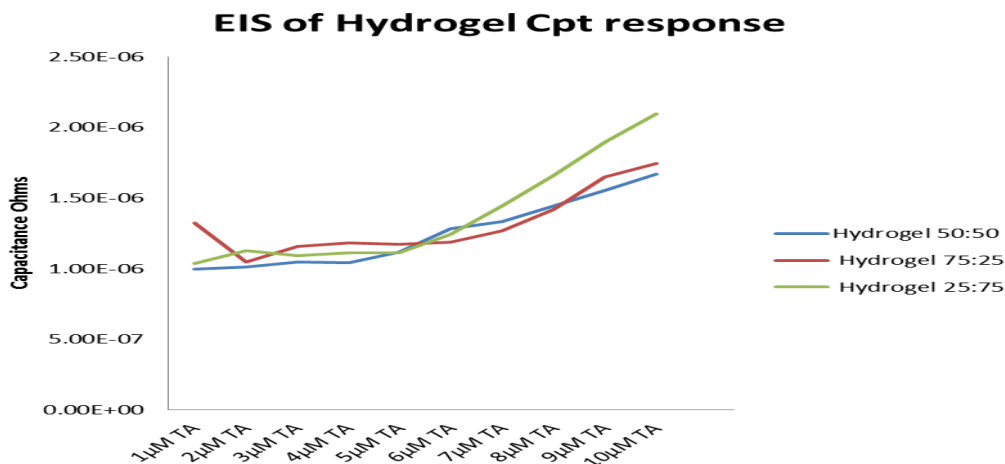


**Figure 5.24:** Electrochemical impedance PSF hydrogels plot of capacitance vs tannic acid concentration

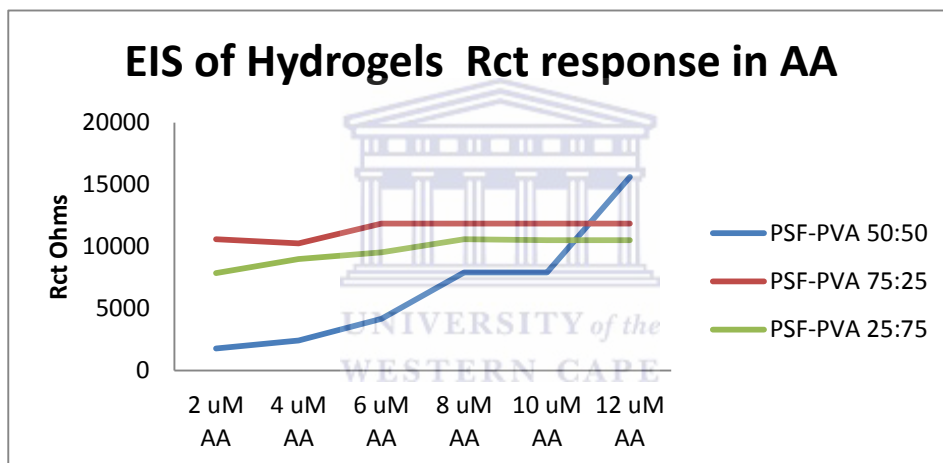


**Figure 5.25:** Electrochemical impedance PSF hydrogels plot of Rct vs alginate acid concentration

The corresponding impedance trend expected for an adsorptive mechanism would be an increase in Rct and an increase in capacitance as the adsorbed analyte material increased the interfacial charge separation and slowed down electron transfer kinetics. However the concentration dependent impedance showed no evidence of a developing trend as a function of concentration, either increasing or decreasing and remained fairly constant in both parameters over the concentration range evaluated (Figure 5.25 and 5.26).



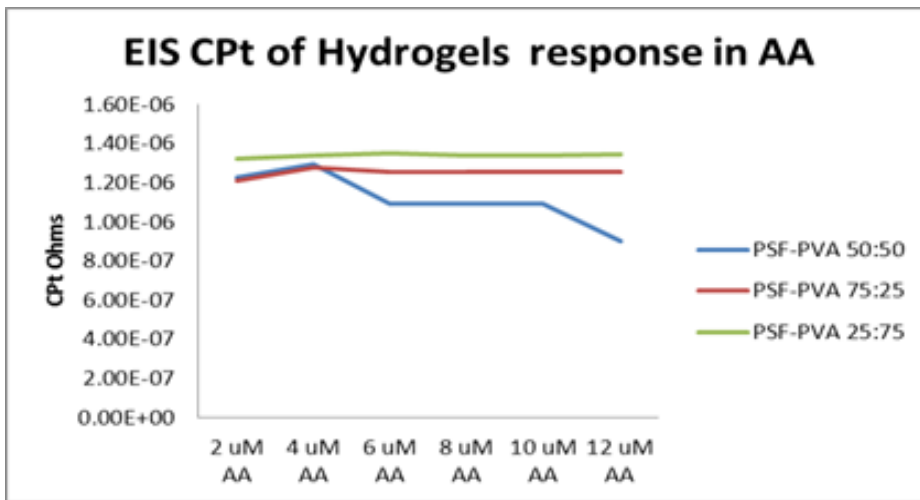


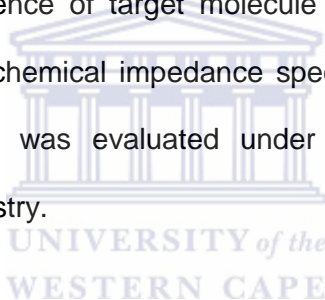
Figure 5.26: Electrochemical impedance PSF hydrogels plot of capacitance vs alginate concentration



# Chapter 6

## 6.1. Conclusion

In the present investigation we have provided evidence in support of polysulfone hydrogel material produced by introducing a conductive hydrophilic polymer (PVA), into the polysulfone (PSF) matrix using glutaraldehyde as crosslinker. The cross linking of PVA and PSF was done at three different ratios i.e. 25:75, 50:50 and 75:25, to produce three unique hydrogel materials, which were characterised using spectroscopic, morphological and electrochemical techniques. Hydrogels performance in the presence of target molecule was evaluated by hydrodynamic voltammetry, and electrochemical impedance spectroscopy. Separation of selected small organic molecules was evaluated under hydrodynamic conditions, using rotating disk electrochemistry.

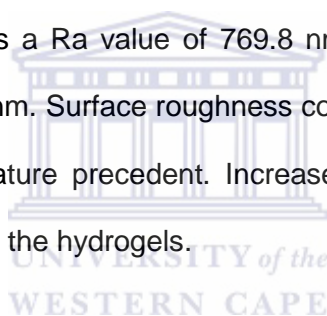


Scan rate dependent cyclic voltammetry confirmed crosslinking of two polymeric unit and the capacitive nature of PSF hydrogels from the block shape curves of the voltammograms and peaks separation between the three voltammograms of PSF.

The SEM images show differences in membranes morphology and porosity for PSF and the synthesised hydrogels. Unmodified PSF shows spherical shape with large pores sized distribution and uniform morphology. The incorporation of the PVA through chemical crosslinking was visible as clusters of much smaller particles distributed onto the PSF template. The morphology was observed to be governed by the dominant polymer concentration.

The hydrogel materials were of nanometer size distribution and the homogeneous incorporation of the PVA morphological into the PSF template was interpreted as confirmation of crosslinking of the two polymers to produce completely new hydrogel materials.

Atomic force microscopic was used to study the surface topography as a surface roughness parameter, which relates to the height distribution of material at the surface. This height distribution was in good agreement with the observed surface features of the polymers in SEM. Surface area (Sa) and surface roughness (Ra) values showed a significant increase in roughness associated with PVA/PSF crosslinking. Polysulfone on its own showed a Ra value of 155.5 nm, and PSF contributions 75:25 shows a Ra value of 769.8 nm, 50:50 Ra value 595.6 nm and 25:75 the value of 791.4 nm. Surface roughness could be associated to hydrophilicity of material, using a literature precedent. Increased roughness was interpreted as increased hydrophilicity of the hydrogels.



The contact angle measurements confirmed that, hydrogels were more hydrophilic as indicated by a decrease in the contact angle with water. The contact angle of the unmodified polysulfone was measured as 103° and upon crosslinking the contact angle decreased by 50% for all hydrogel composites.

Electrochemical characterisation of PSF contributions was done in the presence of target (alginic acid and tannic acid), to study the fouling behaviour on the prepared polysulfone thin films. Cyclic voltammetry, in the absence of analyte confirmed that the charge transport properties of all hydrogels, as measured by diffusion coefficient, were comparable to that of highly conductive polymer systems. The redox chemistry of alginic acid showed no unique analytical peaks that could be distinguished from the transducer. The concentration response of the hydrogels to alginic acid was consistently measured at 110 mV (vs Ag/AgCl) and was observed to follow an adsorptive mechanism. The mechanism was confirmed by EIS as an increase in charge transfer resistance over the analytical concentration range. The redox chemistry of tannic acid was evaluated at its unique oxidation peak at 800 mV (vs Ag/AgCl) and was observed to follow a catalytic mechanism, which resulted in a very wide analytical linear range at all hydrogel interfaces.

Evaluation of hydrodynamic electrochemical using rotating disk electrode confirmed a concentration response to both alginic acid and tannic acid at low rotation speed i.e. below 300 rpm. The detection limit for alginic acid was not affected but the detection limit for tannic acid was greatly reduced under hydrodynamic conditions. From calibration curves based on cyclic voltammetry, the 75:25 hydrogel presented the best performance for quantitative detection of the alginic acid and tannic acid, before saturation of the reactive surface. The saturation point was interpreted as the onset of fouling, since the hydrogel interface at that point becomes insensitive towards the analyte.

## 6.2. Recommendations

The research to date confirmed the successful synthesis of hydrogels through chemical crosslinking. However many physical properties of the hydrogel still remain to be evaluated such as maximum water retention (swellability), temperature degradation profiles by thermogravimetric analysis (TGA, DSC) and surface adsorption area (e.g. BET nitrogen adsorption isotherm analysis).

Furthermore the evaluation of the hydrogel as water treatment membranes requires evaluation in flow through systems such as the wall jet configuration. The wall jet configuration will provide information about laminar flow sensitivity for comparison to mass transport under rotational convection.

The motivation of the research was to present the hydrogels as improved membrane systems for water treatment applications. This implies that the small scale laboratory tests will have to be expanded to be able to report on larger volume testing. The membrane would have to be cast as flat sheet membranes and eventually their suitability for membrane cartridge preparation would have to be assessed. This implies a careful assessment their chemical and mechanical properties.

These hydrogel materials may also be evaluated for their use as host or encapsulating agent in controlled drug release studies. Other aspects such as stability, lifetime, reproducibility of expansion and contraction as well as toxicity and degradation profiling may be necessary, to support the hydrogels as potential materials for controlled drug delivery.

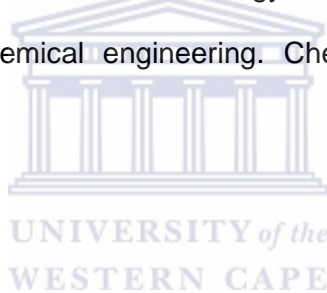
## 7. References

1. Department of Water Affairs and Forestry Republic of South Africa, (2004). National Water Resource Strategy, First Edition, 2004. Online available at <http://www.wrc.org.za/Knowledge%20Hub%20Documents/Other/NWRA%20Sept04.pdf>. [Accessed 10 June 2013].
2. Department of water Affairs, (2011). Green drop report 2010/2011 on water affairs. Online available at [http://www.dwaf.gov.za/dir\\_ws/DWQR/subscr/ViewComDoc.asp?Docid=387](http://www.dwaf.gov.za/dir_ws/DWQR/subscr/ViewComDoc.asp?Docid=387). [Accessed 14 June 2013].
3. Mckinsey global energy and materials efficiency, (2009). Online available at: [www.mckinsey.com/~/.../mckinsey/.../us\\_energy\\_efficiency](http://www.mckinsey.com/~/.../mckinsey/.../us_energy_efficiency). [Accessed 17 August 2013].
4. U.A. Amarasinghe, T Shah, and O.P Singh, (2007). Changing Consumption Patterns: Implications on Food and Water Demand in India, International water management institute R e s e a r c h Report 119, 20 07. Online available at <http://www.iwmi.cgiar.org/publications/iwmi-research-reports>. [Accessed on 17 August 2013].

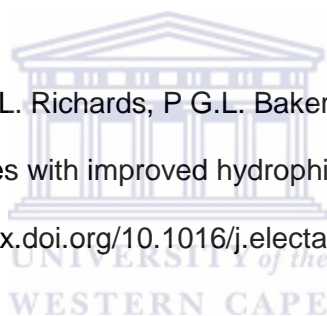


UNIVERSITY OF THE  
WESTERN CAPE

5. U.A Amarasinghe, T. Shah, And O.P Singh, (2007). India's Water Future to 2025-2050: Business-as-Usual Scenario and Deviations. International water management institute Research Report 123, 2007. Online available at <http://www.iwmi.cgiar.org/publications/iwmi-research-reports>. [Accessed 17 August 2013].
  
6. Central Water Commission, (2009). India, P o c k e t B o o k on Water Data 2005/2006 Data monitor, Electricity: Extended Global Industry Guide, 2009
  
7. A. A. Al-Rabiah, (1999). Membrane technology for hydrogen separation in ethylene plants, department of chemical engineering. Chemical Engineering Science, 54, (1999)
  
8. K. H Syed, S. Al-Assaf and G. O Phillips, (2011). Hydrogels Methods of preparation, characterisation and Applications. International Standard Book Number (ISBN) 978-953-307-268-5 (2011). Publisher Intech 2001
  
9. H.L.Richards, PGL.Baker and E. Iwuoha, (2012). Metal nanoparticle modified polysulfone membranes for use in waste water treatment: A Critical review. Sensor lab department of chemistry. Journal of Surface Engineered Materials and Advanced Technology 2 (2012) 183-193



10. A. Guiseppi-Elie, (2010). Electroconductive hydrogels: synthesis, characterization and biomedical application. *Journal on Biomaterias* 31 (2010) 2701-2716
11. T.R. Hoare, D.S. Kohane, (2008). Hydrogels in drug delivery: Progress and challenges. *Journal on Polymer* 49 (2008) 1993-2007.
12. P. Anandao, L. Fumie Sato, H. Weibeck and F.R. Valenzuela-Diaz, (2010). Montmorillonite as a component of polysulfone nana composite membranes. *Journal on Applied clay science* 48(2010) 127-132
13. L. Phelane, F N. Muya, H. L. Richards, P G.L. Baker\*, El Iwuoha, (2013). Polysulfone Nanocomposite Membranes with improved hydrophilicity. *Electrochim. Acta*(2014).  
Online available at <http://dx.doi.org/10.1016/j.electacta.2013.11.156>
14. F.Peng, X.Huang, Anna.Jawor and E.M.V. Hoek, (2010). Transport structural and interfacial properties of poly (vinyl alcohol)-polysulfone composite nanofiltration memembranes. *Journal of membrane science* 353(2010) 169-176
15. A.-hameed, and M. El-Aassar, (2012). Polysulfone-polyvinyl alcohol thin film nano-composite membranes: synthesis, characterisation and application for desalination of saline groundwater. *Journal of Applied Science research*, 8(7) (2012) 3811-3822.





16. A.M. Lowman, and N.A. Peppas, Cross-linking diffusion erosion modelling permeability pore size responsive hydrogen swelling. International Standard Book Number (ISBN): 978-3-642-06068-7 (Print) 978-3-662-06108-4 (Online)
17. S. Tessendorf, et al., (1999). Modeling, Simulation and Optimization of Membrane-Based Gas Separation Systems, *Chemical Engineering Science*, 54, (1999) 943.
18. E.H Schacht, (2004). Polymer chemistry and hydrogel system. *Journal of Physics: Conference Series*. 3 (2004) 22
19. H.Susanto and M. Ulbricht, (2008). High-performance thin layer hydrogel composite membranes for ultrafiltration of natural organic matter. *Journal on water research* 42 (2008) 2827-2835
20. Z. Fan, Z. Wang, M. Duan, J. Wang and S. Wang (2008). Preparation and characterization of membrane. *Journal of membrane science*, 310 (2008) 402-408.
21. J. H. O. Owino, A. Omotayo, PGL. Baker, A. Guiseppi-Elie and E. Iwuoha, (2008). Synthesis and characterisation of poly (2-hydroxyethyl methacrylate) polyaniline based hydrogel composites. *Journal on reactive & functional polymers* 68 (2008) 1239-1244.



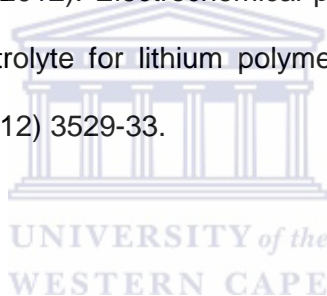
22. Z.F. Fan, Z. Wang, N. Sun, J.X. Wang, S.C. Wang, (2008). Performance improvement of polysulfone ultrafiltration membrane by blending with polyaniline nanofibers. *Journal of membrane Science*. 320 (2008) 363–371.
23. A.J, Dass, L.A. Alhoshan, M.S. Ghasemi, and A.W, Mohammad (2012). Development of polyaniline-modified polysulfone nanocomposite membrane. *Journal on Applied Water Science* 2 (2012) 37-46.
24. X. Wei, Z. Wang, J. Wang and S. Wang, (2012). A novel method of surface modification to polysulfone ultrafiltration membrane by preadsorption of citric acid or sodium bisulfide. *Membrane water treatment*, 3(1) (2012) 35-49
25. H. L. Huang and S. Yang (2006). Filtration characteristics of polysulfone membrane filters. *Journal of Aerosol science* 37(2006) 1198-1208.
26. S. Li, Y Gao, H. Bai, L. Zhang, P. Qu and L. BAi, (2011). Preparation and characteristics of polysulfone dialysis composite membrane modified with nanocrystalline cellulose. *Bioresources International Standard Serial Number (ISSN)* 1930-20126.
27. H. Zhao, L. Wu, Z. Zhou and H. Chen (2013). Improving the antifouling of polysulfone membrane by incorporation of isocyanate-treated grapheme oxide, *Journal societies on Physical. Chemistry*, 15 (2013) 9084—9092.

28. X. Wang, D. Fang, K. Yoon, B. S. Hsiao and B. Chu, (2006). High performance ultrafiltration composite membranes based on poly (vinyl alcohol) hydrogel coating on crosslinked nanofibrous poly (vinyl alcohol) scaffold. *Journal of Membrane Science* 278 (2006) 261–268.
29. C. Dizman, S. Ates, L. Torun and Y. Yagci, (2010). Synthesis, characterization and photoinduced curing of polysulfone with (meth)acrylate functionalities. *Beilstein Journal of organic chemistry*. 6 (2010) 56.
30. G. Jing, L. Wang, H. Yu, W. A. Amer, and L. Zhang, (2012). Recent progress on study of hybrid hydrogels for water treatment. *Journal of physicochemistry. Engineering aspects* 416 (2013) 86– 94.
31. B.V. Slaughter, S.S. Khurshid, O. Z. Fisher, A. Khademhosseini and N.A. Peppas, (2009). Hydrogel in regenerative medicine. *Advanced material* 21 (2009) 3307-3329.
32. S. Sampath, N. A. Choudhury and A .K. Shukla, (2009). Hydrogel membrane electrolyte for electrochemical capacitors. *Journal on chemical science* 121 (5) (2009) 727–734
33. D. Buenger, F. Topuz and J. Groll, (2012). Hydrogels in sensing applications. *Journal of progress in polymer science* 37 (2012) 1678– 1719.

34. T.H. Bae, and T.M. Tak, (2005). Effect of TiO<sub>2</sub> nanoparticles on fouling mitigation of ultrafiltration membranes for activated sludge filtration. *Journal of membrane science* 249 (2005) 1–8.
35. D. Rana, T. Matsuura, (2010). Surface modifications for antifouling membranes. *Chemical review*. 110 (2010) 2448–2471.
36. S.C. Hsu and T. J. Williams, (1982). Evaluation of factors affection the membrane filters technique for testing drinking water. *Apply environmental microbiology*. 44 (2) (1982) 453.
37. S. Dockko, S. Khishigjargal, Il. Kang, H. Oh, S. Choi and I. Hyun, (2010). Physico-chemical characteristics by chemical cleaning on the surface of RO membrane. *Sustain environmental resource*, 20(5) (2010) 305-310.
38. A.F. Ismail, and P.Y.Lai, (2004). Development of defect-free asymmetric polysulfone membranes for gas separation using response surface methodology. *Journal on separation and purification technology* 40 (2004) 191-207.
39. O. Okay, (2009). General properties of hydrogel, hydrogel elasticity swelling and in homogeneity. Digital object identifier (DOI): 10.1007/978-3-540-75645-3-1

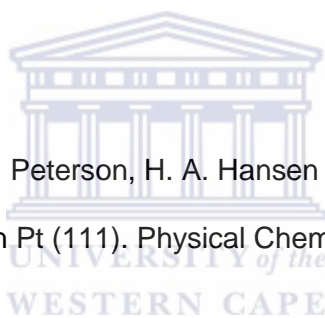
40. B.D. Reid, F.A.R. Trevino, I. H. Musselman, K. J. Balkus and J.P. Ferraris, (2001). Gas permeability properties of polysulfone membranes containing the mesoporous molecular sieve MCM-41. *Chemical materials*, 13 (7) (2001) 517-520
41. K.C. Khulbe, CY. Feng and T. Matsuura, (2013). Water and waste water treatment technology, membrane characterization, *Encyclopaedia of life support systems*. Online available at: <http://www.desware.net/DESWARE-SampleAllChapter.aspx>. [Accessed 6 May 2013].
42. M. Dufresne, P. Bacchin, G. Cerino, J.C Remigy, G.N. Adrianus, P.Aimar and C. Legallais, (2013). Human hepatic cell behaviour on polysulfone membrane with double porosity level. *Journal of Membrane Science* 428 (2013) 454-461.
43. A. V. Bil'dyukevich, N.G Semenkevick, S. A. Pratsenko, and I. L. Zharkevich, (2009). The influence of the porous type on the transport properties of polysulfone membranes. *Theoretical foundations of chemical engineering* 43(4) (2009) 361-365.
44. A.J. Bard, and L.R. Faulkner, (2002). *Electrochemical Methods: Fundamentals and Applications*, 2nd edition, John Wiley & Sons, New York, USA (2002)
45. S. Scally, W. Davison and H. Zhang, (2005). Diffusion coefficients of metal complexes in hydrogels used in diffusive gradients in thin films. *Journal of analytica chemica acta* 558 (2006) 222-229.

46. K. Jamroziak and W. Jargulinski, (2010). The analysis of the electrode potential shift in the examination of plastic-covered metal fatigue strength. *Achieves of materials science and engineering* 41(1) (2010) 21-27.
47. M. J. Aiza, and J. Benavente, (2001). Streaming potential along the surface of polysulfone membranes a comparative study between two different experimental systems and determination of electrokinetic and adsorption parameters. *Journal of membrane science* 190 (2001) 119- 132.
48. K.YD, J.YK, and NJ. Jo, (2012). Electrochemical performance of poly(vinyl alcohol)-based solid polymer electrolyte for lithium polymer batteries. *Journal Nanoscience Nanotechnology*. 12(4) (2012) 3529-33.
49. , X.M Kang., Z. Zou, X. Cai, and P.M. Jinyuan, (2007). A novel glucose biosensor based on immobilization of glucose oxidase in chitosan on a glassy carbon electrode modified with gold-platinum alloy nanoparticles/multiwall carbon nanotubes. *Analytical Biochemistry*. 369(1) (2007) 71-79.
50. N.B. Colthup, L.H. Daly, and S.E. Wiberley, (1990). *Introduction to Infrared and Raman Spectroscopy*, 3rd Edition, Academic Press, 1990.



51. M. A. Aroon, A.F. Ismail, M. M. Montazer-Rahmati and T. Matsuura, (2010). Morphology and permeation properties of polysulfone membranes for gas separation: Effects of non-solvent additives and co-solvent, separation and purification technology 72 (2010) 194-202.
52. N. Savage and M. S. Diallo, (2005). Nanomaterials and Water Purification: Opportunities and Challenges. Journal of Nanoparticle Research 7 (4-5) (2005) 331-342. Digital object identifier (DOI):10.1007/s11051-005-7523-5.
53. K.S. Kim, K.H. Lee, K. Cho, and C.E. Park, (2002). Surface modification of polysulfone ultrafiltration membrane by oxygen plasma treatment. Journal of membrane science 199 (2002) 135-145.
54. R.R.L. De Oliveira, D.A.C. Albuquerque, T.G.S. Cruz, F.M. Yamaji and F.L. Leite<sup>1</sup>, (2005). Measurement of the Nanoscale Roughness by Atomic Force Microscopy: Basic Principles and Applications, Online available at:  
[http://cdn.intechopen.com/pdfs/33450/InTechMeasurement\\_of\\_the\\_nanoscale\\_roughness\\_by\\_atomic\\_force\\_microscopy\\_basic\\_principles\\_and\\_applications.pdf](http://cdn.intechopen.com/pdfs/33450/InTechMeasurement_of_the_nanoscale_roughness_by_atomic_force_microscopy_basic_principles_and_applications.pdf).  
[Accessed 21 September 2013].
55. J. D. Miller, S. Veeramasuneni, J. Drelich, and M. R. Yalamanchili, (1996). Effect of Roughness as Determined by Atomic Force Microscopy on the Wetting Properties of PTFE Thin Films. Polymer engineering and Science 36 (14) (1996) 1849-1855.

56. A Morrin, R.M Moutloali, A.J Killard, M.R Smyth, J Darkwa, and E. Iwuoha, (2004).  
Electrocatalytic sensor devices: (I) cyclopentadienylnickel (II) thiolato Schiff base  
monolayer self-assembled on gold. *Talanta* 64 (2004) 30–38.
57. J. Charkoudian, C. Anthony and E. Allegrezza, Polysulfone copolymer membranes  
and process, United states patent, patent number 5885 (456) (1999) 1-12.
58. R.N Perron, and J.L Brumaghim, (2009). A Review of the Antioxidant Mechanisms of  
polyphenol compounds related to Iron binding cell. *Biochemistry Biophysics* 53 (2009)  
75-100.
59. C.C. P Shi, O. Grady, A. A. Peterson, H. A. Hansen and J. K. Norskov (2013).  
Modelling CO<sub>2</sub> reduction on Pt (111). *Physical Chemistry Chemical Physics* 15 (19)  
(2013) 7114-7122.
60. P. Y. Bruice, (2006). *Essential organic chemistry, peadsoption*, 6<sup>th</sup> Edition.  
International Standard Book Number (ISBN): 13: 978-0321663139
61. R.C. William, and D. Gao, (2009). Properties of membranes used for hemodialysis  
therapy. *Journal of membrane science* 324 (2009) 6-13.





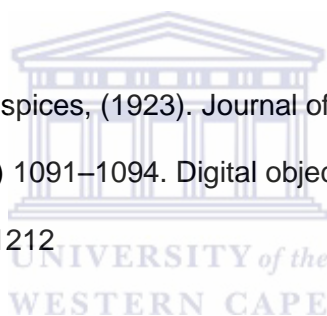
62. J.S. Taurozzi, H. Arul, V. Z. Bosak, A.F. Burban, T.C. Voice, M. L. Bruening and V. V. Tarabara,(2008). Effect of filler incorporation route on the properties of polysulfone silver nanocomposites membranes of different porosities. *Journal of membrane science* 325(2008) 58-68.
63. H. Kim and S.Hong, (1999). The transport properties of CO<sub>2</sub> and CH<sub>4</sub> for Brominated polysulfone membrane. *Korean Journal of chemical engineering* 16(3) (1999) 343-350
64. K.S. Kim, K.H. Lee, K. Cho, and C.E. Park, (2002). Surface modification of polysulfone ultrafiltration membrane by oxygen plasma treatment. *Journal of membrane science* 199 (2002) 135-145.
65. H. Odegaard, B. Eikebrokk, R. Storhaug, (1999). Treatment of water with elevated organic content. *Water Science and Technology* 40 (1999) 37–46.
66. F. Li, J. Sun, H. Zhu, X. Wen, C. Lin and D. Shi, (2011). Preparation and characterization novel polymer-coated magnetic nanoparticles as carries for doxorubicin, *Colloids and surfaces B: Biointerfaces* 88 (2011) 58 -62.
67. D.Li, X. Zhang, J. Yao, G.P. Simon, and H. wang, (2011). Stimuli- responsive polymer hydrogels as new class of draw agent for forward osmosis desalination. *The royal society of chemistry*, 1 5 (2011).

68. A.D. Marshall, P.A. Munro, and G. Trägårdh, (1993). The effect of protein fouling in microfiltration and ultrafiltration on permeate flux, protein retention and selectivity: A literature review. *Desalination* 01/1993; DOI: 10.1016/0011-9164(93)80047-Q
69. D.M Fikai, A.Fikai, G.Voicu, B.S. Vasile, C.Guran and E. Andronescu, (2010). Polysulfone based membranes with desired pores characteristics. *Material plastic*, 47 1 (2010).
70. J. Pretorius, *Encyclopaedia of life support systems, future challenges of providing high quality water- volume II. International protocols regarding global climate change and the impact of water resource*. Online available at: <http://www.eolss.net/sample-chapters/c07/e2-25-02-05.pdf>. [Accessed October 2013].
- 
71. R. Naim, A.F. Ismael, H.Saidi and E.Saion, (2004). Development of sulfonated polysulfone membranes as material for proton exchange membrane. *Proceedings of Regional Symposium on Membrane Science and Technology 2004, 21-25 April 2004*.
72. Y. Yuan and T. Randall Lee, (2013). Contact Angle and Wetting Properties. *Surface Sciences* 51 (2013) 3-34. Digital object identifier (DOI) 10.1007/978-3-642-34243-1\_1
73. L. Huang Lee, (1991). *Contact Chemistry and physics of solid Adhesion. Properties of things* 1290D (1991) 1-346. International Standard Book Number (ISBN) 0-306-43470-9

74. C.R Raymond, P. J. Sheskey, E Marian. E Quinn, (2009). Adipic Acid, Handbook of Pharmaceutical Excipients (Rowe, Handbook of Pharmaceutical Excipients), 6<sup>th</sup> edition, Pharmaceutical (2009) 11–12. International Standard Book Number (ISBN) 0-85369-792-2

75. R. Remminghorst, (2009). Microbial Production of Alginate, biosynthesis and Applications. Microbial Production of Biopolymers and Polymer Precursors. Caister Academic Press. International Standard Book Number (ISBN) 978-1-904455-36-3.

76. Government standards for spices, (1923). Journal of the American Pharmaceutical Association, 12 (12) (1923) 1091–1094. Digital object identifier (DOI):10.1002/jps.3080121212



77. Xu. Wang, (2012). Development of low cost polysulfone based anion exchange membranes and non-platinum oxygen reduction catalysts for fuel cell application. PHD Thesis (2012) School of chemical engineering and material of Newcastle University, June 2012.

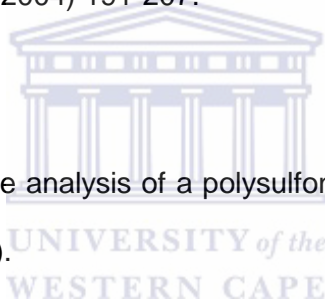
78. A. Cimen, M. Ersoz and S.Yildiz, (2006). Electrochemical characterization of polysulfone membranes with different valence salt solutions. Desalination 194 (2006) 202-210.

79. I Gamry, (2010). Application note. Basic of electrochemical impedance spectroscopy.  
Revised number.1.0.9/3/2010 1990-2009 gamry instrument, Inc.

80. A. Canas. M.J. Ariza, and J.Benavente, (2001). Characterization of active and porous sublayers of a composite reverse osmosis membrane by impedance spectroscopy. Journal of membrane Science 183 (2001) 135-146.

81. A.F. Ismail and P. Y. Lai, (2004). Development of defect-free asymmetric polysulfone membranes for gas separation using response surface methodology. Separation and purification technology 40 (2004) 191-207.

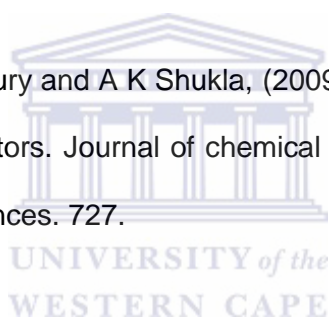
82. J.A. Jansen, (2001). Failure analysis of a polysulfone flow sensor body a case study. Practical failure 1(2) (2001).



83. P.M.S Monk, (2001). Fundamentals of electroanalytical chemistry. Newyork, USA: John Willey & Sons, (2001) 158-159.

84. E.Yeager and R.W. Zurilla. Rotating disk and ring disc techniques, Accession Number: AD0694951. Online available <http://www.dtic.mil/docs/citations/AD0694951>. [Accessed July 2013].

85. A.D. Williams and P.J. Floy, (2003). Analysis of the random configuration of the polycarbonate of diphenylol-2,2'-propane. *Journal of Polymer Science Part A-2: Polymer Physics* 6(12) (2003) 1945–1952. Direct Object identifier (DOI): 10.1002/pol.1968.160061201
86. H.L. Gasparotto, J.F. Gomes and G. Tremiliosi-Filho, (2012). Electrochemical Characteristics of Poly(vinyl pyrrolidone) and Poly(vinyl alcohol) on Single-Crystal Pt Surfaces in Acidic Medium. *ECS Trans.* 43 (1) (2012) 259-266. Direct object identifier DOI: 10.1149/1.4704967.
87. S. Sampath, N. A Choudhury and A K Shukla, (2009). Hydrogel membrane electrolyte for electrochemical capacitors. *Journal of chemical science.* 121 (5) (2009) 727–734. © Indian Academy of Sciences. 727.
88. H. Hou, F. Vacandio, M.L Di Vona, and P. Knauth, (2012). Electropolymerization of sulfonated phenol by cyclic voltammetry. *Journal of Applied Polymer Science* 129 (3) (2013) 1151-1156. Direct object identifier (DOI): 10.1002/app.39074.
89. H. Hou, F. Vacandio, M.L Di Vona, and P. Knauth, (2013). Electropolymerization of sulfonated phenol by cyclic voltammetry. *Journal of Applied Polymer Science* 129 (3) (2013) 1151–1156.



90. J.A. Koehler, M. Ulbricht, G. Belfort, (2000). Intermolecular forces between a protein and a hydrophilic modified polysulfone film with relevance to filtration. *Langmuir* 16 (2000) 10419–10427.
91. H. Susanto, and M. Ulbricht, (2009). Characteristics, performance and stability of polyethersulfone ultrafiltration membranes prepared by phase separation method using different macromolecular additives. *Journal of membrane science*. 327 (2009) 125–135.
92. H.T. Yeo, S.T. Lee, and M.J. Han, (2000). Role of polymer additive in casting solution in preparation of phase inversion polysulfone membranes. *Journal of chemical engineering. Japan*. 33 (2000) 180–185.
93. M.J. Han, and S.T. Nam, (2002). Thermodynamic and rheological variation in polysulfone solution by PVP and its effect in the preparation of phase inversion membrane. *Journal of membrane science*. 202 (2002) 55–61.
94. B. Chakrabarty, A.K. Ghoshal, and M.K. Purkait, (2008). Preparation, characterization and performance studies of polysulfone membranes using PVP as an additive. *Journal of membrane science*. 315 (2008) 36–47.
95. J.H. Kim, and K.H. Lee, (1998). Effect of PEG additive on membrane formation by phase inversion. *Journal of membrane science*. 138 (1998) 153–163.

96. A.K.G Chakrabarty, M.K. Purkait, (2008). Effect of molecular weight of PEG on membrane morphology and transport properties. *Journal of membrane science*. 309 (2008) 209–221.
97. Y.N. Yang, and H.X. Zhang, (2007). The influence of nano-sized TiO<sub>2</sub> fillers on the morphologies and properties of PSF UF membrane. *Journal of membrane science*. 288 (2007) 231–238.
98. J.H. Choi, J. Jegal, and W.N. Kim, (2006). Fabrication and characterization of multiwalled carbon nanotubes/polymer blend membranes. *Journal of membrane science*. 284 (2006) 406–415.
99. S. Qiu, L.G. Wu, X.J. Pan, L. Zhang, H.L. Chen, and C.J. Gao, (2009). Preparation and properties of functionalized carbon nanotube/PSF blend ultrafiltration membranes. *Journal of membrane science*. 342 (2009) 165–172.
100. Z.F. Fan, Z. Wang, N. Sun, J.X. Wang, and S.C. Wang, (2008). Performance improvement of polysulfone ultrafiltration membrane by blending with polyaniline nanofibers. *Journal of membrane science*. 320 (2008) 363–371.

- 101.M. Homayoonfal, and A. Akbari, (2010). Preparation of Polysulfone Nano-Structured Membrane for Sulphate Ions Removal from Water. Journal of environmental. Health. Science. Engineering. 7(5) (2010) 407-412.
- 102.S. Rafiq, Z. Man, S. Maitra, A. Maulud, F. Ahmad, and N. Muhammad, (2011). Preparation of asymmetric polysulfone/polyimide blended membranes for CO<sub>2</sub> separation. Journal of chemical engineering 28 (10) (2011) 2050-2056.
- 103.D. Parker, J. Bussink, HT. van de Grampel, GW. Wheatley, E. Dorf, E. Ostlinning, and K. Reinking, (2002). Polymers, High-Temperature in Ullmann's Encyclopedia of Industrial Chemistry. Direct object identifier (DOI):10.1002/14356007.a21\_449
- 104.H. Grützmacher, and C. M. Marchand, (1997). Heteroatom stabilized carbenium ions. Coordination Chemistry Reviews, 163 (1997) 287-344. Direct object identifier (DOI):10.1016/S0010-8545(97)00043
- 105.A. Canas. M.J.Ariza, and J.Benavente, (2001). Characterization of active and porous sublayers of a composite reverse osmosis membrane by impedance spectroscopy. Journal of membrane Science 183 (2001) 135-146. 2000.
- 106.E Karen, S. Buller, and R.W. De Doncker, (2000). A method for measurement and Interpretation of impedance spectra for industrial batteries. Journal of Power Sources. 85 (1) (2000) 72-78.



- 107.R.O. Akinyeye, (2007). Nanostructured Polypyrrole impedimetric sensors for anthropogenic organic pollutants. PHD thesis 2007. University of the Western Cape: Cape Town, page 271.
- 108.T.C Girija, and M.V. Sangaranarayanan, (2006). Analysis of polyaniline-based nickel electrodes for electrochemical supercapacitors. *Journal of Power Sources*. 156 (2) (2006) 705-711.
- 109.F. Miao, B. Tao, P. Ci, J. Shi, L. Wang, and P.K. Chu, (2009). 3D ordered NiO/silicon MCP array electrode materials for electrochemical supercapacitors. *Materials Research Bulletin* 44(9) (2009) 1920-1925.

